An Assessment of Functionalised Gold Nanoclusters for the Delivery of Doxorubicin to a Breast Cancer Cell Model

By

Akshay Bugwandeen

Thesis presented for the degree of

Master of Science

at

University of KwaZulu-Natal

College of Agriculture, Engineering and Science

School of Life Sciences

Department of Biochemistry

Supervisor: Prof. M Singh

2025

Signature: Prof. M Singh [redacted]

Abstract

Nanotechnology, a rapidly growing field of science, encompasses manipulating materials at the nanoscale with varied applicability to everyday situations. The advent of nanotechnology has facilitated the formulation of novel delivery systems for bioactive molecules. Gold nanoclusters have lured researchers in the field of nanomedicine due to their attractive qualities, which include ultra-small size, photostability, biocompatibility, and efficiency in drug delivery to tumour sites. Breast cancer is among the most common cancers affecting women globally and is a leading cause of death. Chemotherapeutic agents have been traditionally used to treat breast cancer. The anticancer drugs' low solubility is due to their hydrophobic nature, and their non-targeted delivery results in toxicity and high levels of drug resistance. Hence, the need for a smart and efficient drug delivery system is necessary to reduce toxicities and improve therapeutic efficiency. Gold nanoclusters (AuNCs) were synthesised successfully using glutathione, followed by encapsulation using the polymer, chitosan (CS), which was conjugated to the anticancer drug doxorubicin (DOX). High encapsulation was observed, with 83 % for the Au-CS-DOX-loaded nanocomplex (AuCTD) compared to 68 % for the CS-DOX-loaded nanocomplex (CTD). Physico-chemical characterisation included UV-visible spectroscopy, transmission electron microscopy (TEM), Fourier transform infrared (FTIR) spectroscopy, and nanoparticle tracking analysis (NTA). All nanoparticles (NPs) and nanocomplexes were spherical, displayed hydrodynamic sizes of less than 150 nm, had good stability and were mostly monodisperse. Pharmacokinetic studies conducted at physiological and acidic pH levels revealed that the AuCTD nanocomplex displayed a more controlled drug release over time than the CTD nanocomplex. Cytotoxicity studies were conducted using the 3-(4,5-dimethylthiazol-2-yl)- 2,5-diphenyltetrazolium bromide (MTT) assay on the human embryonic kidney (HEK293) and breast adenocarcinoma (MCF-7) cells. The AuCTD nanocomplex showed greater anticancer activity (11.12 % cell survival) compared to the CTD nanocomplex (54.63 % cell survival) and free DOX (32.83 % cell survival) in the MCF-7 cells at the highest concentration of 40 µg/ml. The AuCTD complex showed little cytotoxicity in the HEK293 cells. The high apoptotic indices of the nanocomplex in the MCF-7 cells suggested that apoptosis was a possible mechanism of cell death. Both nanocomplexes displayed no significant differences in the cell cycle analysis, as treatment with both nanocomplexes induced the cells to

remain in the G0/G1 cell cycle phase. Overall, the positive qualities of the AuCTD nanocomplex as a delivery system *in vitro* have been highlighted. These results warrant further studies to determine the mechanisms of action of the nanocomplex and to test these nanocomplexes *in vivo* using a breast cancer animal model.

Keywords: Doxorubicin; gold nanoclusters; chitosan, breast cancer; drug delivery; drug release; anticancer; apoptosis.

PREFACE

The experimental work described in this dissertation was carried out in the Discipline of Biochemistry, School of Life Sciences, University of KwaZulu-Natal, Westville from March 2021 to June 2025, under the supervision of Professor Moganavelli Singh.

These studies represent original work by the author and have not otherwise been submitted in any form for any degree or diploma to any tertiary institution. Where use has been made of the work of others it is duly acknowledged in the text.

COLLEGE OF AGRICULTURE, ENGINEERING AND SCIENCE

DECLARATION I - PLAGIARISM

I, Akshay Bugwandeen, declare that

1. The research reported in this thesis, except where otherwise indicated, is my original research.
2. This thesis has not been submitted for any degree or examination at any other university.
3. This thesis does not contain other persons' data, pictures, graphs or other information, unless specifically acknowledged as being sourced from other persons.
4. This thesis does not contain other persons' writing unless specifically acknowledged as being sourced from other researchers. Where other written sources have been quoted then:

a. Their words have been re-written but the general information attributed to them has been referenced.

b. Where their exact words have been used, then their writing has been placed in italics and inside quotation marks, and referenced.

5. This thesis does not contain text, graphics or tables copied and pasted from the Internet, unless specifically acknowledged, and the source being detailed in the thesis and in the References sections.

Signed: 

Date: 13/07/2025

Thanks, and Dedications

I'd like to firstly thank God for everything, during this academic period, I was met with some ofthe most challenging obstacles, thankyou forgiving me the strength during my darkest times. I'd like to thank my family for their support- Rajan Bugwandeen (father), Priya Bugwandeen (mother) and Sohum Bugwandeen (brother). Lastly a big thankyou to my mentor Professor. M Singh for all of herpriceless guidance, patience and advice.

I'd like to dedicate this thesis to my late grandparents, Askran and Indookumari Bugwandeen (father's side), Chanderdutt and Bimla Devi Rughubar (mother's side). Thankyou for always looking over me, showering me with guidance and blessings.

ACKNOWLEDGEMENTS

I wish to express my sincere gratitude and appreciation to the following individuals and institutions:

- Professor. M Singh, thank you for all of your effort which has gone into this thesis. Your mentoring, patience, and support have been thoroughly valuable throughout this process.
- Dr. Saffiya Habib, thank you very much for your advice and time in this project. I appreciate your kind-hearted motivation during lab work.
- Mr Subashen Naidu of the Microscopy and Microanalysis Unit (UKZN, Westville) for his assistance with Transmission Electron Microscopy-Energy Dispersive X-ray (TEM-EDX) and for supplying formvar coated grids and staining solutions.
- The staff of the Discipline of Biochemistry and all colleagues who I now regard as family, of the Non-viral Gene and Drug Delivery and Mammalian Tissue Culture Laboratory (UKZN, Westville) for providing a pleasant work environment. Thank you for all of the help, guidance, and motivation, this work would not be possible without you. I appreciate each and every one of you.
- Ms. Kiya Madaree, thank you for your support and assisting me with keeping track of time during the drug release kinetics experimentation. I will always be grateful.
- The **University of KwaZulu-Natal** for supporting my research and providing me with the facilities that I needed to achieve my goals.

TABLE OF CONTENTS

List of Figures

Appendix A

List of Tables

List of Abbreviations

Acridine Orange: AO
Actual drug content: ADC
Aggregation-induced emission: AIE
AuNCs-CS-TPP-DOX nanocomposite: AuCTD

Chitosan: CS
CS-TPP-DOX nanocomposite: CTD

Daltons: Da
Deoxyribonucleic acid: DNA
Dicycohexyl carbodiimide: DCC
Dimethyl Sulfoxide: DMSO
Doxorubicin: DOX
Doxorubicin hydrochloride: DOX-HCl
Drug Delivery Systems: DDS
Ductal carcinoma in situ: DCIS

Energy Dispersive X-ray: EDX
Encapsulation efficiency: EE
Enhanced Permeability and Retention: EPR
Ethidium bromide: EtBr

Fourier Transform Infrared: FTIR

Gold: Au
Gold nanoclusters: AuNCs
Glutathione: GSH

High-Resolution Transmission Electron Microscope: HRTEM

Infiltrating ductal carcinoma: IDC
Infiltrating lobular carcinoma: ILC

Lobular carcinoma in situ: LCIS

3-[(4,5-dimethylthiazol-2-yl)-2,5-diphenyl tetrazolium bromide]: MTT
Minimum Essential Medium: MEM
Molecular weight: Mw
Molecular Weight Cut-Off: MWCO

Nanoparticle Tracking Analysis: NTA

N-hydroxysuccinimide: NHS

Polydispersity Index: PDI
Polyethylene glycol: PEG
Phosphate Buffered Saline: PBS

Revolutions per minute: rpm
Sodium tripolyphosphate: TPP
Standard Deviation: SD

Topoisomerase II: TOP2
Theoretical drug content: TDC
Transmission Electron Microscopy-Energy Dispersive X-ray: TEM-EDX

United States of America: USA

Chapter 1

Introduction and Significance of study

CHAPTER ONE

1. Introduction

1.1 Background to study

Cancer is a worldwide health issue, with around 19.3 million people diagnosed with this disease in 2020, with an estimated ten million mortalities (Debela *et al*., 2021). Cancer is characterized by aberrant cell growth caused by changes in gene expression due to mutations, resulting in dysregulated cell proliferation and apoptosis. Breast cancer is the most common type of cancer in women and the second highest cause of death in the USA. In 2023, there were a projected 609820 cancer mortalities and 1958310 new cancer cases, highlighting the seriousness of this issue (Siegel *et al*., 2023). In South Africa, from 2000 to 2020, the number of new breast cancer cases has more than doubled (Dlamini *et al*., 2024), emphasizing the need for research into innovative treatment interventions for cancer therapy.

Cancer treatment can be separated into conventional and novel or advanced therapy (Debela *et al*., 2021). The three primary modalities of conventional treatment are surgery, radiotherapy (radiation treatment), and chemotherapy, with surgery being one of the oldest forms of cancer treatment (Tannock, 1998). However, these treatment methods have been challenged due to severe side effects experienced by patients (Moses *et al*., 2003). Chemotherapeutic agents have limitations due to their aqueous solubility, systemic cytotoxicity, drug clearance, and multidrug resistance (Akinyelu *et al*., 2022). Multidrug resistance is primarily due to the efflux pumps in the cell that cause anticancer drugs to exit the cells. Most chemotherapeutic agents also exhibit a lack of selectivity towards cancer cells, resulting in normal cells also being affected (Chidambaram *et al*., 2011). These are some of the challenges facing conventional cancer therapy.

Doxorubicin (DOX) is a highly potent antineoplastic drug, usually administered alone or in combination with other treatments. The side effects related to DOX are cardiotoxicity, neurological disruption, gastrointestinal disruption, increased microbial infection, balding, nausea, and vomiting (Carvalho *et al*., 2009). Hence, developing

novel drug delivery systems that can reduce these effects may be beneficial to advance cancer treatment.

Nanotechnology has gained significant attention in cancer research, diagnosis, and therapeutic management. Nanotechnology is the manipulation of materials at a nanometer scale (usually between 1 and 100 nm) for the advancement of biological and chemical needs. There are usually two standard methods of nano-level manufacturing: the top-down approach and the bottom-up approach (Emerich and Thanos, 2003; Bhushan, 2016). Due to the nanosize of these particles, they provide great value in nanomedicine. The applications of nanomedicine include use in biosensors, bioimaging, regenerative healing, wound care and healing, and drug and gene therapy delivery systems (Haleem *et al*., 2023).

Gold nanoclusters (AuNCs) have attracted researchers in the field of nanotechnology and nanomedicine due to their qualities, such as ultra-small size, photostability, and biocompatibility that can be used in biosensing and bioimaging (Pavelka *et al*., 2023). AuNCs have displayed high efficiency in delivering drugs to tumour tissue with increased circulation times, low cytotoxicity, and high renal clearance (Yahia-Ammar *et al*., 2016). This makes them suitable candidates for *in vitro* and *in vivo* drug delivery studies.

This investigation primarily focused on breast cancer and the treatment via chitosan-functionalized gold nanoclusters for doxorubicin delivery. Chitosan was included to enhance drug encapsulation and delivery to cancer cells and for better biocompatibility and stability of the AuNCs.

1.2 Novelty of study

This investigation describes the use of AuNCs as an anticancer drug (DOX) delivery system for minimizing the drug's side effects and enhancing anticancer activity in breast cancer cells. Although spherical AuNPs and, to some extent, Au nanorods have been investigated for drug delivery, the use of AuNCs to deliver DOX to a breast cancer model has not yet been fully explored.

1.3 Aims and Objectives

This investigation aimed at synthesizing chitosan functionalized AuNCs that can efficiently bind and deliver the anticancer drug DOX to breast cancer cells with little or no effect on normal cells.

The objectives of the study were:

- To synthesize ultra-small AuNCs and functionalize them with chitosan ensuring colloidal stability biocompatibility and responsiveness.
- To encapsulate the anticancer drug, doxorubicin, with high efficiency and high loading of doxorubicin onto chitosan-functionalised AuNCs.
- Characterization of the physicochemical properties AuNCs and their drug nanocomposites using nanoparticle tracking analysis (NTA) for size distribution and concentration, transmission electron microscopy to identify morphology (TEM), Fourier transform infrared to investigate surface chemistry and bonding (FTIR) and UV-visible spectroscopy to observe optical properties. This was conducted to ensure a full characterization profile.
- To determine the drug release kinetics by monitoring the DOX release at different pHs from the nanocomplexes over 72 hours representing physiological and tumour microenvironments, and to model the release mechanism.
- To determine the cytotoxicity of DOX versus the drug nanocomplexes on the breast cancer (MCF-7) and embryonic kidney (HEK293) cells using the MTT assay, with confirmation from the apoptosis and cell cycle assays. To elucidate mechanisms and selectivity.

1.4 Outline of dissertation

The dissertation comprises 5 main chapters.

Chapter 1 provides a background to the study, its novelty, and the aims and objectives of the research.

Chapter 2 is a detailed literature review discussing breast cancer, gold nanoclusters, the need to functionalize using polymers, doxorubicin, and cellular uptake mechanisms.

Chapter 3 provides the experimental protocols used in the study.

Chapter 4 presents all data obtained from the study, including figures, tables, and statistical analyses. The results are further critically discussed against the literature.

Chapter 5 summarises the key points of the thesis together with a conclusion and recommendations for future studies.

Chapter 2

Literature Review

CHAPTER TWO

2. Literature Review

2.1 Breast Cancer

Cancer can be traced to ancient times, with initial evidence of tumours located in fossilised bones. Early archaeological findings indicated that cancer was present for a long time. Although the word "cancer" was not used, phrases for the word "tumour" were found on wall illustrations in ancient Egypt, ancient China, and Mesopotamia (Paduch, 2015; Jassim *et al*., 2023). Surgical intervention was one of the oldest forms of treatment for breast cancer.

Today, breast cancer is the most common cancer and the leading cause of mortality in women globally (Azamjah *et al*., 2019). Breast cancer can be hereditary or due to hormonal changes, lifestyle, and diet (McGuinn *et al*., 2012; Kripke *et al*., 2020). Genetic mutations to the breast cancer susceptibility 1 and 2 (BRCA1/2) genes validate risk assessment screening (Watkins, 2019). Malignant neoplasms tend to infiltrate adjacent tissues and subsequently metastasize to remote locations, leading to additional tumours (McGuinn *et al*., 2012; Kripke *et al*., 2020). Mutations to proto-oncogenes and tumour suppressor genes contribute to the disease (Venkitaraman, 2019). Hence, cancer is noted for uncontrollable cellular division with dysfunctional cell signalling pathways.

The stages of breast cancer range from stage 0 to stage 4 (Table 2.1) (Sharma *et al*., 2010). *In situ* breast cancers refer to the localised cancer which has not yet spread to nearby tissues (Obeagu and Obeagu, 2024). The lower the stage (stage 1 to 4) of cancer, the less the cancer has metastasised (Trayes and Cokenakes, 2021). Factors that affect the staging of cancer are the size of the tumour, the spread of the cancer to the lymph nodes, metastasis to distant sites, and the grade of the tumour (Moo *et al*., 2018).

Table 2.1: The different stages of cancer (Sharma *et al*., 2010).

Stage	Description
In situ carcinoma	
0	The tumour is confined to the milk-producing glands as well as the milk duct, and has not spread to other parts of the breast tissue.
Localised and regional invasive cancer	
I	The size of the tumour would be than ¾ inch in diameter, and has not gone beyond the breast.
IIA	The size of the tumour is less than ¾ inch in diameter, and it would have invaded one to three lymph nodes located in the armpit. Microscopic quantities would have invaded the lymph node in close proximity to the breastbone in accordance with the side of the tumour or both. The tumour could also be larger than ¾ inch but less than 2 inches, yet would not have spread past the breast.
IIB	The size of the tumour would be greater than ¾ inch but less than 2 inches in diameter, and has spread to one to three lymph nodes in the armpit. Microscopic quantities would have invaded the lymph node in close proximity to the breastbone in accordance with the side of the tumour or both. The tumour could also be larger than 2 inches, and would not have spread past the breast.
IIIA	The size of the tumour is 2 inches or less in diameter and has spread to four to nine lymph nodes in the armpit, or one lymph node near the breastbone would be enlarged on the same side of the tumour. The tumour could have also been greater than 2 inches and would have spread to four to nine lymph nodes near the breastbone or in the armpit.
IIIB	The tumour has spread to the chest wall or skin and had caused inflammatory breast cancer.
IIIC	The tumour can be of any size and found as one of the following; The tumour has spread to 10 or more lymph nodes in the armpit. The tumour has spread to the lymph nodes above or below the collarbone. The tumour has spread to lymph nodes in the armpit, and at least one lymph node is enlarged, located near the breast bone on the same side as the tumour. The tumour has spread to four or more lymph nodes in the armpit and microscopic quantities to lymph nodes located near the breast bone on the same side of the tumour.
Metastatic cancer	
IV	Regardless of the tumour size, it has invaded other tissues or organs such as the lungs or bones, or lymph nodes that are distant to the breast.

The breast has two primary tissues: the glandular tissue, which contains the ducts and lobules, and the stromal tissue. The ducts serve as milk passages, while the lobules serve as housing units. The stromal tissue is made of fibroid connective tissue and fatty tissue. The lymphatic tissue is also a component of the breast and is responsible for the drainage of waste products and cellular fluids (Sharma *et al*., 2010).

Breast cancer is classified into three major subtypes based on the presence or absence of molecular indicators for estrogen or progesterone receptors. These include the human epidermal growth factor 2 (ERBB2), triple-negative (15% of patients, tumours without any molecular indicators), ERBB2 negative (70% of patients), and ERBB2 positive (15%-20% of patients) (Waks and Winer, 2019). The two broad categories of breast cancer are non-invasive and invasive breast cancer. Non-invasive breast cancer is when the cancer cells are confined to the area of origin (ducts or lobules) and have not metastasized to fatty or fibrous tissue. Standard forms are ductal carcinoma *in situ* (DCIS), which makes up about 90% of non-invasive cancers, lobular carcinoma *in situ* (LCIS), which is less common and is more likely used as a marker in cases of higher risk (Watkins, 2019). In invasive breast cancers, the cancer cells burst through ducts and lobular walls, invading surrounding tissues (connective and fatty tissue) (Sharma *et al*., 2010; Iacopetta *et al*., 2023). These cover a broad spectrum of breast cancers that require diagnostics and treatment.

Infiltrating carcinomas such as lobular carcinoma (ILC) originate in the breast's lobules, metastasise to other areas of the body, and are usually progesterone and estrogen-receptor-positive (Watkins, 2019). Infiltrating ductal carcinoma (IDC) originates in the milk ducts and metastasizes to adjacent breast tissue by penetrating the duct walls. IDC is the most common type of breast cancer, making up 80% of all cancer cases, with 70% of women being human receptor positive or negative (Watkins, 2019; Sharma *et al*., 2010).

Globally, breast cancer is a cause for concern, with over 500 000 deaths and affecting 1 in 8 to 10 women regardless of ethnicity. It is predicted that almost 12 million females will be diagnosed with human receptor-positive cancer, with an expected survival of 5 years (Gholami *et al*., 2024). This highlights the need for the

formulation of innovative drug delivery systems. Drug delivery systems should be able to minimise toxicity to healthy cells, prolong circulation time, increase the bioavailability and uptake of the drug at the tumour site, and prevent premature degradation of the therapeutic drugs (Bae and Park, 2011; Iacopetta *et al*., 2023).

2.2 Doxorubicin (DOX)

Doxorubicin (DOX) is an antitumoral antibiotic that can be used on a wide spectrum of cancers (Rivankar, 2014). DOX belongs to the group of anthracyclines, which was first isolated from the bacterium *Streptomyces peucetius* (Thorn *et al*., 2011; Jones and Dass, 2022). It has been routinely used as treatment for a variety of cancers, such as breast cancer, lung cancer, ovarian cancer, Hodgkin's lymphoma, some leukaemias, as well as malignancies associated with the head. Apart from cancer, it is also used for the inhibition of malaria and AIDS related sarcomas (Rivankar, 2014). DOX is a highly potent antineoplastic drug (Carvalho *et al*., 2009; Jones and Dass, 2022) that can be used on both solid tumours and soft (liquid) tumours and can be used in combination therapy or alone (Rivankar, 2014). DOX is a glucoside containing a tetracyclic quinoid aglycone, adriamycinone, linked to the amino sugar daunosamine (Figure 2.1) (Yang *et al*., 2014; Alghorabi *et al*., 2019).

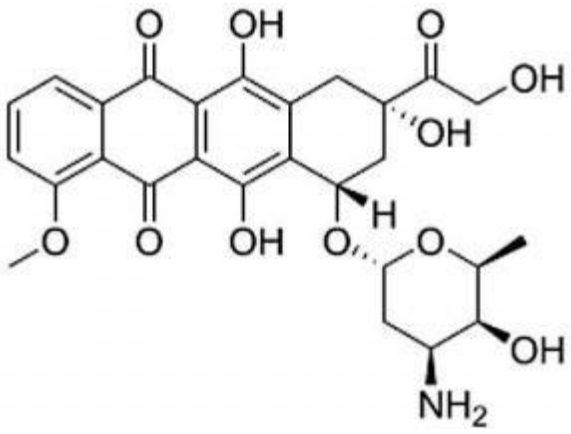

Figure 2.1: The chemical structure of doxorubicin (Alghorabi *et al.,* 2019).

The intravenous administration of DOX is conventionally performed at 21-day intervals. Incompatibility issues arise when combining this medication with heparin or 5-fluorouracil, as precipitation may occur (Sritharan and Sivalingam, 2021). The rapid distribution profile exhibited by DOX enables swift tissue penetration, with the primary mode of biotransformation for DOX (Johnson-Arbour and Dubey, 2017).

The antitumoral action of DOX can be attributed to the establishment of free radicals, which cause oxidative stress, destroying DNA, cellular membranes, and proteins (Yang *et al*., 2014). The intercalation of DOX into the DNA hinders DNA and RNA synthesis. Intercalation occurs at the connecting points amid the nucleotide bases of the DNA strands (Norouzi *et al*., 2020). DOX also suppresses topoisomerase II (TOP2) activity, an enzyme that regulates DNA topology by impeding replication, transcription, and DNA repair (Norouzi *et al*., 2020). These lead to the formation of free radicals, as mentioned above. However, DOX lacks specificity and targets both healthy and cancer tissue, leading to adverse effects on the patients that include oral ulcers, nausea, vomiting, fatigue, hormonal changes, hypertension, alopecia, and bone marrow depression. The chronic impact of DOX is cardiomyopathy, which leads to congestive cardiac failure (Rivankar, 2014; Aloss and Hamar, 2023). More severe side effects include nephrotoxicity, hepatoxicity, and cardiotoxicity due to free radical-induced damage to the myocardium. (Alghorabi *et al*., 2019). DOX augments the matrix production of metalloproteinases 2 and 9, contributing to cardiomyopathy due to the weakening of the collagenous matrix, which serves as a structural support for the cardiomyocytes (Sobiborowicz-Sadowska *et al*., 2023).

Although DOX is an efficient chemotherapeutic, its adverse side effects hinder its use. Hence, suitable delivery vehicles are needed to limit the induced toxicity and improve efficacy by targeting the drug specifically to cancer cells and minimising harm to healthy tissue.

2.3 Chemotherapeutic Drug Delivery Systems

Chemotherapeutic agents have been the conventional form of treatment for cancer. There are three main types of clinical administration of chemotherapy. Primary induction therapy is used for advanced cancer types, where no other treatment

would provide efficacy (Chu and Sartorelli, 2018). Neoadjuvant therapy is usually used for patients who display localised cancer, for which radiation and surgery would not be effective. Neoadjuvant treatment is provided to patients with locally advanced cases of breast cancer and is provided before surgery (Wang and Mao, 2020).

Adjuvant therapy is often combined with radiation, surgery, or both (Chu and Sartorelli, 2018). The mechanism of interaction of a drug delivery system with malignant formations and the limiting factors after administration need to be investigated before the treatment process.

Drug delivery systems (DDS) have been extensively investigated, with few technologies impacting cancer (Moses *et al*., 2003). DDS has aided in cancer prevention and cancer-associated pain. The concept of DDS is based on the controlled release of the associated chemotherapeutic agent and the duration of the chemotherapeutic at the targeted site (Zhang *et al*., 2013; Wakaskar, 2018). A DDS facilitates the introduction of therapeutic substances into the body while optimizing efficiency and safety by regulating the rate, location, and volumetric parameters governing drug release. This process encompasses therapeutic administration, active ingredient discharge, and transfer across biological membranes to the target site for optimal impact (Jain, 2020).

Creating new pharmaceutical drugs or altering existing formulations to enhance efficacy holds little value if the vehicles responsible for their dissemination are ineffective (Adepu and Ramakrishna, 2021). Most progress in targeted drug delivery has been made in cancer therapy. However, delivering therapeutic drugs to the brain via the blood-brain barrier presents with a multitude of obstacles due to short half-life, poor uptake, lack of solubility (Avramović *et al*., 2020), high dose dumping causing toxicity, high first-pass metabolism and premature excretion from the body (Adepu and Ramakrishna, 2021). Systemic side effects can also be attributed to non-specific biodistribution, uncontrolled drug release, and low levels of drug payloads at specific target sites (Liu *et al*., 2016; Panda *et al*., 2020). The formulation of smart and efficient DDS is necessary to reduce toxicities and improve overall therapeutic efficiency (Kalaydina *et al*., 2018)

The targeted delivery of chemotherapeutic agents into solid tumours has been of interest for disease abrogation and cure (Lu and Qiao, 2018). Limiting factors such

as the difficulty of cancer therapeutics to target cancer stem cells as well as difficulty in invading tumour sites due to lack of specificity and the internal pressure (increased interstitial fluid pressure) of the tumour, make it difficult for drugs to enter the tumour core where uncontrolled proliferation and angiogenesis occurs (Chakraborty and Rahman, 2012; Panda *et al*., 2020). In addition to these limitations, some chemotherapeutic agents show low solubility levels due to their hydrophobic nature, and their non-targeted delivery results in toxicity and high levels of drug resistance (Kachalaki *et al*., 2016). The levels of drug resistance can be attributed to the enhanced removal of drugs via efflux pumps in the cell membrane through proteins such as P-glycoprotein (Baguley, 2010). They aid in the distribution, excretion, or absorption of many chemical compounds. This can become a challenge in administration due to decreased bioavailability, therapeutic levels, and reduced movement across the blood-barrier (Bukowski *et al*., 2020).

Chemotherapeutic agents have a major role in cancer treatment, used alone or in combination (Chidambaram *et al*., 2011). However, the current efficiency of DDS is limited as damage also occurs to proliferating and normal cells due to a lack of specificity (Pan *et al*., 2016). Side effects reported include nausea and vomiting (Schirrmacher, 2019) and increased toxicity to organs (kidneys, digestive passages and organs, liver, and areas of the bone marrow) (van den Boogaard *et al*., 2022).

An ideal DDS must protect healthy cells from high toxicity and enhance current chemotherapeutic agents while reducing side effects. Furthermore, it should have increased drug bioavailability, control drug release, site-specific interaction, stability under physiological conditions, improved circulation and bio-dispersion, ease of administration, and cost-effectiveness (Jain, 2020). Using nanobased DDS may be advantageous for medical treatment. These systems have demonstrated their efficacy through diverse formulations targeting a range of ailments. They exhibit specific attributes such as reduced size, biodegradability and hydrophobic/hydrophilic tendencies alongside superior compatibility in biological environments, resulting in low toxicity and immunogenicity, that contribute to high effectiveness against different forms of cancer pathology (Forouhari *et al*, 2022).

The advent of nanotechnology has facilitated the formulation of novel delivery systems for bioactive molecules (Hu *et al*., 2018). Nanoparticles (NPs) in the form of nanoclusters (NCs) offer an array of benefits, stemming from the development and

utilization of materials engineered at the nanoscale level. These novel materials possess unique properties (Villela Zumaya *et al*., 2022), which include the capacity to encapsulate or bind drugs for efficient and targeted delivery to specific tissues while improving bioavailability, reducing dosages and toxicity levels, and facilitating transport across biological barriers. These NCs can contribute to medical issues related to theranostics, tissue engineering, and drug administration with improved accuracy that is aided by imaging techniques (Villela Zumaya *et al*., 2022).

2.4 Nanotechnology

Nanotechnology, a rapidly growing field of science, encompasses manipulating material at the nano-level with varied applicability to everyday situations (Nasrollahzadeh *et al*., 2019). It involves formulating and implementing chemical, physical, and biological systems at various scales - from single atoms or molecules to submicron dimensions. Additionally, it involves the incorporation of these nanomaterials into more comprehensive systems (Hornyak *et al*., 2018). Nanotechnology can modify, enhance, and optimize the characteristics of materials and products (Mohammed *et al*., 2024). The current era may be called the "Nano Era" based on its positive impacts, especially in water treatment, engineering, and medicine (Bhushan, 2016; Nasrollahzadeh *et al*., 2019).

Nanotechnology's most notable influence is observed in biomedical research and medicine. This manipulation of material at a nanoscale that emphasizes medical advancement and medical substitutions is termed nanomedicine (Satalkar *et al*., 2016). Nanostructures range from 1 nm to 100 nm, providing greater efficacy than their bulk counterparts (Mansoori, 2017). They have shown potential in cancer therapeutics as anticancer nanocarriers. This is due to their distinct structural dimensions and outstanding mechanical, electrical, thermal, optical, and chemical properties (Haleem *et al*., 2023). Nanosystems have shown improved antitumour drug specificity for uptake into tumour sites, lowered toxicity, and achieved steady-state drug levels (Chatterjee and Kumar, 2022).

The exploitation of nanotechnology in cancer therapy can circumvent limitations in the central nervous system (CNS) and blood-brain barriers (Tang *et al*., 2019). NPs can engage and accommodate many small molecules and are amenable to functionalization with ligands, polymers, DNA or RNA strands, peptides, antibodies, and drugs (Gmeiner and Ghosh, 2014). NPs need functionalization with suitable polymers to enhance the encapsulation of therapeutic molecules and to improve stability (Bugwandeen *et al*., 2023).

2.5 Gold Nanoclusters (AuNCs)

2.5.1 Background

In early civilizations, gold (Au) was often associated with divine figures and rulers. It held great value and was sought after in tribute to their glory. Throughout history, this precious metal has long been revered as a symbol of power, beauty, and cultural elitism. Some of the first uses of Au date back to 2600 BC (Habashi, 2016), when Au was used as jewellery and in the creation of deities for worship. Au is one of the least complicated metals due to its inert nature and workability. It is also highly pure, making it attractive in therapeutics and diagnostics (Harrison, 2010). Over the last three decades, we have seen remarkable progress in nanoscience and nanotechnology. Studies of Au nanoclusters (AuNCs) provide precise nanomaterials and properties such as homogeneity of particles, the same atomic crystalline metal phases, the phenomenon of periodicity and quantum confinement in nanoclusters, and the development of hierarchical complexity in nanosystems (Zeng, 2018).

The term "colloidal gold" refers to a suspension of sub-micrometer-sized particles of Au in either water or an organic solvent (Mingos, 2014). The properties and uses of these colloidal particles are influenced mainly by their size and shape, making them invaluable across various industries, including electronics, electron microscopy, nanotechnology, materials science, and medicine (Lohse and Murphy, 2013; Voliani, 2020). Recent breakthroughs have been achieved by isolating molecular cluster compounds containing Au that can be stabilized using phosphine or organothiolato-ligands. Characterization of metal particles comprising 3-100 atoms at the atomic level has revealed their intriguing chemical, physical, and catalytic attributes (Mingos, 2014; Voliani, 2020). Chitosan is a prominent choice as a drug-delivery carrier

associated with AuNCs due to its high levels of improving stability, improving adhesion, and temporarily widening tight junctions of cells, increasing drug delivery (Rodrigues *et al*., 2012). Chitosan has high cross-linking abilities when used with sodium tripolyphosphate, being able to increase levels of bound drug (Gounden and Singh, 2024). This improves treatment by lowering dose-dependent treatment by increasing the therapeutic drug index. Drug targeting is site-specific when incorporated with chitosan making chitosan modified-gold nanoclusters ideal drug delivery carriers (Faid *et al.,* 2022).

2.5.2 Applications of Gold Nanoclusters

Over the last twenty years, AuNCs have presented themselves as versatile tools in cancer diagnosis and treatment (Zheng *et al*., 2021). This could be due to their ultrasmall size (1 nm to 3 nm in diameter), improved photonic characteristics, and reduced plasmonic responses compared to the more prominent AuNPs (Jin *et al*., 2016). AuNCs have native luminescent properties upon formation. Modification with proteins, peptides, polymers, capping ligands, or other biomolecules as structural scaffolds is deemed necessary for stabilizing AuNCs. This enhances the biocompatibility of these AuNCs and preserves their unique optical characteristics for use in theranostics (Figure 2.2) (van de Looij *et al*., 2021).

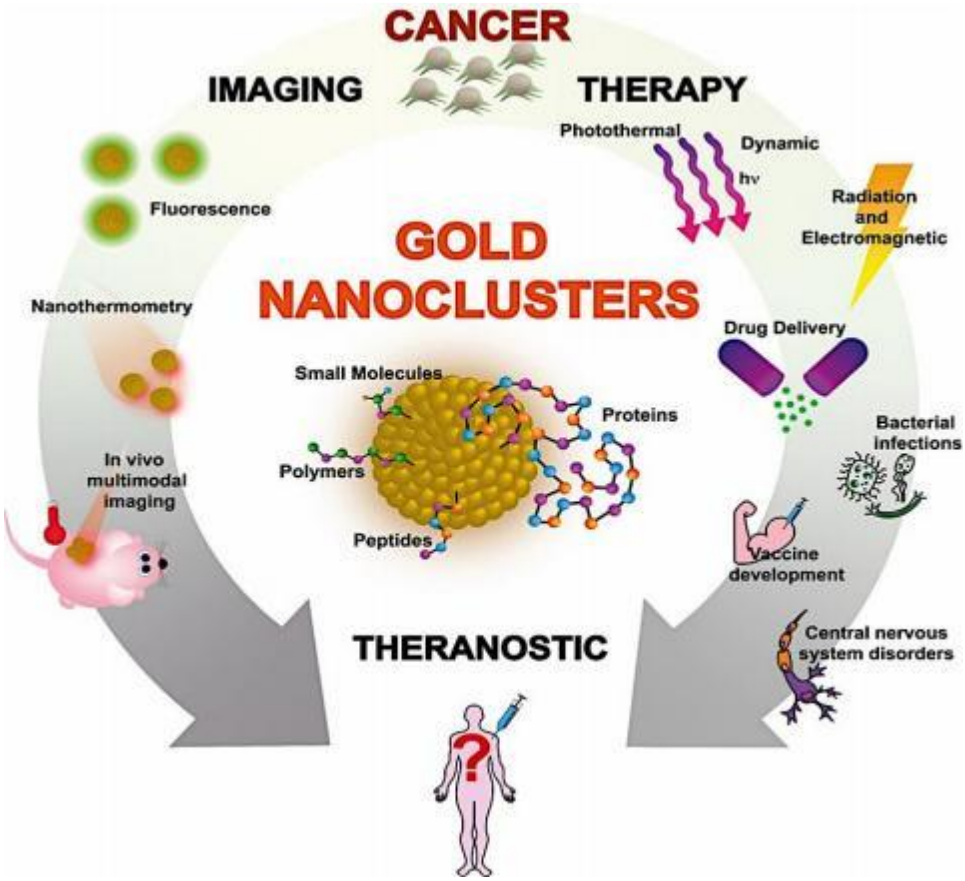

Figure 2.2: Illustration of the uses of AuNCs (van de Looij *et al*., 2021).

Due to their uncomplicated yet efficient surface modification, Au-based nanostructures have received widespread use in detecting analytes, bio-imaging, delivering pharmaceutical drugs, and treating diseases. AuNCs can assist in drug delivery technology, encompassing duration and dosage parameters in drug distribution. This results in enhanced drug utilization efficiency, reduced costs, and lower toxicity (Cui *et al*., 2020).

It has been reported that AuNCs can easily penetrate the core of mature cells, including lymphocytes and granulocytes (Qu *et al*., 2015; Bai *et al*., 2020). The function of these AuNCs in biological systems was elucidated by a series of tests, including assessments of pH-dependent stability and resilience under conditions with excess salinity. AuNCs have the potential to act as fluorescent platforms for imaging

and sensing applications in biology and deep-tissue imaging *in vivo* (Kaur *et al*., 2018). AuNCs may serve as drug delivery vehicles or as monitors of pharmaceuticaltherapeutics in drug administration. The advantages of AuNCs include their use in radiation, electromagnetic therapy, photothermal therapy, and photodynamic therapy. The luminescent feature of AuNCs can be used to detect drug release mechanisms. DOX-loaded AuNCs were shown to deliver DOX to cancer cells due to the cleavage of the disulfide bonds, with tumour reduction noted after nineteen days (Cui *et al*., 2020).

In vivo studies using a concurrent treatment of photothermal and photodynamic therapy with AuNCs displayed 41.1% photothermal conversion, and the internal thermal tumoral conditions increased by 28.1 ± 6.8 °C compared to 8.4 ± 2.1 °C in mice treated only with laser therapy. It was also noted that the tumour size and volume increased in the control mice, while mice receiving the AuNC photothermal therapy showed a reduction in tumour volume (Liu *et al*., 2019).

2.5.3 Gold Nanoclusters as Drug Delivery Systems

The use of NPs as drug delivery systems holds promise for treating many diseases due to their potential to limit toxicity and dosage required for efficient treatment. They are attractive due to their ability to deliver drug payloads to specific tissue sites (Wang and Kohane, 2017; Bai *et al*., 2020). AuNCs have shown increased drug circulation and biodistribution, in addition to targeting and triggering drugs at specific sites to reach therapeutic levels. This increases the drug's efficacy while limiting the dosage to off-target sites (Chakraborty and Pradeep, 2017). Cells mostly take up NPs due to the enhanced permeability and retention (EPR) effect (Li *et al*., 2018).

AuNCs combined with graphene oxide and loaded with DOX were used for drug delivery and imaging in hepatocellular carcinoma. It was observed that the DOX-loaded AuNC complex had increased distribution and absorption of DOX in the cell compared to DOX alone. The complex also inhibited greater cellular growth compared to free DOX. This was attributed to the ease of internalisation of the complex (Wang *et al*., 2011; Tan *et al*., 2024). A study using AuNCs conjugated to a block copolymer with the anticancer drug camptothecin investigated the cytotoxic

effects of the free drug and drug-loaded nanocomplexes in the uterine cervix carcinoma and human lung adenocarcinoma cells. The study noted that the camptothecin-loaded AuNCs had a higher level of cytotoxicity on both cell lines than free camptothecin (Chen *et al*., 2012; Tan *et al*., 2024).

A study using AuNC drug delivery systems as an "all-in-one" system to aid in the passive uptake by tumours through the EPR effect and to inhibit tumour growth by producing reactive oxygen species using near-infrared light. The study noted that gold nano-species in the 5 nm to 200 nm range showed low levels in the liver due to the reticuloendothelial system removing the NPs, and high renal clearance (Kong *et al*., 2021). Due to the efficacy of AuNCs in bioimaging, diagnostics, and treatment, the synthesis of these nanocarriers has gained popularity.

2.5.4 Synthesis of Gold Nanoclusters

Their ultrasmall size (1 nm to 5 nm), stability, increased surface area, and high luminescence are only a few capabilities of AuNCs that make them highly attractive for research in nanomedicine.

One of the most important phenomena observed in the synthesis of AuNCs is the aggregation-induced emission (AIE) mechanism, in which non-luminescent gold (I)-thiolate oligomeric complexes formed highly luminescent AuNCs upon aggregation. The colour and intensity of the luminescence and quantum yields are attributed to the level of aggregation. The core shell of the nanocluster has a high level of gold (I)-thiolate complexes, which gives the AuNC its highly luminescent photo-qualities (Luo *et al*., 2012). The three steps of attaining gold nanoclusters are shown in Figure 2.3.

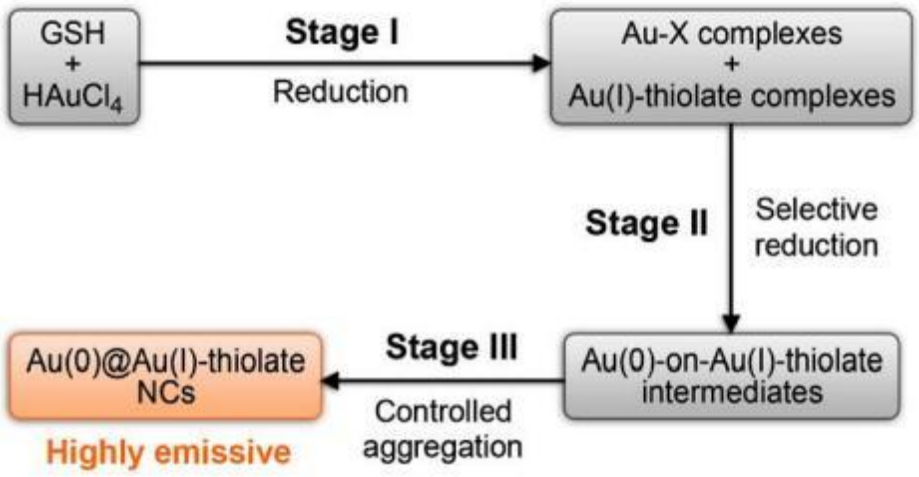

Figure 2.3: The process to synthesize luminescent gold nanoclusters (X represents any nonthiolate ligand) (Luo *et al.,* 2012).

The strategy to synthesize the AuNCs was to compact the Au (I)-thiolate complexes into a dense shell onto the Au(0) core. Glutathione (GSH) is added as a ligand for steric stabilization, water solubility and as the reducing and protective agent in the synthesis process. In the three-step synthesis process (Figure 2.3), the initial step is the GSH reduction of Au(III) into Au(I) due to the thiol (Au(I)-thiol) group on GSH. If oxidized GSH were used, this would be attributed to the disulfide bonds. Selective reduction occurs when the Au(I)-X particles are reduced to Au(0) atoms. The Au(0) core then forms on the Au(I)-thiolate group, forming intermediates. The last stage is the controlled aggregation of the Au(0) atoms into the Au core, with the Au(I)-thiolate complexes forming a shell around the core. The highly stable luminescent AuNCs would have formed through the AIE mechanism (Luo *et al*., 2012). Figure 2.4 depicts a scheme for the formation of the AuNC.

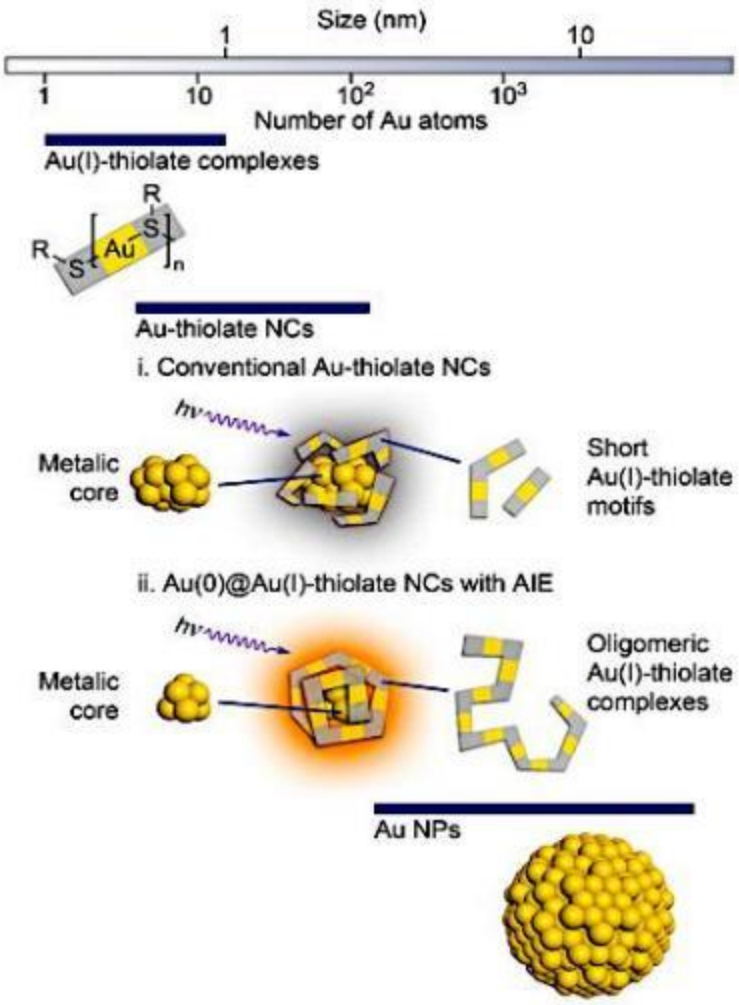

Figure 2.4: Schematic representation of the mechanism of AIE and the conventional method using short Au(I)−thiolate motifs (Luo *et al.,* 2012).

2.6 Surface modification and Zeta potential

The characteristics of AUNCs have gained much attention from the scientific community, with their surface chemistry seen as a critical determinant for selecting their ideal application. Surface modifications are essential to reduce toxicity, enable targeted delivery, attachment of therapeutic agents, prevent aggregation by improving stability, and improve the circulation time to avoid removal by the reticuloendothelial system (Pissuwan *et al*., 2011; Cui *et al*., 2020).

One of the focal aspects of AuNCs is their unique properties that can arise using distinct thiol ligands. Ligands can determine the properties of the AuNC, such as size, distribution, dispersity, and solubility (Yan *et al*., 2016). This study used glutathione

(GSH) as a capping ligand for the synthesis process. GSH is a low molecular weight thiol that reduces and prevents oxidative stress and regulates redox homeostasis needed for cellular growth and function. GSH can directly interact with free radicals and enzymes such as glutathione transhydrogenase and glutathione peroxidase. The presence of GSH in tissues and bodily fluids is important in some diseases and for the type of therapy required (Tian *et al*., 2012). Higher levels of stability were reported when GSH was used as a capping ligand, in addition to increased quantum yield, water dispersibility, and stability against photo irradiation and salts. The advantages of GSH include improved selectivity, sensitivity, and cost-effectiveness. GSH-prepared AuNCs exhibited improved fluorescent intensity and were highly efficient (Wu *et al*., 2017).

Zeta potential measurements assist with assessing the stability of NPs in colloidal solutions/suspensions due to the electrostatic forces between particles. The zeta potential is also known as the electrokinetic potential. It can be defined as the potential of the shear plane of a colloidal nanocomplex that can move within an electric field (Bhattacharjee, 2016). The liquid encompassing the particle is termed the electrical double layer and comprises an inner region (Stern layer) and an outer region (diffuse layer). There is a hypothetical barrier within the boundaries of the diffuse layer containing ions that form an impenetrable unit. When the NP is exposed to an electrical field, the ions on the exterior of the barrier migrate individually, displacing the fluid and resulting in the zeta potential. The term surface of hydrodynamic shear explains the particle surface interaction among the particles (Lowry *et al*., 2016).

The range of the electrostatic forces can be defined as highly stable, moderately stable, relatively stable, and highly unstable. The greater the magnitude of the zeta potential (negative or positive), the greater the extent of the repulsion forces, preventing the aggregation of particles. However, stability can also be attributed to van der Waals forces, which are not considered in zeta potential measurements. Some factors affecting the zeta potential are pH, concentration of the colloidal solution, and ionic strength (Bhattacharjee, 2016). Zeta potential measurement is useful in pharmaceutics, medicine, mineral processing, chemical production, and water and soil purification (Lunardi *et al*., 2021). Functionalisation with polymeric material is needed to improve the efficacy and stability of NPs for drug delivery. In

this study, chitosan was used as the polymer of choice for the added stability of the AuNCs.

2.7 Chitosan

The use of naturally occurring polysaccharides and their derivatives has gained more attention in DDS due to their many advantages (Barclay *et al*., 2019). Natural polysaccharides have an affinity for covalent crosslinking in polymer-based nanocarrier preparations (Liu *et al*., 2008; Zhang *et al*., 2021). Polysaccharides are advantageous because of their abundance, cost-effectiveness, biocompatibility, and biodegradability. In the case of chitosan (CS), upon degradation, amino sugars are released that can be absorbed by the body and are non-toxic and non-reactive. They also possess physicochemical qualities that allow easy modification and simple construction of stable nanocarriers for delivery purposes (Barclay *et al*., 2019).

CS is a derivative of chitin, produced through its deacetylation (Figure 2.5). Chitin is found in the shells of crustaceans such as prawns and crabs and the cellular walls of fungi (Mohammed *et al*, 2017). CS comprises β-1,4-linked D-glucosamine units, similar to cellulose. Functional groups such as hydroxyls, primary amines, and esters provide the polymer with exceptional properties for functionalizing AuNCs (Murugadoss and Sakurai, 2011; Zhang *et al*., 2021).

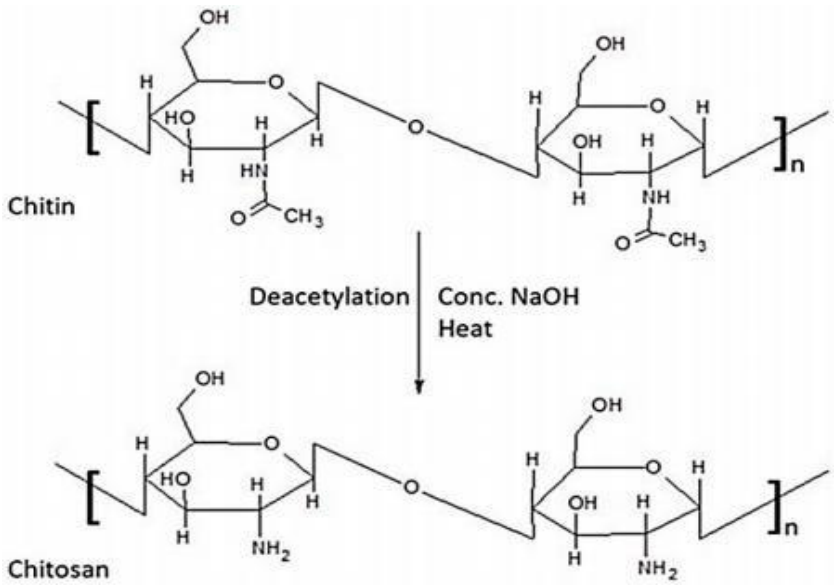

Figure 2.5: Scheme showing the deacetylation of chitin to chitosan (Mohammed *et al.,* 2017).

Polymer-based nanocarriers are usually designed in a sub-microscopic manner and are below 1000 nm in size. Using CS-based nanocarriers in DDS is highly advantageous due to their small size, allowing transport through most capillaries and preventing premature clearance (Liu *et al*., 2008). They have an affinity for cellular penetration (especially the epithelium) and tissue gaps into site-specific areas (Mohammed *et al.*, 2017). CS-based nanocarriers display controlled release of therapeutic agents (drug or gene) due to biodegradability, pH, ion, or temperature. Hence, they can improve the therapeutic index of drugs and significantly relieve associated side effects (Liu *et al*., 2008; Turcsányi *et al*., 2020). Recently, CS has been used in applications that benefit hydrogels and films for therapeutics (Turcsányi *et al*., 2020; Gounden and Singh, 2024; Gounden and Singh, 2025).

CS-based nanocarriers can be formulated by crosslinking, self-assembly, ionic crosslinking, and polyelectrolyte complexation (Liu *et al*., 2008; Plucinski *et al*., 2021), with simple complexation and ionic gelation being the most common methods (Babu and Ramesh, 2017). The enhancement of CS occurs through the modifications at active sites, such as the primary amine group (NH_2) and hydroxyl group (OH), which results in improved stability and increased drug encapsulation (Shukla *et al*., 2013).

The drug release mechanism of CS-based nanocarriers varies and may occur via polymer swelling, diffusion of the adsorbed drug, diffusion of the drug from the polymeric matrix, or drug release through polymer degradation or erosion or a combination of both (Figure 2.6) (Liu *et al*., 2018; David and Singh, 2025). The initial release of the therapeutic drugs occurs through a burst system due to either polymeric swelling, diffusion, or pore creation. CS-based nanocarriers exhibit pH-dependent drug release due to their acidic solubility (Mohammed *et al.*, 2017; David and Singh, 2025).

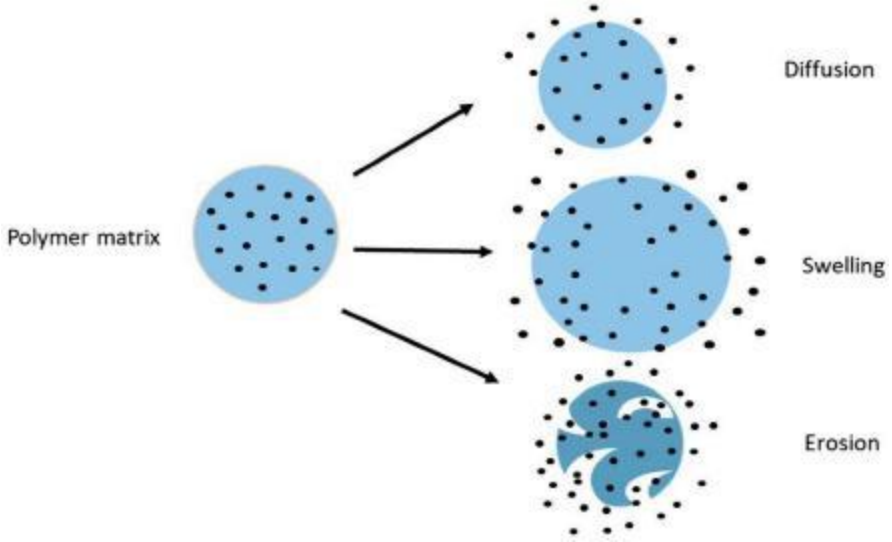

Figure 2.6: Scheme showing the modes of release from the chitosan matrix (Mohammed *et al.,* 2017).

CS-based AuNCs with spiropyran displayed good biocompatibility and internalisation in MCF-7 cells for fluorescent bioimaging purposes (Cong *et al*., 2021). Furthermore, CS-based AuNCs carrying methotrexate effectively targeted the lungs, resulting in improved drug retention, active tumour-targeting, and suppressed tumour growth *in vivo* while displaying a reduction in systemic side effects (Guo *et al*., 2018). The use of CS-based DOX-nanocomplexes with an antibody ligand showed that this nanocomplex was more effective in targeting MCF-7 cells than the just CS-based DOX-nanocomplexes and free DOX (Yousefpour *et al*., 2022).

The polycationic qualities of CS allow for its favourable interaction with the mucus membrane, making it a mucoadhesive. Hence, it is suitable for chemotherapeutic agents. However, CS does have low solubility levels in water but is soluble in acidic solutions due to the protonation of the amine groups. The amine group has also been noted to efficiently condense DNA and allow for intracellular trafficking of nanocarriers through endosomal disruption. The efficacy and stability of CS-based nanocarriers depend on the degree of deacetylation and molecular weight (Babu and Ramesh, 2017). The ability of CS to open tight joints linking epithelial cells allows for enhanced uptake of therapeutics in circulation (Mohammed *et al.*, 2017).

2.8 Biological Barriers to Drug Delivery

There are several biological hurdles that a nanocarrier will have to overcome before it can reach the desired treatment site. These include the gastrointestinal tract, blood-brain barrier, and solid tumours (extracellular or intracellular) (Wang *et al*., 2016; Gao *et al.*, 2023). Other issues that arise are clearance by the reticuloendothelial and phagocytic systems, immune responses, activation of the complement cascade, which responds to allergy-type reactions, glomerular filtration resulting in quick renal excretion and the blood vascular structure, where the cells of the endothelial lining and base membranes cause interference to access to tissues or organs (Rabanel *et al*., 2012; Liu *et al*., 2024).

Nanocarriers smaller than 200 nm have shown improved permeabilization of biological barriers (Finbloom *et al*., 2020). In the case of oral therapeutics, barriers such as the gastrointestinal tract, epithelial lining, and mucus-lined epithelium limit their bioavailability and distribution into the blood system (Waheed *et al*., 2022). The intravenous route has provided DDS with greater efficacy than oral therapeutics. Upon injection, the nanocarrier is opsonized in a biological medium. The opsonins are plasma proteins comprising apolipoproteins, fibronectin, immunoglobulin G, and immunoglobulin M (Rabanel *et al*., 2012). The reticuloendothelial system can also clear the therapeutics from circulation. Macrophages within the blood also entrap DDS by recognizing the adsorbed opsonin proteins and engulfing them by phagocytosis via the opsonin receptors (Schwartz, 2017; Rabanel *et al*., 2012). Polymeric material or targeting moieties as a coating can evade opsonization, premature clearance, or any immune-related response (Waheed *et al*., 2022).

Tumour vasculature limits drug delivery and penetration into target sites. Tumours have an irregular internal vascular structure and lack blood vessel organization. The increased surface area of the tumour vasculature results in enhanced vascular leakiness. The process of angiogenesis and the tumour endothelium can introduce wider endothelial junctions, leading to increased leakiness of pores. Other barriers include vessel co-option, vasculogenic mimicry, and insufficient vascular density, where the tumour cells undergo mitosis more rapidly than the endothelial cells, causing disorganized and hypoxic areas. The increased interstitial pressure from poor lymphatic drainage, the amplified fluid build-up from the leaky tumoral blood

vessels, and pressure due to the proliferation of cells in blood vessels impact the efficiency of chemotherapeutic agents (Kim *et al*., 2017). Another limiting factor with current chemotherapeutic agents is the lack of specificity to cancer cells, the tumour micro-environment, nanocarrier size, morphology and surface charge, and multi-drug resistance (Blanco *et al*., 2015: Nag and Delehanty, 2019).

Using biodegradable polymers such as CS, polyamidoamine, and polylactic acid in formulating novel DDS introduces favourable attributes to the system. The removal of nanocomplexes has not been thoroughly researched, but it is noted in the literature that the ultrasmall particles of approximately 10 nm can be rapidly filtered by the kidneys and liver and excreted in the urine. Polymeric functionalization of these particles can prevent this rapid excretion (Waheed *et al*., 2022). Figure 2.7 summarises the various biological barriers encountered in drug delivery.

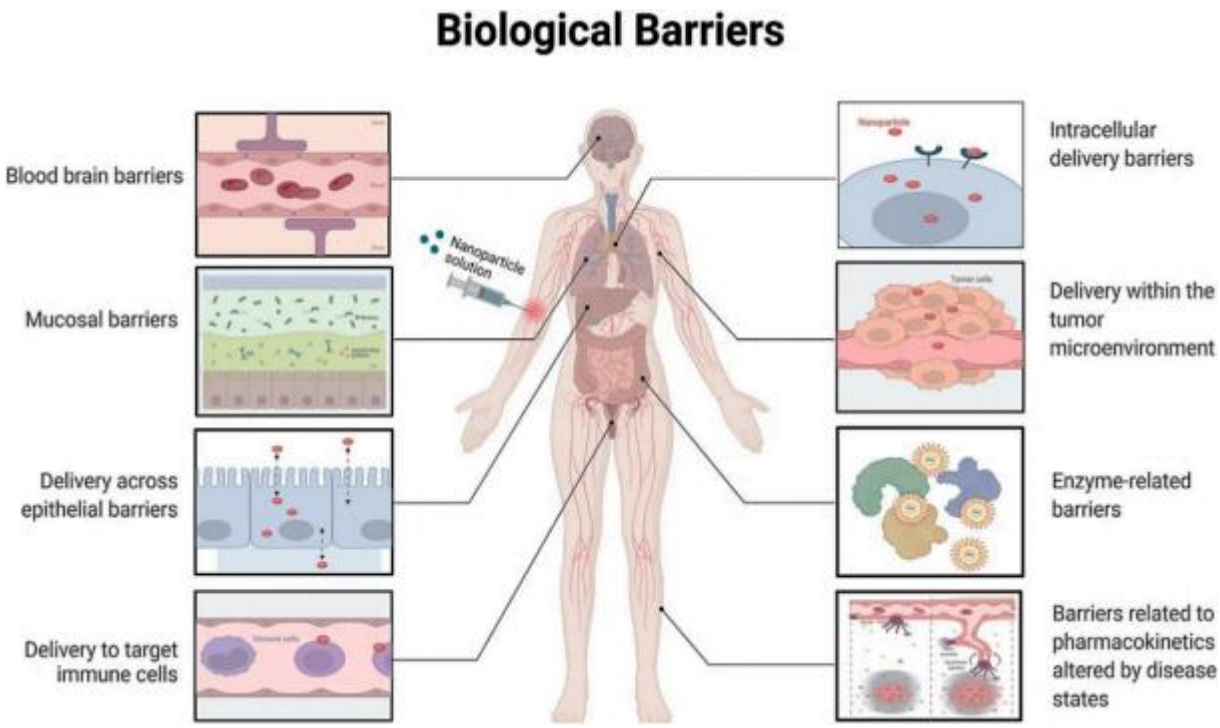

Figure 2.7: Diagram depicting different biological barriers (Waheed *et al.,* 2022).

2.9 Cellular Uptake

Cellular uptake of NPs can occur passively or actively (Figure 2.8). Passive uptake is the diffusion of the NP through the nuclear pore, and active uptake occurs by the diffusion of the NP through the nuclear membrane pore complex (Augustine *et al*., 2020). The principal biological factors that lead to the identification of NPs are their physiochemical properties, such as size, morphology, charge, polydispersity, surface chemistry, and surface nature (hydrophobic or hydrophilic). Before the nanocomplexes can reach the tumour cells, they must encounter the tumour microenvironment. The dense extracellular and extensive fibrous matrix, pH, and increased interstitial fluid pressure can affect the NP's interactions with the cellular membrane and their internalization (Behzadi *et al.,* 2017).

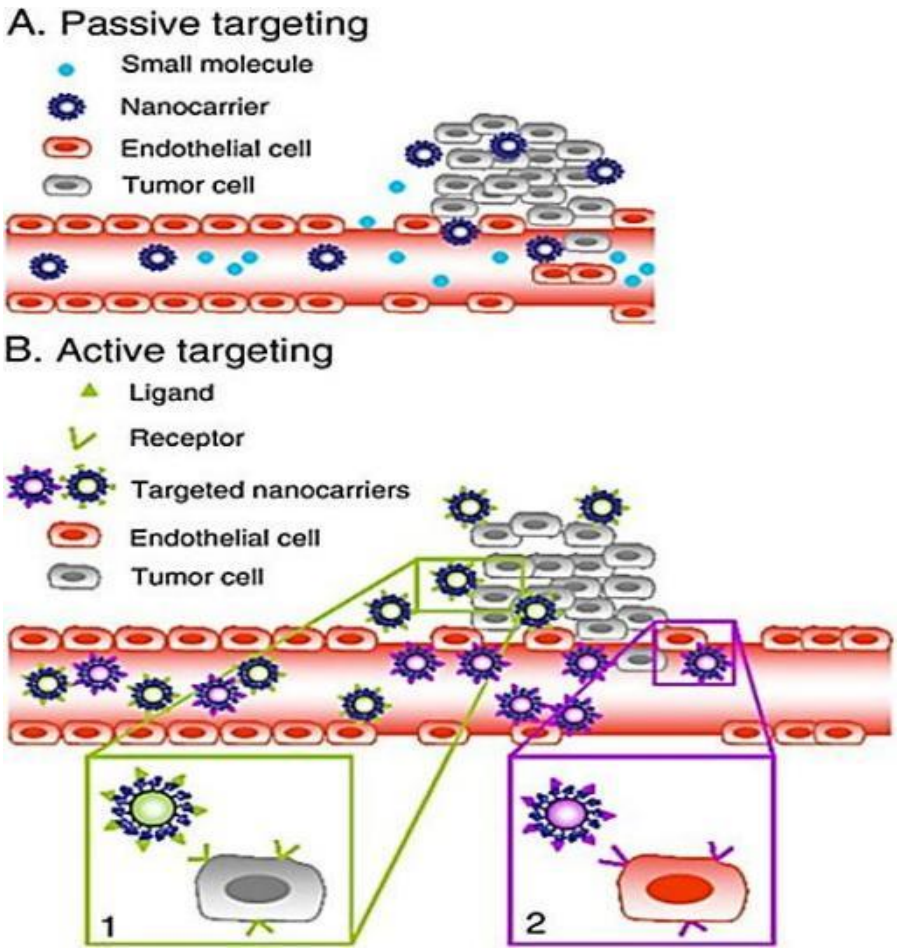

Figure 2.8: Illustration of the mechanisms of passive and active uptake (Danhier *et al*., 2010).

Passive targeting refers to the transfer of NPs that contain therapeutic agents through the endothelial lining of leaky blood vessels that have become more permeable and into the interstitial area of the cells. Passive targeting exploits the NP's physicochemical properties, the tumor's leaky vascular bed, and the tumour microenvironment. Particles ranging from 10 nm to 500 nm have been reported to leave the leaky vascular tissue and accumulate in the interstitial space (Torchilin, 2010; Tewabe *et al*., 2021). Other studies have noted similar accumulations for NPs ranging from 1 nm to 1000 nm. The physicochemical attributes of the NPs can be optimized to control the efficiency of drug delivery to the tumour sites (Rabanel *et al*., 2012; Tewabe *et al*., 2021).

The enhanced permeability and retention (EPR) effect in targeting looks at the prolonged circulation of drugs without interference through opsonization and premature excretion via the reticuloendothelial system. The EPR effect allows the therapeutic to accumulate within the target site, not within healthy cells/tissue. This selectivity decreases the chance of toxicity. A study using DOX and the polymer polyethylene glycol (PEG) found that the PEG-based DOX-loaded nanocomplexes displayed an increased EPR effect at tumour sites with significantly reduced side effects compared to the free drug (Torchilin, 2010).

Active targeting aims to internalize the drug-loaded NP by the tumour cells due to interactions between the functional moiety of the nanocarrier and the overexpressed receptors on the cancer cell surface (Torchilin, 2010; Attia *et al*., 2019). The targeting ligands that are attached to the surface of the NP, would bind to over-expressed receptors on the cancer cell surface. Targeting ligands include monoclonal antibodies, antibody ligands (peptides or non-peptides), and antibody fragments (Danhier *et al.,* 2010; He *et al*., 2020). Using these targeting moieties ensures that the therapeutic reaches the specific cancer cell.

Overall, understanding the tumour microenvironment is vital for researchers in producing acceptable therapeutic interventions to aid treatment. Compared to normal tissue, the cancer cell vascular structure differs in saturated oxygen, pH, perfusion, vascular anomalies, and metabolic conditions (Figure 2.9). (Danhier *et al.,* 2010: Dessale *et al*., 2022).

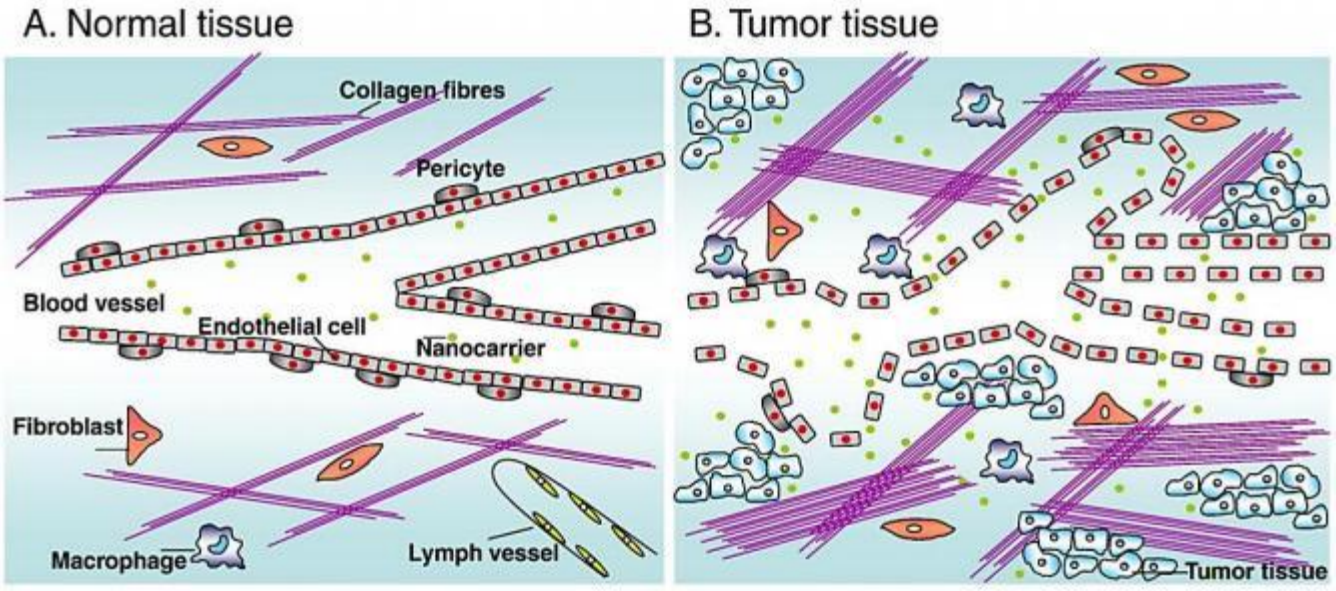

Figure 2.9: Diagram showing differences between normal and tumour tissue (Danhier *et al*., 2010).

2.10 Internalization and Intracellular Trafficking

The mechanisms of cellular uptake have been widely investigated, but the clarity of the uptake mechanism is still a grey area. Endocytosis is one of the main cellular uptake processes, which allows the cell to take up nutrients, solutes, and other molecules. The term endocytosis can be described by two sub-categories: phagocytosis, which takes up large particles, and pinocytosis, which is the uptake of fluids and minerals (solutes). Pinocytosis can be further divided into sub-categories such as macropinocytosis, caveolae-mediated endocytosis, clathrin-mediated endocytosis, and clathrin- and caveolae-independent endocytosis (Nelemans *et al*., 2020). Figure 2.10 depicts the main mechanisms of internalization.

Phagocytosis usually occurs in macrophages. The phagocytosis of NPs usually occurs after opsonization. When phagocytes engulf the intended material, phagosomes are formed, which eventually bind to the lysosomes. The material within the lysosome can be digested due to

the acidic environment of the lysosomal lumen. Particles ranging between 200 and 2000 nm can be phagocytosed (Behzadi *et al.,* 2017). Pinocytosis usually assists in the internalization of smaller particles. This process occurs when the cellular membrane configures an infolding of the membrane, which internalizes a small amount of extracellular fluid containing dissolved particles (Ramsden, 2023).

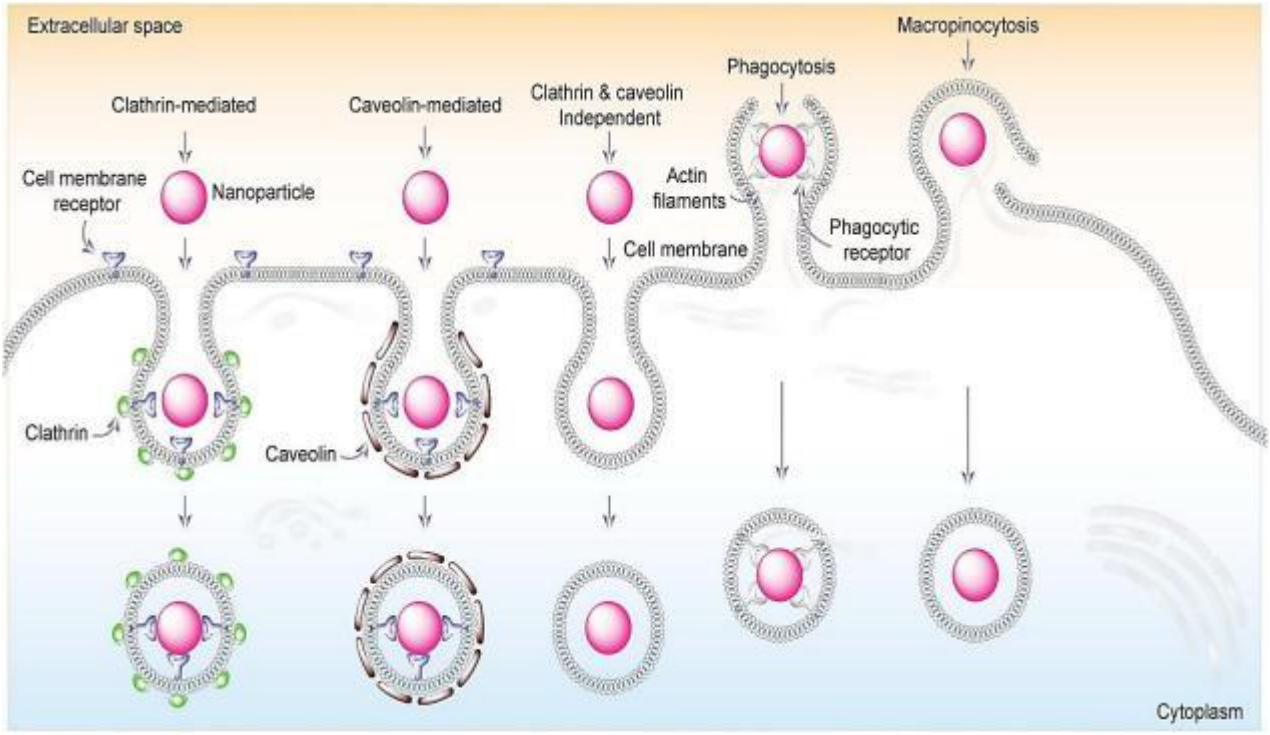

Figure 2.10: Diagram showing cellular uptake and intracellular trafficking of nanocomplexes (Ausgustine *et al.,* 2020).

Macropinocytosis is the internalization of foreign material, such as viruses, bacteria, and antigens. This pathway also internalizes necrotic and apoptotic cells. Caveolae- mediated endocytosis involves the use of infoldings of the membrane into a flask shape called caveolae, which can be found in adipocytes, endothelial, epithelial, muscle, and fibroblast cells (Foroozandeh and Aziz, 2018). The mechanism occurs through cellular signaling pathways and the control of membrane proteins. Usually, material ranging from 20 nm to 100 nm can be internalized. Caveosomes protect the integrity of the contents from enzymes (Augustine *et al.,* 2020).

Clathrin-mediated endocytosis is a mechanism that allows for the internalization of selected compounds. The mechanism operates on the formation of ligand-receptor complexes that form on the surface of the cellular membrane. The complexes then migrate to a cell membrane region with a concentrated number of clathrin-coated pits. The NP eventually reaches the endo-lysosomal pathway (Foroozandeh and Aziz, 2018). The size of NPs that the clathrin-mediated endocytosis pathway can take up ranges from 100 nm to 350 nm (Augustine *et al.,* 2020). Clathrin- and caveolae- independent endocytosis usually occurs when clathrin and caveolin are absent. This mode of action occurs through extracellular fluids, growth hormones, glycosylphosphatidylinositol-linked proteins, and interleukin-2 proteins that internalize the material. It was noted that polymeric nanocarriers can be internalized by this method (Foroozandeh and Aziz, 2018).

Studies have shown that NPs less than 200 nm can avoid the reticuloendothelial system and increase their half-life. Furthermore, increased cellular uptake was noted for NPs ranging from 100 nm to 200 nm in physiological barriers such as the blood-brain barrier and the gastrointestinal lining (Kulkarni and Feng, 2013; Navya *et al*., 2019). The internalization of NPs ranging from below 50 nm to 200 nm was investigated in hepatocellular carcinoma cells. NPs below 50 nm were internalized through energy-independent insertion and diffusion, while those ranging from 50 nm to 100 nm were internalized and could migrate to the nucleus. The NPs ranging from 100 nm to 200 nm were found to accumulate in the cell's cytoplasm (Li *et al*., 2017).

Chapter 3

Materials and Methods

CHAPTER THREE

3. Materials and Methods

3.1 Materials

Gold (III) chloride trihydrate (Mw: 393.83 g/mol, $HAuCl_4.3H_2O$), L-glutathione reduced (Mw: 307.32 g/mol, $C_{10}H_{17}N_3O_6S$), chitosan (CS)-medium molecular weight (≥ 75% deacetylation, $C_{12}H_{24}N_2O_9$), doxorubicin hydrochloride (DOX-HCl) (Mw: 579.98 g/mol, $C_{27}H_{29}NO_{11}.HCl$), sodium tripolyphosphate (Mw: 367.86 g/mol, $Na_5P_3O_{10}$), ethidium bromide solution (Mw: 394.31 g/mol, $C_{21}H_{20}BrN_3$) dialysis tubing (MWCO 14 000 Da and MWCO 2000 Da) were all purchased from Sigma-Aldrich (St. Louis, MO, USA). Glycerol anhydrous extrapure AR, 99.5% (Mw: 92.10 g/mol, $C_3H_8O_3$) was sourced from Sisco Research Laboratories Pvt. Ltd, (MH, India). Dimethyl sulfoxide (DMSO) (Mw: 78.13 g/mol), acridine hydrochloride zinc chloride double salt (Mw: 438.11 g/mol, $C_{17}H_{20}Cl_3N_3Zn$), 3-[(4,5-dimethylthiazol-2-yl)-2,5-diphenyl tetrazolium bromide] (MTT) (Mw: 414.32 g/mol, $C_{18}H_{16}BrN_5S$), and phosphate buffered saline (PBS) were obtained from Merck (Darmstadt, Germany). Luminex (TX, USA) supplied the Muse® cell cycle kit (MCH100106). The human embryonic kidney cells (HEK293) and breast adenocarcinoma (Michigan Cancer Foundation-7 cells, MCF-7 cells), were sourced through the American type culture collection (ATCC, Manassas, VA, USA). Minimum Essential Medium (MEM) with Earle's salts with L-glutamine, was acquired from Capricorn Scientific (Ebsdorfergrund, Germany). The penicillin/ streptomycin and Amphotericin B (100x) in respective concentrations (10 000 U/ml, 10 000 µg/ml, 25 µg/ml) and trypsin versene was purchased through Lonza BioWhittaker (Walkersville, MD, USA). Sterile fetal bovine serum had been obtained from Cytiva, Hyclone (UT, USA). All sterile tissue culture plasticware were purchased from NEST (Wuxi, Jiangsu, China). 18 MΩ ultrapure water, from Millipore Co, Direct Q3 was used throughout the study (Molsheim, France). All other reagents used were of a research grade quality. All cell culture and biological assays were conducted under aseptic conditions in a

Airvolution Class II biosafety Laminar flow hood (United Scientific, Cape Town South Africa).

3.2 Methods

3.2.1 Synthesis of Gold Nanoclusters

Gold nanoclusters (AuNCs) were synthesized as described previously with modifications (Luo *et al.,* 2012). Aqueous solutions of gold (III) chloride trihydrate ($HAuCl_4 . 3H_2O$) (20 mM, 0.5 ml) and L-glutathione (GSH) (100 mM, 0.15 ml) were mixed with 4.35 ml of 18 MΩ water in a 10 ml conical flask at 25 °C, and then gently stirred at 500 rpm. The reaction mixture was slightly submerged in anhydrous glycerol, which was then gently heated to 70 °C while the mixture was stirred gently for 24 hours (Wiggens, Wuppertal, Germany). The AuNC mixture was then purified through dialysis (14 000 Da MWCO) against 18 MΩ water for 24 hours at 25 °C. The final AuNC sample was stored at 4 °C.

3.2.2 Functionalization of gold nanoclusters with chitosan

A chitosan (CS) solution (0.25 mg/ml in 2% acetic acid) was freshly prepared at 25 °C, and the pH was adjusted to pH 4 (Maney and Singh, 2017). A 3:1 (v/v) ratio of CS to AuNCs was used for functionalization. Approximately 3 ml of the CS solution was pipetted into a conical flask with gentle stirring (500 rpm). To this was added 1 ml of the AuNCs solution dropwise at 3-minute intervals. The reaction mixture was stirred for 24 hours at 25 °C. The functionalized sample (CS-AuNCs) was dialyzed as in 3.2.1. and stored at 4 °C.

3.2.3 Drug (Doxorubicin) loading of CS functionalized AuNC

The protocol was adapted from that reported previously (Maney and Singh, 2017). Approximately, 1 ml of a 1 mM doxorubicin (DOX) solution was added to 1 ml of sodium tripolyphosphate (TPP, pH 2), and mixed gently for 30 minutes. The mixture

was allowed to settle for 10 minutes and then stirred gently, with 3 ml of CS (0.25 mg/ml, pH 4) added to the DOX-TPP solution in a dropwise manner every minute. Thereafter 1 ml of the AuNCs was added dropwise every 3 minutes to prevent aggregation. The solution was stirred for 2 hours for the reaction to reach completion. The final AuNCs-CS-TPP-DOX (AuCTD) nanocomposite with a ratio of 1:3:1:1 (v/v) was produced.

A further nanocomposite of CS-TPP-DOX (CTD), was synthesized as a control. Approximately, 1 ml of 1 mM DOX solution was added to 1 ml of 0.35 mg/ml of TPP solution (pH 2). The DOX-TPP solution was mixed for 30 minutes and allowed to settle for 10 minutes. Thereafter, 3 ml of CS (pH 4) was added dropwise to the DOX-TPP solution at 1-minute intervals with stirring. The CS-TPP-DOX (CTD) nanocomposite ratio was maintained at 3:1:1 (v/v/v). Both the nanocomposites were subjected to dialysis (2000 Da MWCO) for 24 hours against deionized water. The final nanocomposites were stored at 4 °C.

3.2.4 UV-visible (UV-vis) spectroscopy

Approximately 10 µl of each sample was analyzed in a UV-vis spectrophotometer (JASCO, Tokyo, Japan) at a wavelength range of 200 nm to 800 nm. This was done to confirm the CS binding to the AuNCs as well as DOX encapsulation by the AuNCs, with reference to the literature.

3.2.5 Transmission Electron Microscopy-Energy Dispersive X-ray (TEM-EDX)

About 100 µl of the respective sample was sonicated for 15 minutes before use. A Formvar-coated carbon grid was submerged in the solution and air-dried. Images were acquired using a JEOL 2100 High-Resolution Transmission Electron Microscope (HRTEM) (JOEL Ltd, Akishima, Tokyo, Japan). The EDX data was obtained using the X-Max EDX detector (Oxford Instruments, Abingdon, United Kingdom).

3.2.6 Nanoparticle Tracking Analysis (NTA)

Nanoparticle tracking analysis (NTA) (Nanosight NS500, Malvern, Worcestershire, UK) was used to assess the size, zeta potential, and particle distribution of the AuNCs, CS-AuNCs, the drug containing nanocomposites CTD and AuCTD. The instrument was primed and flushed, and the zero-position set. The samples were diluted 1:50 using 18 MΩ water before measurement at 25 ºC and 24 V. Videos captured the movement of the particles, which were analyzed using the NTA 3.2. software (Malvern Instruments, Worcestershire, UK). The hydrodynamic diameters were calculated using the Stokes-Einstein equation, and zeta potential using Smoluchowski approximation.

3.2.7 Fourier transform infra-red (FTIR) Spectroscopy

Fourier transform infrared (FTIR) spectroscopy was utilized to verify the existence of important functional groups and chemical bonds in the AuNCs by observing their specific peak characteristics. Approximately, 200 µl of each synthesized sample was analyzed using a Spectrum Perkin Elmer instrument (Waltham, MA, USA), from 4000–400 cm^{-1}. The IR spectra were generated using the associated Spectrum Analysis Software version 10.

3.2.8 Encapsulation efficiency (EE%)

The encapsulation efficiency (%) was calculated to determine the amount of drug bound to the nanocomplexes. This was done by the removal of unbound DOX through dialysis due to the nanocomplexes being in the colloidal state. The absorbance at 481 nm was used to analyze the samples. The samples were analyzed before and after dialysis to determine the encapsulation efficiency. The nanocomposite was placed into dialysis tubing (2000 Da MWCO) for 24 hours in a 1000 ml beaker containing deionized water. Thereafter, the samples were stored at 4°C. The theoretical drug content (TDC), encapsulation efficiency (EE) and actual drug content (ADC) of the drug-loaded nanocomposites were calculated using the following formulae (3.1-3.3) (Maney and Singh, 2017; Moodley and Singh, 2020). Due to the nanocomposites being in a collodial state, their expression was displayed in a volumetric ratio (Maney and Singh, 2017). This was also applied to drug release experimental analysis UV-vis spectrometer was calibrated for 30 minutes prior use and was blanked using deionised water prior to readings.

$$\text{TDC } (\mu g) = \frac{\text{Weight of DOX}}{\text{Weight of nanocomposite}} \quad (3.1)$$

$$\text{EE } (\%) = \frac{\text{Absorbance before dialysis} - \text{Absorbance after dialysis}}{\text{Absorbance before dialysis}} \times 100 \quad (3.2)$$

$$\text{ADC } (\mu g) = \text{TDC} \times \text{EE } (\%) \quad (3.3)$$

3.2.9 Drug Release

The drug release was conducted as reported previously (David *et al*., 2023). The prepared nanocomposite solutions, AuCTD and CTD solutions (400 µl) were dialyzed (2000 Da MWCO) separately against phosphate buffer saline (PBS, 5 ml) at different pH levels of 4.5, 5.5, 7.4. with gentle shaking (Infors HT Ecotron Shaking Incubator, Lasec, Cape Town, South Africa) at 80 rpm at 37°C. At 4-hour intervals, 20 µl of the dialysate was removed and replenished with PBS to maintain the sink volume, over 72 hours. Each dialysate aliquot was analyzed by UV-vis spectroscopy (JASCO, Tokyo, Japan) at a wavelength 481 nm. The readings were used to produce a drug release profile for each nanocomplex under the various pH conditions. Drug release was calculated using formula 3.4.

$$\text{Cumulative DOX-HCl release } (\%) = \frac{\text{Absorbance of free DOX}}{\text{Absorbance of total DOX}} \times 100\% \quad (3.4)$$

The models used to determine the pharmacokinetics studies R^2 values were the First-Order kinetics, Korsmeyer Peppas, Zero-order kinetics, and the Higuchi and Hixson Crowell models (Damodharan, 2020; Akinyelu *et al*., 2022; Akinyelu and Singh, 2019).

3.2.10 Cell culture

The human embryonic kidney (HEK293) (Figure 3.1A) and the breast adenocarcinoma cells (MCF-7) (Figure 3.1B) were propagated in 25 cm^2 tissue culture flasks containing 5 ml of MEM (supplemented with 10% FBS and 1% antibiotics), and incubated in a Hepa Class 100 Stericult incubator at 37°C and 5% CO_2 (Thermo-Electron Corporation, Waltham, Massachusetts, USA). The cells were routinely monitored using a Nikon TMS inverted microscope (Nikon, Tokyo,

Japan). Upon confluency, the cells were trypsinized and seeded into multiwell plates for assays, or cryopreserved. All cell culture protocols were conducted under aseptic conditions in a Class II biological safety laminar cabinet.

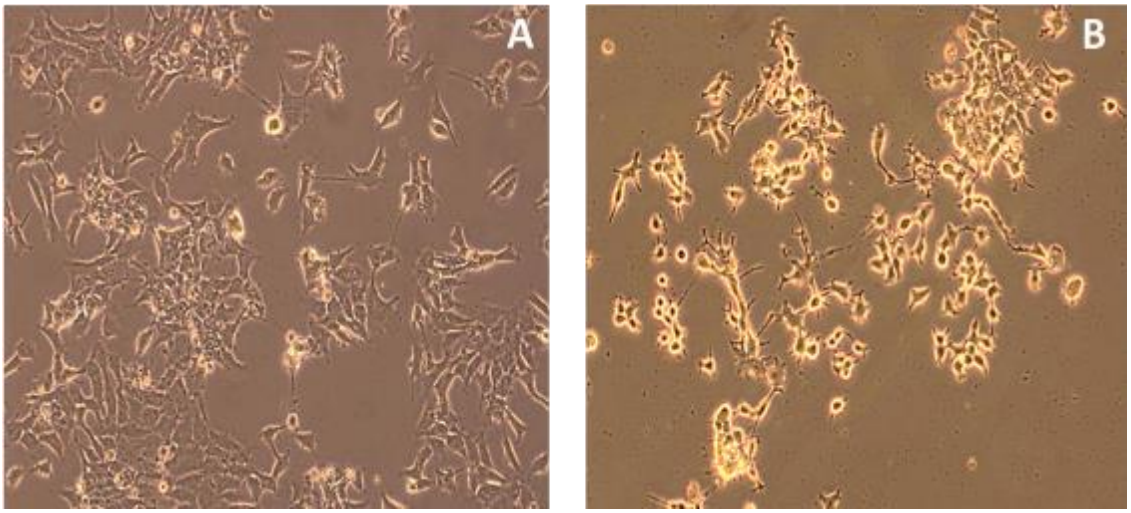

Figure 3.1: (A) HEK293 cells, and (B) MCF-7 cells at 20x magnification.

3.2.11 Cytotoxicity Assay

Cytotoxicity was determined using the standard (3-(4,5-dimethylthiazol-2-yl)- 2,5-diphenyltetrazolium bromide (MTT) assay (Mossman, 1983). HEK293 and MCF-7 cells near confluency were trypsinized and seeded at a density of 2.5 x 10^4 cells per well into 96-well plates containing 100 µl of complete MEM. Cells were incubated for 24 hours at 37 °C, to allow for the attachment of the cells. Following this, the spent medium was substituted with 100 µl of fresh medium followed by treatment with the AuNCs, nanocomplexes (CTD and AuCTD) and DOX at varying concentrations (10 µg/ml, 20 µg/ml, 30 µg/ml, 40 µg/ml). Positive controls consisting solely of cells wereincluded and documented as a survival rate of 100%. The assay was conducted in triplicate. Cells were incubated at 37 °C in 5% CO2 for 48 hours. Thereafter, the medium from each well was replaced with 100 µl fresh medium containing 10 µl MTT (5 mg/mL in PBS), and the cells were incubated at 37 °C for a further 4 hours. The MTT-media were then aspirated from each well, and 100 µl of DMSO was added to solub ilize the resulting formazan crystals. The cells were briefly shaken on a platform rocker (Stuart Scientific, Nottingham, UK), and absorbance readings at 570 nm were taken using a Mindray MR-96A microplate reader (Vacutec, Hamburg,

Germany). DMSO was used as the blank. Absorbance values were used to calculate the cell viability using formula 3.5.

$$\text{Cell Viability (\%)} = \frac{Absorbance\ of\ test}{Absorbance\ of\ control} \times 100 \qquad (3.5)$$

A linear regression curve was created of log transformation concentration values against cell viability, and the concentration at which 50% cell viability (IC50) was recorded, and was used for subsequent cell-based assays.

3.2.12 Fluorescent apoptosis assay

The dual dye fluorescent apoptosis assay was used to determine if apoptosis played a role in the cell death (Maiyo *et al*., 2016). The assay utilises a dual staining method of acridine orange (AO) and ethidium bromide (EB) in a 1:1 ratio. Each dye was prepared in PBS at a concentration of 100 µg/ml. The HEK293 and MCF-7 cells were seeded at a density of 5.0 x 10^4 cells per well in 48-well plates containing 250 µl growth medium, and incubated for 24 hours at 37 °C. After the 24-hour incubation, the spent media was removed and replaced with 250 µl of fresh media followed by the addition of the AuNC's, CS-AuNC's, CTD, AuCTD and DOX at their IC50 concentrations. Untreated cells were considered as positive controls. The assay was done in triplicate. After the 24-hour incubation the spent medium was removed and the cells were washed twice with 250 µl of PBS, followed by the addition of 10 µl of AO/EB (1:1 v/v) solution to each well. Cells were gently shaken for 5 minutes at 30 rpm in the dark. The excess dye was removed by rinsing with PBS (250 µl). The cells were then viewed and images captured using an Olympus inverted fluorescence microscope (Olympus Co., Tokyo, Japan), which was equipped with a CC12 fluorescence camera (Olympus Co., Tokyo, Japan). Formula 3.6 was used to calculate the apoptotic indices from the images.

$$\text{Apoptotic Index} = \frac{Number\ of\ Apoptotic\ cells}{Total\ number\ of\ cells\ counted} \qquad (3.6)$$

3.2.13 Cell cycle analysis

The Muse™ cell cycle kit allowed for a quantitative measurement of the percentage of cells within the different phases of the cell cycle. HEK293 and MCF-7 cells were seeded into 24-well plates containing 500 µl MEM, at a density of 1.0×10^5 cells per well, and incubated for 24 hours at 37 °C. Thereafter, the spent media was removed and replaced with 500 µl of fresh medium, followed by the addition of the AuNC's, CS-AuNC's, CTD, AuCTD and DOX at their IC50 concentrations. Untreated cells were used as controls. Cells were then incubated for 48-hours as previously. After the incubation period the assay was conducted as per manufacturer's instructions. Briefly, the cells were centrifuged for 5 minutes at 300 x g, washed with PBS, and finally resuspended in 200 µl of 70% (v/v) cold ethanol. The cells were then incubated overnight at -20°C. Thereafter, the cells were centrifuged and washed with PBS as previously. After the Muse® cell cycle reagent (200 µl; propidium iodide, RNase A), was added, the cells were incubated at room temperature for 30 minutes, and then analyzed in a Muse™ Cell Analyzer (Luminex, TX, USA).

3.2.14 Statistical analysis

All data were subjected to statistical analyses using ANOVA (one-way analysis of variance) (GraphPad Prism version 9, GraphPad Software Inc., CA, USA). All assays were done in triplicate and represented as mean ± SD (n= 3). The Tukeys multiple comparison test were done as post hoc tests. The *p* values that were less than 0.05 were considered to be significant. Microsoft Excel 2018™ was used to evaluate the dissolution parameters of drug release kinetic studies.

Chapter 4

Results and Discussion

CHAPTER FOUR

4. Results and Discussion

4.1 Ultraviolet-visible (UV-vis) spectroscopy

UV-vis spectroscopy is a popular and trusted method to analyze and characterize compounds within a UV range of 200 nm to 800 nm. It is based on the absorption of UV or visible light by specific compounds, producing a unique spectrum that confirms the composition of a sample (Mandru, 2023). Figure 4.1 displays the UV-vis spectra of the AuNCs, CS-AuNCs and the drug- encapsulated nanocomplex (AuCTD). At approximately 400 nm, there is a shoulder peak, and the onset occurs at approximately 500 nm. This confirmed the successful synthesis of the AuNCs and sizing through the aggregation-induced emission adopted in literature (Luo *et al*., 2012). A colour changed to orange upon the addition of GSH, before becoming colourless with further stirring, providing visual confirmation of synthesis.

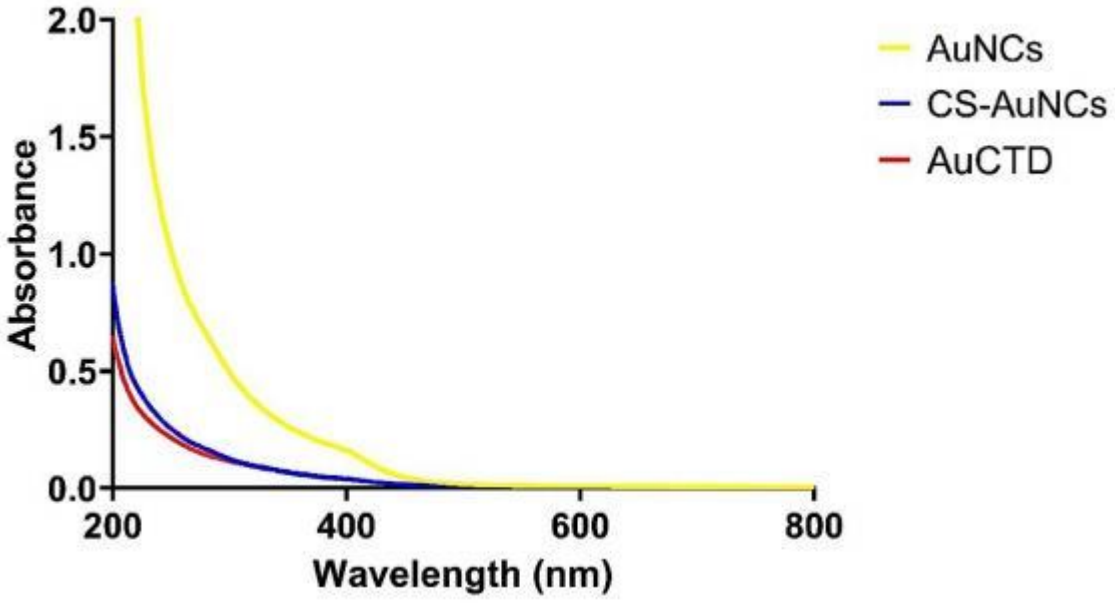

Figure 4.1: UV-visible spectroscopy of the gold nanoclusters (AuNCs), chitosan-functionalized gold nanoclusters (CS-AuNCs), and doxorubicin (DOX) loaded-chitosan-gold nanoclusters (AuCTD).

Conventional synthesis methods produce AuNCs with peaks greater than 500 nm, attributed to AuNCs comprising more than 15 atoms (Wu *et al*., 2020; Luo *et al*., 2012). No peaks were observed above 500 nm, which could indicate that the synthesized AuNCs were less than and/or equal to 15 atoms. The lack of peaks at 324 nm indicated the potential of a complete reduction of the Au (III) to Au (0) ions (Moreaud *et al*., 2022). This is in contrast to Au nanoparticles (AuNPs) that produce a peak in the range of 520 nm to 570 nm (Pal and Kryschi, 2015; David and Singh, 2025). The lack of a peak could indicate the successful synthesis of AuNCs smaller than 3 nm (Moreaud *et al*., 2022). The absence of this shoulder peak in the spectra of may be due to differences in charge transfer in the CS-coated AuNC.

Using chitosan (CS) to functionalise the AuNCs and encapsulate DOX resulted in a Stokes shift in the surface plasmon absorbance peak. This suggests the successful synthesis of CS-AuNCs with the onset at wavelengths greater than 400 nm, confirming their small size. It has been reported that DOX has absorptive peaks ranging from 480 nm to 490 nm, and at 232 nm in solution (Maney and Singh, 2017). The slight red shift of AuCTD in comparison to the CS-AuNCs can be indicative of the successful encapsulation of DOX, however, due to the small size of AuNCs, the onset of the AuCTD absorptive spectra rather than a peak at 232 nm could indicate the small size of the AuCTD complex. The anionic carboxylic group from GSH present in the AuNCs binds to the cationic amine group of the CS, resulting in the spectral shift (Goswami *et al*., 2016; Mao *et al*., 2021), and confirming the successful functionalization of the AuNCs.

4.2 Transmission Electron Microscopy (TEM) and Energy Dispersive X-ray (EDX)

The dry-weight size of the various AuNCs and their nanocomplexes from TEM is represented in Table 4.1.

Table 4.1: The TEM size of the AuNCs and their nanocomplexes.

Nanoparticle	TEM Size (nm)
AuNCs	2.51 ± 0.05
CS-AuNCs	2.38 ± 0.13
CTD	2.15 ± 0.10
AuCTD	2.45 ± 0.07

All AuNCs and their drug nanocomplexes were below 3 nm in size. The CS-AuNCs were approximately 2.38 nm and were marginally smaller than the AuNCs (2.51 nm), which can be attributed to the electrostatic forces between the CS and AuNCs due to ionic gelation. The stronger electrostatic forces generated can create compact NPs during synthesis and functionalization. The CS-drug nanocomplex (CTD) was the smallest (2.15 nm) due to the absence of the AuNC, while the CS-AuNC-drug nanocomplex (AuCTD) was slightly larger (2.45 nm) than the CS-AuNCs. This can be attributed to the successful encapsulation of the DOX. The AuCTD nanocomplex was slightly smaller than the AuNCs nanocomplex owing to the ionic interactions within the AuCTD nanocomplex, resulting in a tighter and more compact nanocomplex. The TEM size changes also served to confirm the synthesis of AuNCs. Furthermore, there was a correlation with the absorption spectra from UV-vis spectroscopy, alluding to smaller NPs being produced. The AuNCs and their nanocomplexes appeared as dark spots in the TEM images (Figure 4.2 A-D).

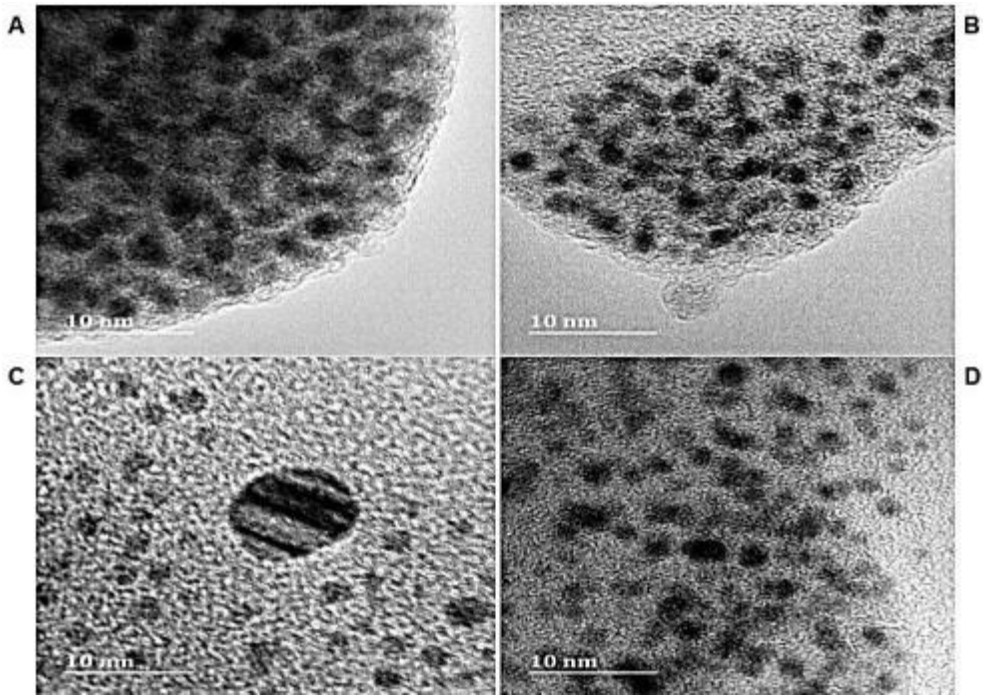

Figure 4.2: Selected TEM images of (A) AuNCs, (B) CS-AuNCs, (C) CTD and (D) AuCTD. Scale bar = 10 nm.

The AuNCs were spherical with little or no variation in size and shape being noted, similar to that reported in literature (Tian *et al*., 2012; Xie *et al*., 2020). TEM imaging is based on electron diffraction, which was able to provide information about a particle's morphology through its symmetry and nano-crystalline structure (Zhao *et al*., 2023). According to the literature, CS-DOX loaded nanocomplexes have a spherical and smooth morphology and sometimes resemble a core-shell structure (Yousefpour *et al*., 2022). A similar spherical and smooth morphology was observed for the AuNCs and the drug-nanocomplexes. The AuNCs and the nanocomplexes were mostly monodisperse, with minimal agglomeration. The morphology of CS often resembles a film but can take on the morphology of the NP during modification (Bugwandeen *et al*., 2023). A faint layer of CS can be seen surrounding the CS-AuNCs and the nanocomplexes. (Figure 4.2 B-D).

EDX is based on two physical foundational events, which are elastic and inelastic scattering. EDX can be used to assess the elemental composition of the constituents of a colloidal solution and to prompt the X-ray characteristic of atoms through the incident beam electrons (Scimeca *et al*., 2018). The results obtained from EDX (Table 4.2 - 4.5) correlated with those seen in the literature, with the element Au

present in the assessed samples (Kuo *et al*., 2021). The amount Au present varied per sample, with the AuNCs having the highest weight percentage (Table 4.2).

Table 4.2: TEM-EDX displaying elemental composition of AuNCs.

Element	Peak Area	Area Sigma	k Factor	Abs Corrn.	Weight %	Weight % Sigma	Atomic %
C K	37155	603	1.431	1.000	50.14	0.67	85.77
N K	2072	490	1.794	1.000	3.51	0.80	5.14
O K	3570	274	1.069	1.000	3.60	0.27	4.62
Au L	28891	399	1.569	1.000	42.76	0.61	4.46
Totals	100.00						

Table 4.3: TEM-EDX displaying elemental composition of CS-AuNCs.

Element	Peak Area	Area Sigma	k Factor	Abs Corrn.	Weight %	Weight % Sigma	Atomic %
C K	36008	674	1.431	1.000	65.49	1.10	81.21
N K	-44	597	1.794	1.000	-0.10	1.36	0.11
O K	6453	381	1.069	1.000	8.77	0.50	8.16
Na K	13541	314	0.681	1.000	11.72	0.33	7.59
S K	7647	277	0.548	1.000	5.33	0.21	2.47
Au L	4409	197	1.569	1.000	8.79	0.40	0.66
Totals	100.00						

Table 4.4: TEM-EDX displaying elemental composition of CTD.

Element	Peak Area	Area Sigma	k Factor	Abs Corrn.	Weight %	Weight % Sigma	Atomic %
C K	41108	778	1.431	1.000	33.64	0.45	49.16
O K	47598	509	1.069	1.000	29.10	0.30	31.93
Na K	18514	341	0.681	1.000	7.21	0.13	5.50
P K	47868	513	0.579	1.000	15.85	0.19	8.98
Cl K	9856	227	0.562	1.000	3.17	0.07	1.57
Fe K	21402	262	0.681	1.000	8.33	0.11	2.62
Au L	3024	202	1.569	1.000	2.72	0.18	0.24
Totals	100.00						

Table 4.5: TEM-EDX displaying elemental composition of AuCTD.

Element	Peak Area	Area Sigma	k Factor	Abs Corrn.	Weight %	Weight % Sigma	Atomic %
C K	76152	669	1.431	1.000	80.12	0.47	89.81
N K	7496	376	1.794	1.000	9.89	0.45	9.50
Au L	8665	236	1.569	1.000	10.00	0.26	0.68
Totals	100.00						

Other elements such as carbon, potassium, oxygen, nitrogen, sodium, iron, and chlorine were also seen and could be due to the chemicals used in the synthesis, CS, DOX, and the reagents and grids used in preparing the sample for analysis.

4.3 Nanoparticle Tracking Analysis (NTA)

Nanoparticle tracking analysis (NTA) is a popular method that is used to measure the size and stability of NPs in colloidal solutions using their Brownian motion (Fukuda *et al*., 2023). Zeta potential can be defined as the electrostatic potential of the shear plane of a colloidal NP suspension and provides an indication of the colloidal stability of a system (Carvalho *et al*., 2018). Zeta potential measurements that range between ± 20 mV and 30 mV are moderately stable, and measurements greater than +30 mV or less than -30 mV are regarded as being exceptionally stable (Bhattacharjee, 2016). The zeta potential and sizes from NTA are shown in Table 4.6 and Appendix A.

Table 4.6: Hydrodynamic sizes (nm) and zeta potentials (mV) obtained from NTA.

Sample	Hydrodynamic Size (nm)	Zeta Potential (mV)	Polydispersity Index (PDI)
AuNCs	93.3 ± 11.0	-41.3 ± 0.1	0.014
CS-AuNCs	141.6 ± 25.5	22.7 ± 1.4	0.032
CTD	134.3 ± 40.0	22.0 ± 2.9	0.089
AuCTD	144.9 ± 36.6	18.9 ± 3.6	0.064

The zeta potential of the AuNCs was -41.3 ± 0.1 mV, which is considered highly stable. The CS-AuNCs, CTD, and AuCTD nanocomplexes had zeta potentials of 22.7 ± 1.4 mV, 22.0 ± 2.9 mV, and 18.9 ± 3.6 mV, respectively, suggesting that these nanocomplexes are moderately stable. CS has also been reported to have a high positive zeta potential, making it a very stable polymer (Bugwandeen *et al*., 2023). The high overall negative charge of the AuNCs enables electrostatic bond formation between the negative charges of the carboxyl group (-COOH) of the AuNCs core and the positive charges of the amine ($-NH_3^+$) groups of CS during ionic gelation (Luo *et al*., 2012; Saeedi *et al*., 2022).

Nanocarriers smaller than 200 nm show better permeabilization of biological barriers (Finbloom *et al*., 2020). The hydrodynamic sizing of the AuNCs and the

nanocomplexes was less than 200 nm, indicating that they may be suitable therapeutic carriers *in vivo*. The size increase of the AuNCs from 93.3 nm to 141.6 nm for the CS-AuNCs indicated successful coating of CS onto the AuNCs. The further increase in the size of the CS-AuNCs from 141.6 nm to 144.9 nm for the AuCTD indicated the successful loading and encapsulation of DOX. CS is reported to display a swelling mechanism in solution, allowing for functionalization of the AuNCs (Akakuru and Isiuku, 2017), which also results in a size increase. Overall, the size of TEM and NTA differs, with that of NTA being much larger. This is due to the preparation of the samples with TEM using dry samples and NTA using samples in an aqueous medium. The latter provides and hydrodynamic size which is more in keeping with what one can expect in an *in vivo* system (David and Singh, 2025; Akinyelu and Singh, 2019).

In accordance with the literature, the dispersity of a nanocomplex solution is determined by PDI values; lower values display greater monodispersity, while higher values display polydispersity. Samples in a range of 0-0.05 are considered monodisperse, range of 0.05-0.08 are nearly monodisperse systems, and samples in the 0.08-0.7 range are regarded as mid-range polydisperse samples. Samples with PDI values greater than 0.7 are considered highly polydisperse (Muhesen and Rajab, 2023). From Table 4.6, the low PDIs for the AuNCs and CS-AuNCs suggest that they are monodisperse. Synthesised nanocomplexes, CTD and AuCTD, can be considered monodispersed systems, and they have low PDI values.

4.4 Fourier transform infrared (FTIR) Spectroscopy

FTIR spectroscopy is utilized to assess the chemical constituents through the recognition of the specific functional groups, based on their vibrational energy changes that coincide with the transitional energy (Mohamed *et al*., 2017). The FTIR spectra for the AuNCs are illustrated in Figure 4.3.

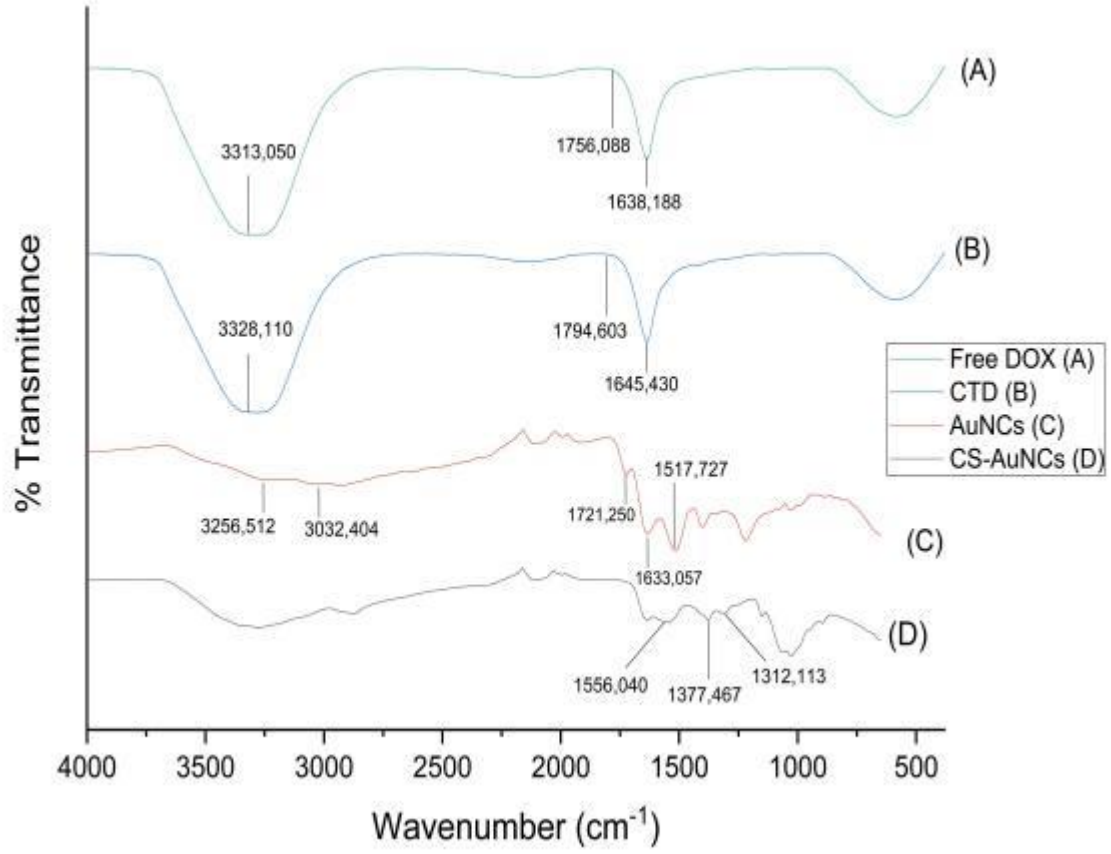

Figure 4.3: FTIR spectra of DOX, CTD, AuNCs and CS-AuNCs.

The absorptive spectra of DOX displayed peaks at 1756 cm^{-1}, which is the stretching band of the carbonyl group (C=O), as reported in the literature (Bansal *et al*., 2021). The peaks at 1638 cm^{-1} and 3313 cm^{-1} indicated the N-H stretching and the presence of -OH bands. Upon successful encapsulation of DOX into CS, there were slight chemical shifts of functional groups, as reported previously. Upon DOX encapsulation into CS, the carbonyl group shifted slightly from 1756 cm^{-1} to 1794 cm^{-1}, the peaks at 1645 cm^{-1} (from 1638 cm^{-1}) and 3328 cm^{-1} (from 3313 cm^{-1}) indicated the N-H stretching and the presence of OH bands, respectively (Abo Mansour *et al*., 2020).

The spectra of the AuNCs displayed peaks at 3256 cm^{-1} and 3032 cm^{-1}, confirming the presence of the N−H stretching bands. The peaks at 1633 cm^{-1} and 1721 cm^{-1} confirmed the C=O stretching bands, and the peak at 1517 cm^{-1} indicated that there was deformation of the amide bonds upon successful AuNC synthesis (Kuo *et al*.,

2021). Most of the differences for the CS-AuNCs occurred in the 1800–1300 cm^{-1} region of the spectra. The -NH vibrational bending at 1556 cm^{-1} was at a lower frequency shift reported in the literature, indicating the interaction of CS with the AuNCs. The vibration bending and the shift to 1377 cm^{-1} and 1312 cm^{-1} indicated the interaction between the -OH group of CS and the AuNCs (Murugadoss and Sakurai, 2011). All peaks were assigned according to that reported in the literature.

4.5 Encapsulation efficiency (EE%)

The UV-vis spectroscopy was used to determine the encapsulation efficiency (EE) of the CTD and AuCTD nanocomplexes at a fixed wavelength of 481 nm (Islam *et al*., 2017). Studies were also conducted where the AuNCs were used as detection vectors of DOX rather than nanocarriers of the drug (Meng *et al*., 2019). It was reported that high molecular weight CS with DOX-loaded AuNPs displayed an encapsulation efficiency of 20% (Fathy *et al*., 2018). In this study, the CS used was of a medium-molecular weight, which could be attributed to a less dense CS matrix, allowing for an increased drug-loading efficiency. The CTD displayed an EE of 68.64 %, while the AuCTD had a greater EE of 83.10 % (Table 4.7).

Table 4.7: Theoretical drug content, encapsulation efficiency, and actual drug content.

Nanocomplex	Theoretical Drug Content (µg)	Encapsulation Efficiency (%)	Actual Drug Content (µg)
CTD	600.00	68.64	411.84
AuCTD	600.00	83.10	498.60

Smaller AuNCs are reported to be better organised compared to the larger AuNPs (Yougbare *et al*., 2019), with a greater number of clusters per unit of surface area (Li and Jin, 2013). This can be attributed to the physical properties of the AuNCs with an increased surface area to volume ratio, resulting in a higher encapsulation efficiency. The use of CS and TPP in the process of ionic gelation was successful for the encapsulation of DOX. This was facilitated by the positively charged amine groups of CS and the polyanionic crosslinking properties of TPP. It was previously reported

that a 4:1(w/w) CS:TPP ratio created 200 nm particles (Pedroso-Santana and Fleitas-Salazar, 2020), which is in keeping with this study, although our nanocomplexes were smaller and between 130 and 145 nm with a 3:1 (v/v) CS:TPP ratio. DOX-loaded CS-TPP particles have been reported to usually range from 10 to 500 nm (Pedroso-Santana and Fleitas-Salazar, 2020).

4.6 Drug Release

The *in vitro* drug release studies were conducted at three pH levels, which were pH 4.5, 5.5 and 7.4. This was done to investigate the amount of doxorubicin (DOX) released from the CTD and AuCTD nanocomplexes under the simulated micro-environment of acidic tumours and physiological conditions *in vivo* (Akinyelu and Singh, 2019). The drug release was also conducted at 37 °C. Figure 4.4 displays the pH-dependent release of DOX from CTD. At pH 4.5, 5.5 and 7.4, approximately 79%, 80% and 58% of DOX was released, respectively. Figure 4.5 displays the pH-dependent release of DOX from AuCTD, with approximately 93%, 91% and 35% released at pH 4.5, 5.5 and 7.4, respectively, after 72 hours. Both the CTD and AuCTD nanocomplexes displayed increased drug release under acidic conditions compared to neutral/physiological conditions. This could be due to the potentially increased protonation of CS's amine groups. It was reported that a solidification process of CS at a physiological pH can lead to sustained drug release, while at acidic pH, CS can become more soluble, leading to a burst release of the drug (Kumar *et al*., 2015). The observations of DOX release correlate with previous studies, which also observed that polymer-coated DOX-loaded nanocomplexes display high levels of release under acidic conditions (Akinyelu *et al*., 2022). Overall, Figures 4.4 and 4.5 clearly display a sustained drug release over 72 hours with minor fluctuations after 44 hours.

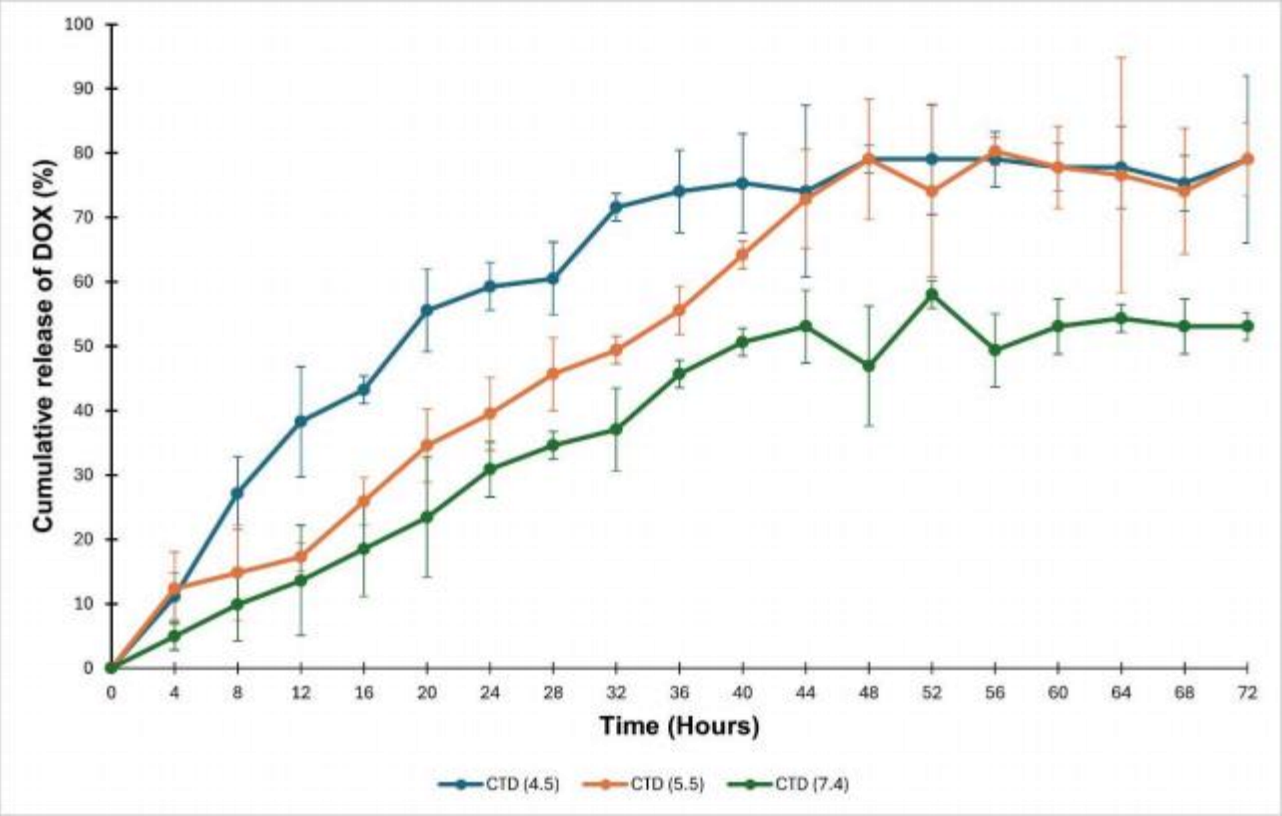

Figure 4.4: *In vitro* drug release profile of CTD nanocomplex at pH 4.5, 5.5 and 7.4. Data are represented as means ±SD (n=3).

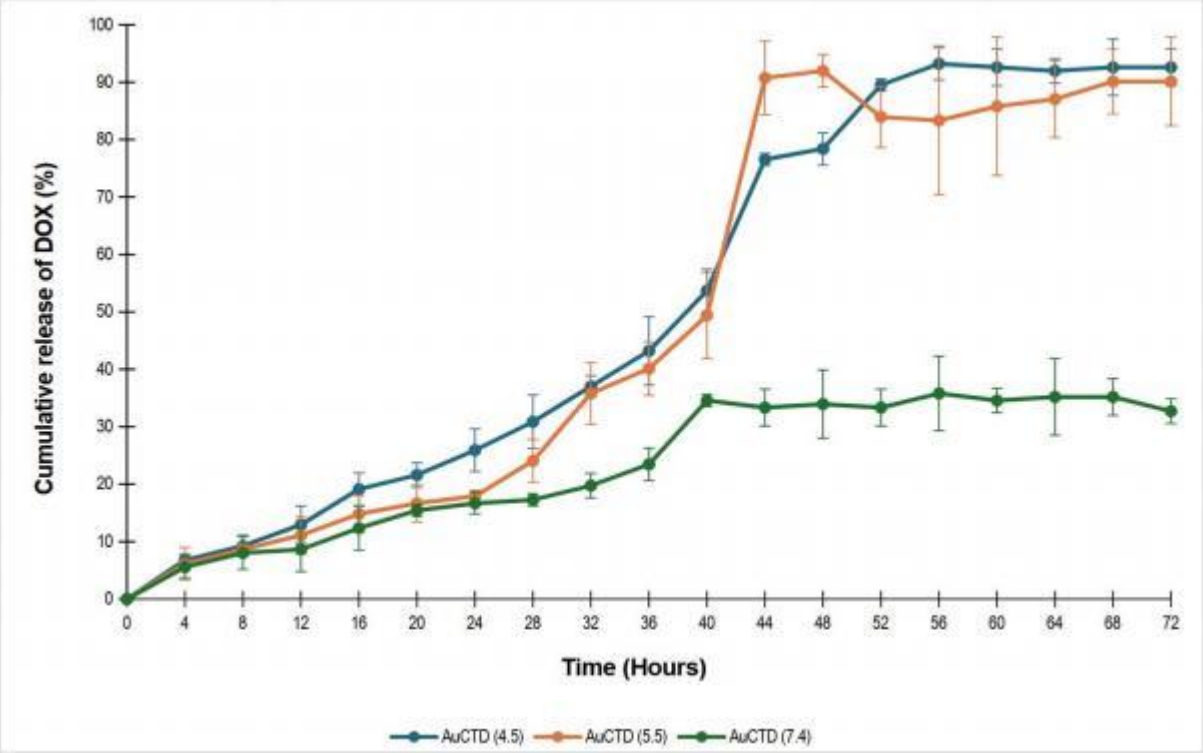

Figure 4.5: *In vitro* drug release profile of AuCTD nanocomplex at pH 4.5, 5.5 and 7.4. Data are represented as means ±SD (n=3).

The drug release pharmacokinetics were resolved by correlating and fitting the release data (Tables 4.8 and 4.9) into selected kinetic mathematical models (zero order, first order, Higuchi, Hixson-Crowell and Korsmeyer-Peppas). From Table 4.8 it can be seen that the CTD nanocomplex release kinetics model of pH 4.5, 5.5 and 7.4 fitted best into the Hixson-Crowell model. This occurs when there are changes to the diameter and surface area of the nanocomplex in the DDS. The model is based on drug-loaded NPs. The dissolution rate was taken as the rate of drug release is restricted and not through diffusion, which is very similar to the pharmaceutical dosing using tablets and capsules. (Damodharan, 2020).

From Table 4.9, it can be observed that the release kinetics for the AuCTD nanocomplex fitted into the Korsmeyer-Peppas model. The model is based on the Fickian release, which adheres to the Fickian laws that are based on polymeric swelling or non-swelling, due to the n-values ranging from 0.665 to 1.107. The Fickian diffusion law also complies with the Zero-order kinetics model, which is based on the dissolution of a drug at different dosages that does not segregate but displays a controlled manner of drug release (Damodharan, 2020; Akinyelu *et al*., 2022).

The n-values acquired through the Korsmeyer-Peppas model ranged from 0.710 to 1.003 for the CTD nanocomplexes and from 0.665 to 1.107 for the AuCTD nanocomplexes (Tables 4.8 and 4.9). The n-values display non-Fickian release and do not follow the Fickian laws but indicate zero-order kinetics and super case-II transport, suggesting that there could be more than one drug-release kinetic model involved (Akinyelu and Singh, 2019; Damodharan, 2020; Akinyelu *et al*., 2022). Zero–order release may assist in forecasting the bioavailability status of drugs, resulting in improved treatment cycles (Akinyelu and Singh, 2019).

Table 4.8: Correlation coefficients (R^2) obtained from CTD through release kinetic models at pH 4.5, 5.5 and 7.4.

	Zero-Order	First-order	Higuchi	Hixson-Crowell	Korsmeyer-Peppas	n-value
pH						
Correlation value (R^2) – CTD						
4.5	0.9567	0.9814	0.9632	0.9803	0.9525	0.710
5.5	0.9825	0.9817	0.9222	0.9838	0.943	0.877
7.4	0.9939	0.9897	0.908	0.9919	0.9976	1.003

*n: Korsmeyer-Peppas diffusion exponent.

Table 4.9: Correlation coefficients (R^2) obtained from AuCTD through release kinetic models at pH 4.5, 5.5 and 7.4.

	Zero-Order	First-order	Higuchi	Hixson-Crowell	Korsmeyer - Peppas	n-value
pH						
Correlation value (R^2) – AuCTD						
4.5	0.9922	0.9836	0.911	0.9876	0.9814	0,970
5.5	0.9199	0.8842	0.8194	0.8974	0.9671	1.107
7.4	0.959	0.9678	0.9695	0.9649	0.9664	0.665

*n: Korsmeyer-Peppas diffusion exponent.

4.7 Cytotoxicity Assay

The 3-[(4,5-dimethylthiazol-2-yl)-2,5-diphenyl tetrazolium bromide] (MTT) assay is a colorimetric assay that has become a standard for assessing the metabolic activity of living cells, and was used to assess the cytotoxic effect of nanoclusters and drugs on the mitochondrial activity *in vitro*. MTT is a positively charged salt, which upon incubation with cells in culture can lead to the formation of insoluble formazan crystals, which need to be solubilized by a reagent such as dimethyl sulfoxide (DMSO) (Ghasemi *et al*., 2021). Once dissolved, the optical density can be measured at a wavelength of 570 nm. The intracellular reduction of MTT occurs

through enzymes such as oxidoreductases and dehydrogenases, as well as the electron-donating effect of NAD(P)H (Ghazali *et al*., 2020).

The HEK293 cell line is a healthy non-cancer cell line that was used as a control in the investigation to assess the cytotoxicity profile of the various NPs and nanocomplexes (AuNCs, CS-AuNCs, CTD, AuCTD and DOX). In the HEK293 cells (Figure 4.6), it was observed that the free DOX displayed the highest level of cell death and cell survival ranged between 17.85 % and 31.44 % across the various (10 µg/ml to 40 µg/ml). This can be attributed to the induction of oxidative stress, destroying cellular DNA and organelles, the intercalation of genetic material affecting DNA and RNA synthesis, or the suppression of topoisomerase II (TOP2) activity (Norouzi *et al*., 2020). The AuNCs also displayed levels of cytotoxicity with cell viabilities of 37.02 %, 43.29 %, 32.39 % and 27.84 % at concentrations of 10 µg/ml, 20 µg/ml, 30 µg/ml and 40 µg/ml, respectively. AuNCs have been reported to show high cytotoxicity (Wang *et al*., 2011). The GSH-capped AuNCs have been shown to hinder the progress of healthy human cells due to the changes in epigenetic modifications (van de Looij *et al*., 2021). Once the AuNCs were functionalised with CS, their biocompatibility improved (Essawy and El-Nggar, 2019). The CS-AuNCs and the CTD complex displayed increased cell viabilities (over 100%), which can be attributed to the biocompatible properties of CS (Charoenwongpaiboon *et al*., 2019). However, at 40 µg/ml of CTD, cell viability was low (14.47 %). CS is a highly biodegradable polymeric material which is converted to aminos and sugars (Wrońska *et al*., 2023). Cells require additional aminos and sugars for mitosis, and upon degradation of CS, there is leaching of DOX. The AuCTD nanocomplex displayed a maximum cell viability of 114.44 % at 40 µg/ml and the lowest cell viability of 67 % at 30 µg/ml. This was much higher than the cell survival of the AuNCs and DOX treatments. This can be due to the increased biocompatibility of the nanocomplex through the electrostatic interactions with CS (Essawy and El-Nggar, 2019).

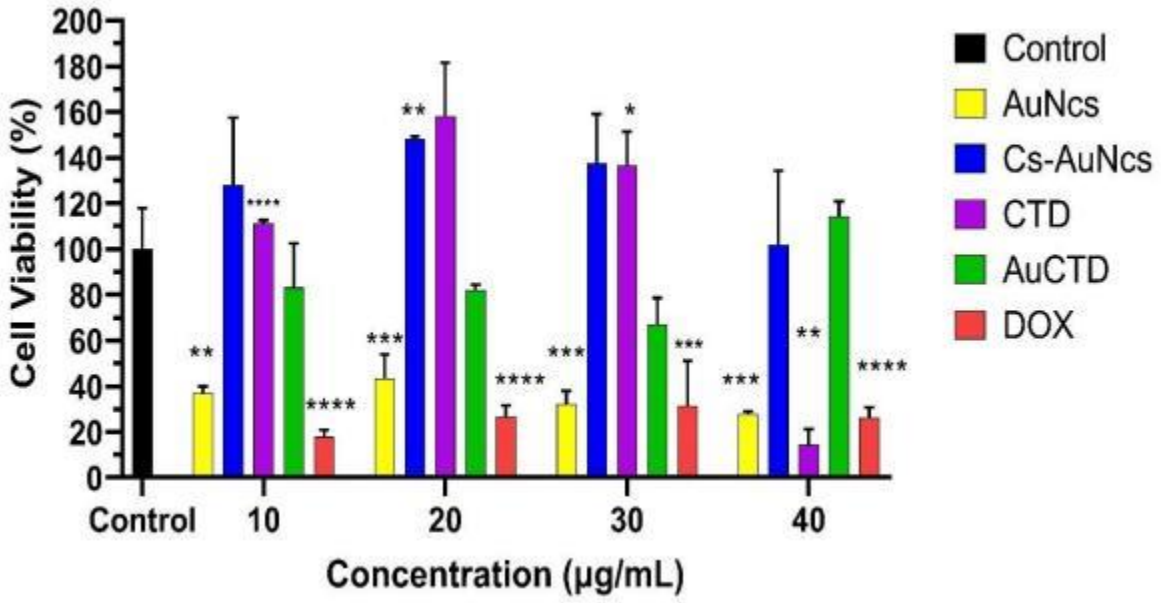

Figure 4.6: The effect of different treatments on the growth of HEK293 cells after 48-hour exposure. Data are represented as means ±SD (n=3). $^{*}p< 0.05$; $^{**}p< 0.01$; $^{***}p< 0.001$; $^{****}p< 0.0001$ vs. the control. *p<0.05 considered statistically significant.

In the MCF-7 cells (Figure 4.7), the AuNCs displayed a cell viability of 68.11 %. This can be due to oxidative stress induced by the charged AuNCs. It was reported that AUNPs can cause cytotoxicity in triple negative breast cancer cells through oxidative stress and disruption of signally pathways (Surapaneni *et al*., 2018). Furthermore, the zeta potential of the MCF-7 cells had been proposed to be around −20.32 mV and after incubation with the NPs, the cells' measurements tend to become more negative (Zhang *et al*., 2008). It was shown earlier (Table 4.6) that AuCTD was positive; this can increase the affinity of the nanocomplex to the surface of the negatively charged MCF-7 cells through electrostatic interactions. Cancer cells use greater amounts of glucose than healthy cells, which increases the acidic microenvironment of the tumours and cancer cells (Bogdanov *et al*., 2022). From Figure 4.7, it could be seen that the CTD displayed a declining or dose-dependent trend in the MCF-7 cells, with cell viabilities dropping from 76.51% to 54.63% as the concentrations of the nanocomplex increased from 10 µg/ml to 40 µg/ml. From Figure 4.7, it can be seen that the AuCTD displayed a decreasing or dose-dependent trend in the MCF-7 cells with cell viabilities of 61.19 %, 45.69 %, 23.33 % and 11.12 % at the respective concentrations of 10 µg/ml, 20 µg/ml, 30 µg/ml and 40

µg/ml. This anticancer activity was greater than that of DOX, which displayed cell viabilities of 64.78 %, 61.10 %, 46.58 % and 32.83 % in the MCF-7 cells at the same to concentrations. The AuCTD nanocomplex displayed more selective targeting than DOX with CS, causing the nanocomplex to have a greater affinity for cellular uptake (Mohammed *et al*, 2017).

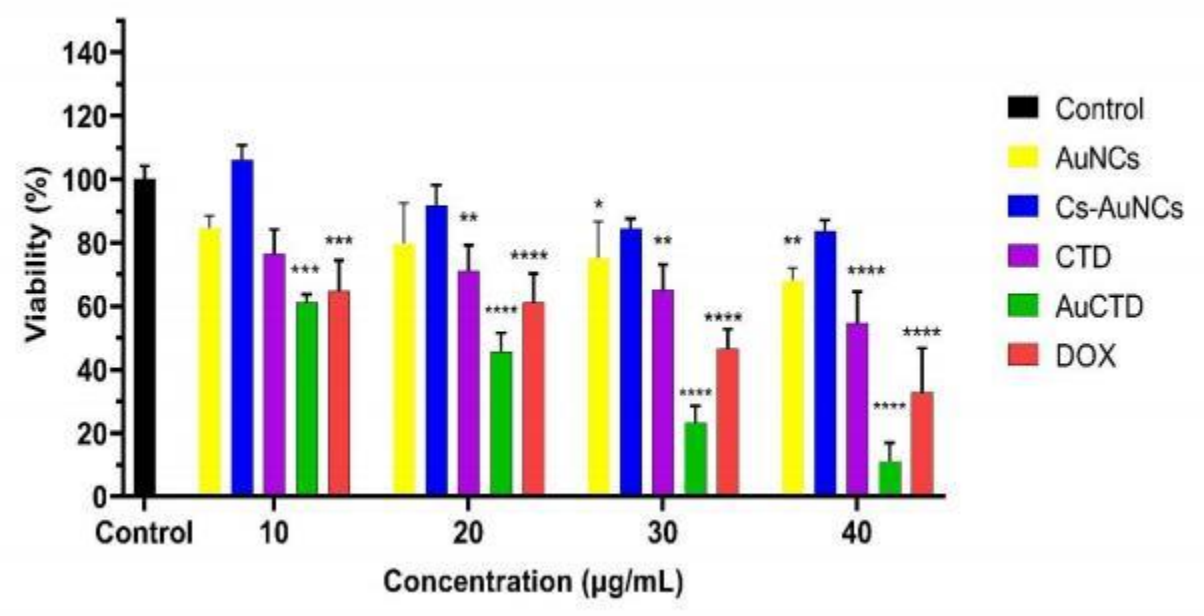

Figure 4.7: The effect of different treatments on the growth of MCF-7 cells after 48-hour exposure. Data are represented as means ±SD (n=3). $^{*}p< 0.05$; $^{**}p< 0.01$; $^{***}p< 0.001$; $^{****}p< 0.0001$ vs. the control. $*p<0.05$ considered statistically significant.

As seen earlier, the AuCTD displayed low drug release in the HEK293 cells, suggesting that the nanocomplex is pH-sensitive. This was further highlighted by the low levels of cytotoxicity in the HEK293 cells and higher levels of cytotoxicity in the MCF-7 cells. Furthermore, CS is less soluble at a physiological pH than at acidic pH, which confirms the sustained drug release and with increased solubility at lower pH, leading to an eventual burst release of the drug (Kumar *et al*., 2015). The CTD nanocomplex showed a dose-dependent profile in the MCF-7 cells (Figure 4.7). The AuCTD nanocomplex, however, was more effective than the CTD nanocomplex, possibly due to the presence of the AuNCs, which have been shown to increase the surface area to volume ratio (Yougbare *et al*., 2019), leading to the enhanced treatment of the MCF-7 cells.

Table 4.10 exhibits the IC50 values calculated from the MTT data for the MCF-7 cells. IC50 is commonly referred to as half-maximal inhibitory concentration, which is used to assess the effectiveness of pharmaceutical-based drugs (Aykul and Martinez-Hackert, 2016). The half-maximal inhibitory concentration stipulates the amount of drug that is required to impede a biological assay by half, this leads to producing a measurement of the strength of the drug needed for research (Aykul and Martinez-Hackert, 2016). The AuCTD with the lowest IC50 (14.8 µg/ml) confirmed that it was the most suitable and efficient of the carriers tested and was even better than the free drug, DOX, in the breast cancer cells. Hence this suggests that the these nanocomplexes have a a cell-specific dependency, in this case for breast cancer cells.

Table 4.10: The concentrations of 50 % cell survival of the different treatments in the MCF-7 cells.

NP/Nanocomplex	IC50 Values (µg/ml)
AuNCs	239.8
CS-AuNCs	249.4
CTD	69.9
AuCTD	14.8
DOX	23.5

4.8 Fluorescent apoptosis assay

Apoptosis is a physiological process that is commonly referred to as programmed cell death. Cell death can occur through various processes, either in response to external or internal stimuli. When treating cancer, it is essential to induce as much cancer cell death, without affecting the normal healthy cells, tissues or organs. This has led to the formulation of several anticancer treatments that take advantage of the natural cell death process, such as apoptosis, which removes damaged or harmful cells in a regulated manner (Baig *et al*., 2016). To analyse whether the synthesised nanocomplexes may or may not cause cell death via the process of programmed cell death or apoptosis, a dual staining using acridine orange/ethidium bromide (AO/EtBr) dye was conducted.

The use of the AO/EtBr dye methodology is based on foundational processes in which the AO dye enters into the cells that have intact plasma membranes to bind to DNA, producing a green fluorescence. On the other hand, the EtBr dye enters cells that have a compromised plasma membrane and, upon interacting with DNA, an orange-red fluorescence is produced (Singh *et al*., 2022). The observations made on the nuclear morphology enabled the differentiation between the late apoptotic and the early apoptotic cells (Figures 4.8 and 4.9).

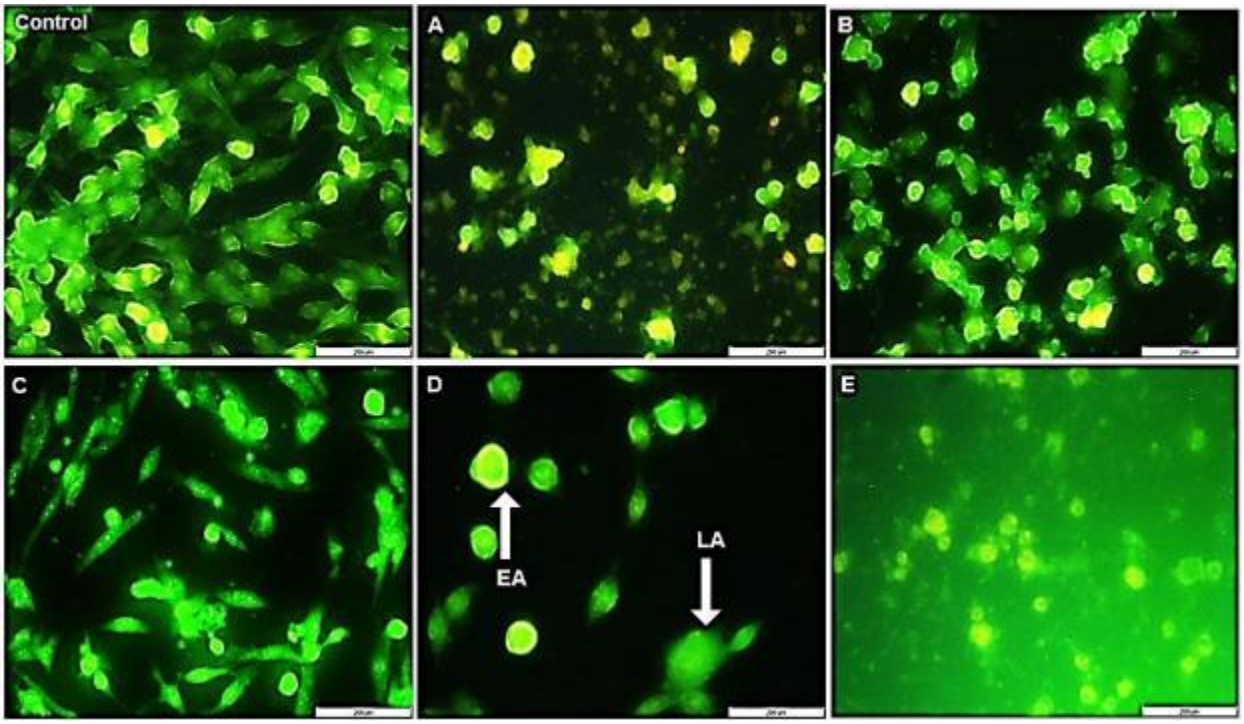

Figure 4.8: Acridine orange/ethidium bromide staining of the HEK293 cells (control) and HEK293 treated with AuNC's (A), CS-AuNC's (B), CTD (C), AuCTD (D) and DOX (E). **EA=** Early apoptosis, **LA=** Late apoptosis. (x 200).

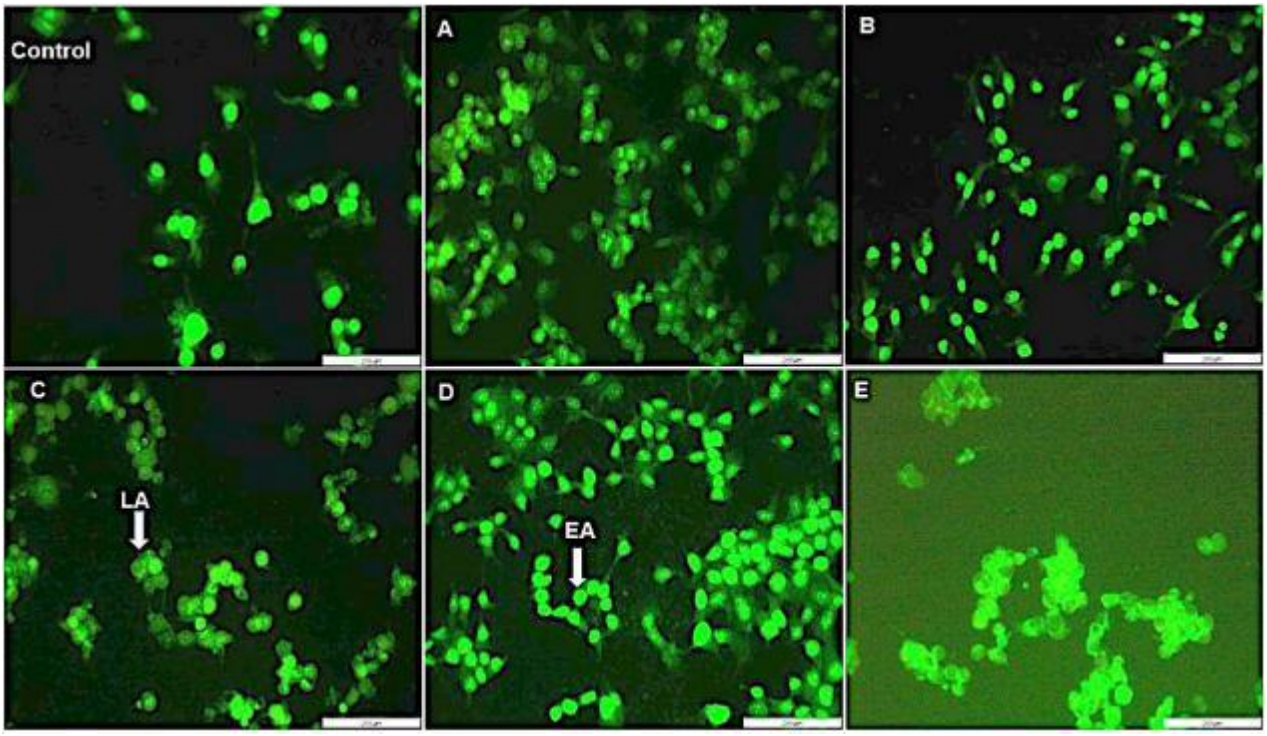

Figure 4.9: representing fluorescent apoptosis assay of the MCF-7 control cells and HEK293 treated with AuNC's (A), CS-AuNC's (B), CTD (C), AuCTD (D) and DOX (E). **EA=** Early apoptosis, **LA=** Late apoptosis. (x 200).

Early apoptotic cells with unaltered plasma membranes had shortened, condensed-like, or fragmented nuclei and emitted a green fluorescence. Late apoptotic cells displayed damaged plasma membranes with evidence of fragmentation and condensation and had a dull green-orange fluorescence. No necrotic cells were observed. Necrotic cells generally display a bright orange fluorescence with no alterations to the plasma membrane (Ribble *et al*., 2005).

From Figures 4.8 and 4.9, it was observed that the cells treated by DOX (E) were not as integral as those treated by the nanocomplexes. This could be attributed to the mode of action of DOX, which caused the establishment of free radicals, resulting in oxidative stress and the destruction of DNA, cellular membranes and proteins (Yang *et al*., 2014). This compromised the staining of the highly damaged cellular membranes. Similar studies have shown that functionalized DOX-loaded AuNPs with CS are highly effective at inducing apoptosis in breast cancer cells (Akinyelu *et al*., 2022; Manivasagan *et al*., 2016; Ignatova *et al*., 2011). This could be linked to mitochondrial membrane depolarisation and caspase activation (Akinyelu *et al*., 2022) due to DOX. Necrosis is a form of cell death that lacks specificity and is usually

triggered via an inflammatory reaction (Fulda, 2015). There were no necrotic cells observed, suggesting that the CS-Au-drug loaded nanocomplexes were highly effective against the MCF-7 cells. Tables 4.11 and 4.12 show the calculated apoptotic indices, which were all high, suggesting that apoptosis may have played a role in cell death.

Table 4.11: Apoptotic indices in HEK293 cells treated with various nanocomplexes and DOX.

Nanocomplex	Apoptotic Index ± SD (n=3)
AuNC's	0.60 ± 0.01
CS-AuNC's	0.55 ± 0.09
CTD	0.64 ± 0.04
AuCTD	0.59 ± 0.00
DOX	0.81 ± 0.04

Table 4.12: Apoptotic indices in MCF-7 cells treated with various nanocomplexes and DOX.

Nanocomplex	Apoptotic Index ± SD (n=3)
AuNC's	0.72 ± 0.06
CS-AuNC's	0.60 ± 0.04
CTD	0.73 ± 0.07
AuCTD	0.90 ± 0.03
DOX	0.92 ± 0.03

4.9 Cell Cycle Analysis

Flow cytometry allows for cellular analysis of morphological traits such as DNA/RNA content, cell counting, expression of molecular targeting, cellular sizing, granulation and many other features. The cytometer functions on the principle that cells flow through a capillary with a concentrated light source. Photodetectors are utilised to capture data to assess the cells' morphological characteristics. Cell cycle analysis is

commonly done using flow cytometry due to the ability to identify the different phases of the cell cycle, such as the G0/G1, S, and G2/M. It also enables the identification of apoptotic cells below the G0/G1 phase (Bajgelman, 2019).

Cell cycle control is primarily focused on two aspects, which are genomic DNA replication followed by the segregation of daughter cells. It has been commonly understood that cancer is the uncontrollable progression through the different cell cycle phases. However, the cell cycle checkpoints at various phases need to be defective to produce cancer cells (Matthews *et al*., 2022). A typical cell cycle is comprised of four stages, G0/G1, S and G2, considered as the interphase and M phase or mitosis phase. Cells in the G1 stage can either progress to the replication stages or exit the cell cycle and enter the G0 phase, also known as the quiescent state (Molina and Pituello, 2017). If the cell enters the progression of the cell cycle, it will enter the S phase, in which DNA replication occurs. Thereafter, the cell enters the G2 phase, in which the cell undergoes preparation for mitosis. The final M phase occurs when two daughter cells are produced (Cecchini *et al*., 2012). The cell cycle has highly intricate processes that oversee checkpoints and restrictions to maintain the integrity of DNA for the replication process (Molina and Pituello, 2017).

From Figures 4.10 and 4.11, the control HEK293 cells were mainly in the G0/G1 phase (99.6%), and 0.4 % were in the S phase. It was observed that the various nanocomplex treatments on the HEK293 cells displayed no major changes in the cell cycle G0/G1 phase with more that 81% of the cells in this phase [(AuNCs= 99% (G0/G1), 0.9% (S phase) and 0.1% (G2/M), CS-AuNCs= 81.1% (G0/G1), 15.6% (S phase) and 3.3% (G2/M), CTD= 87.9% (G0/G1), 9.4% (S phase) and 2.7% (G2/M), AuCTD= 99.2% (G0/G1), 0.7% (S phase) and 0.1 (G2/M)] compared to the controls (99.6%). For DOX-treated cells, 85.7% of the HEK293 cells were in the G0/G1 phase, with 11.9% progressing into the S phase. From Figures 4.12 and 4.13 the control MCF-7 cells were mainly in the G0/G1 phase (88.3%) and 7.9 % was in the S phase and 3.8% in the G2/M phase. The various nanocomplex treatments on the MCF-7 cells displayed no major significant changes in the cells' G0/G1 phase [(AuNCs = 87% (G0/G1), 10.1% (S phase), and 2.9% (G2/M), CS-AuNCs = 84.5% (G0/G1), 13.4% (S phase) and 2.1% (G2/M), CTD = 96.1% (G0/G1), 2.5% (S phase) and 1.3% (G2/M), AuCTD = 89.9% (G0/G1), 7.1% (S phase) and 3.0% (G2/M)], relevant

to the controls (88.3%). DOX treatment showed that 100% of cells stayed in the G0/G1 phase.

The progression of cell cycle phases occurs in a systematic manner and is controlled by serine/threonine kinases. Cyclin-dependent kinases attach to the subunit of cyclin, leading to activation through the phosphorylation of the threonine residues that activate cyclin-dependent kinases at the various phases of the cell cycle (Molina and Pituello, 2017). It had been observed from literature that the G0/G1 cell cycle arrest is initiated through p^{53}-dependent pathways, which then leads to effects in p21 and the inhibition of D and E cyclins (Matthews *et al*., 2022; Oladimeji *et al.,* 2021). G0/G1 cell cycle arrest was observed in both HEK293 and MCF-7 cells that were treated with the gold nanocomplexes. G0/G1 cell cycle arrest had been observed to cause high levels of DNA damage, replication stress, unattached kinetochores or partial to incomplete spindle formation, leading to induced apoptosis. Incomplete spindle formation can be due to the overexpression of MAD1 or MAD2, which weakens or causes hyperactivation of the spindle assembly checkpoint complex, respectively (Matthews *et al*., 2022).

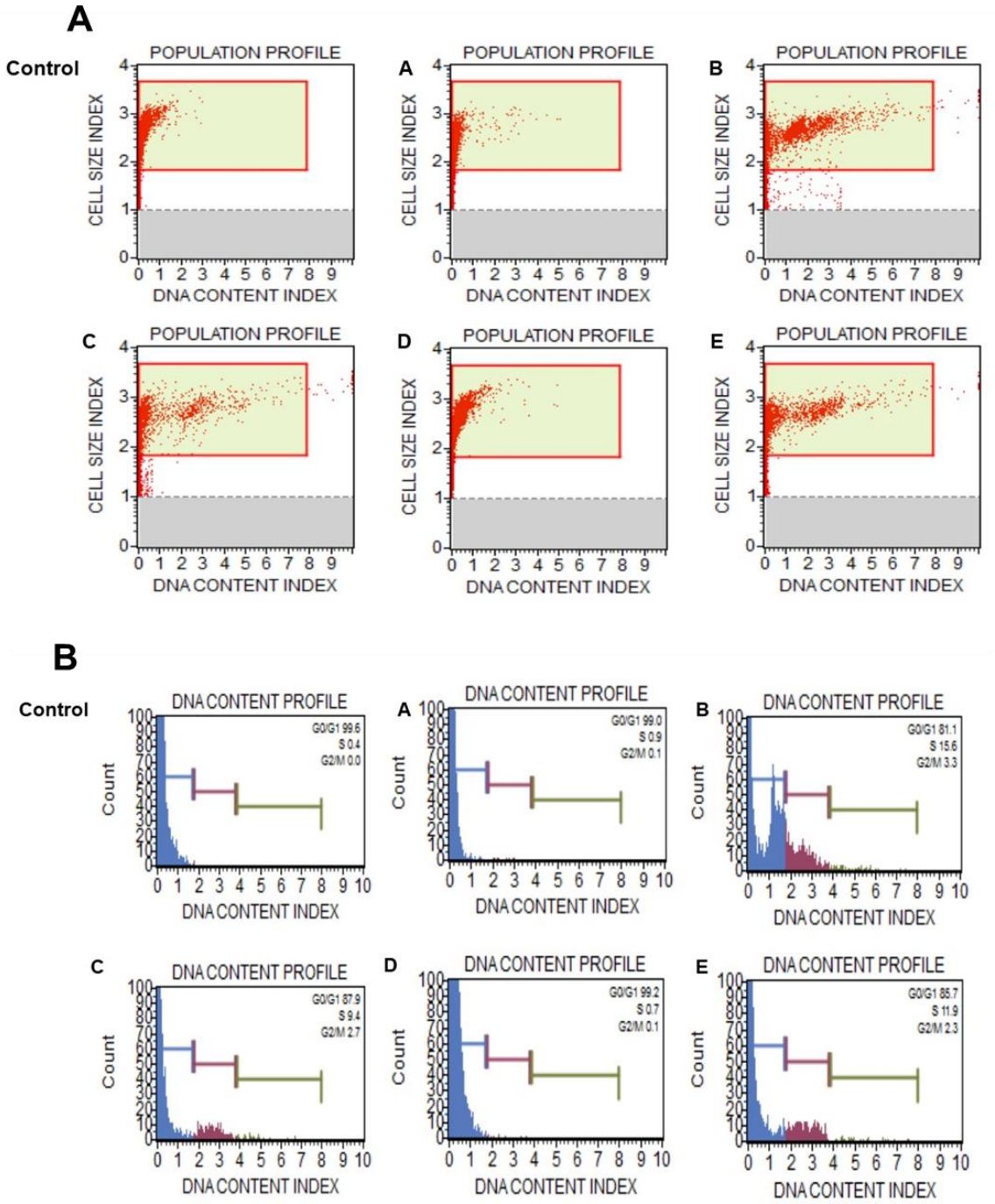

Figure 4.10: Cytographs of cell cycle analysis of HEK293 cells after treatment at the half-maximal inhibitory concentrations obtained from the cytotoxicity assay. (A) cell population profile. (B) DNA content profile. A= AuNCs, B= CS-AuNCs, C= CTD, D= AuCTD, E= DOX.

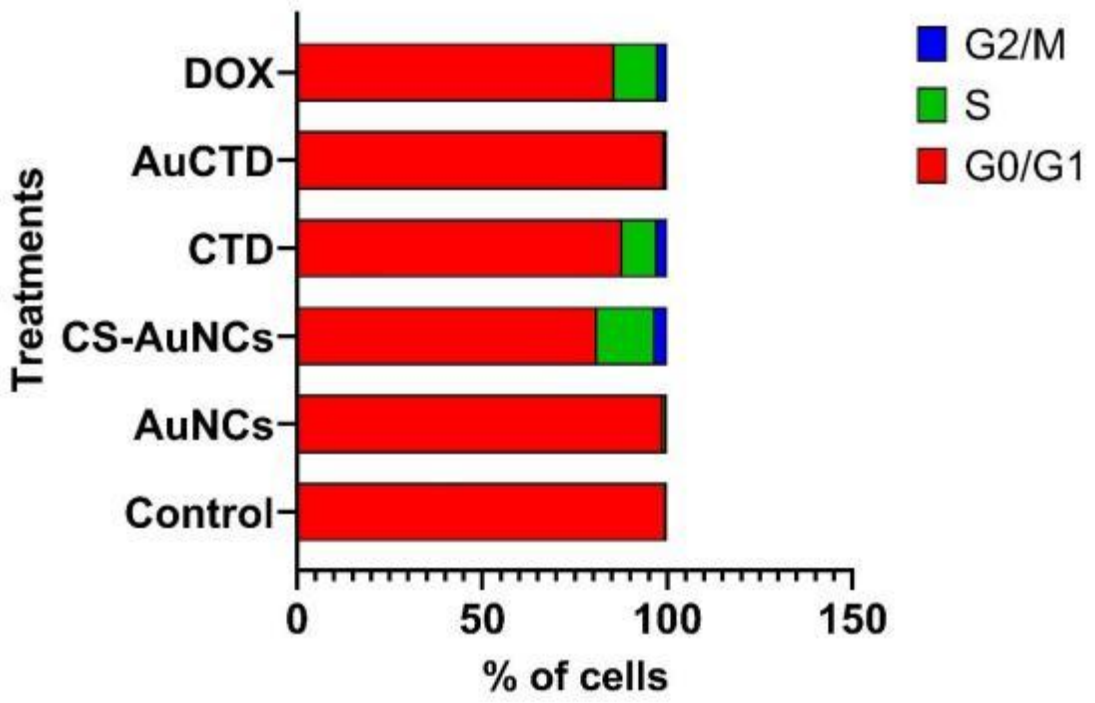

Figure 4.11: Graphical representation of the cell cycle analysis of HEK293 cells after treatment at the half-maximal inhibitory concentrations obtained from the cytotoxicity assay.

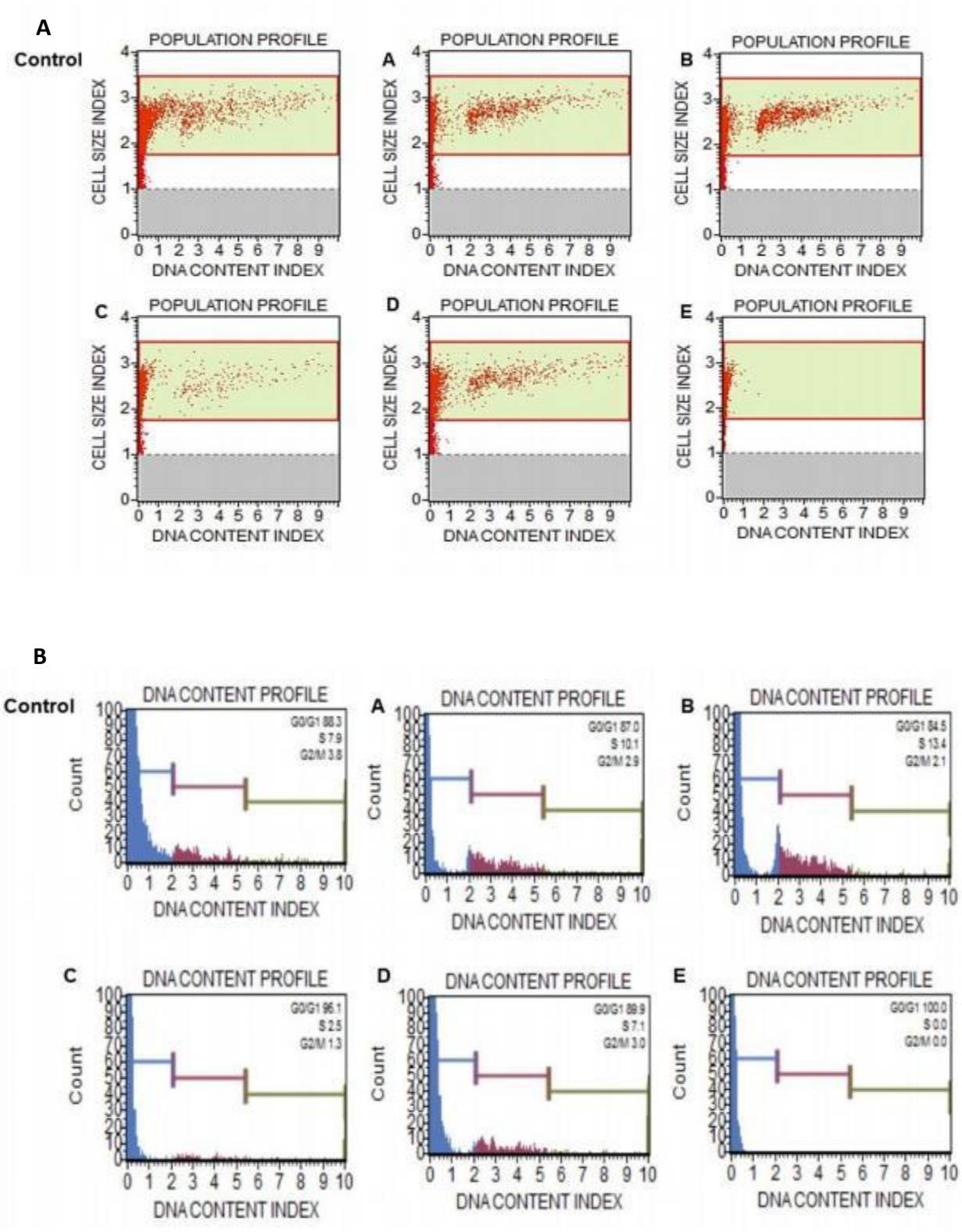

Figure 4.12: Cytographs of cell cycle analysis of the MCF-7 cells after treatment at the half-maximal inhibitory concentrations obtained from the cytotoxicity assay. (A) Cell population profile. (B) DNA content profile. A= AuNCs, B= CS-AuNCs, C= CTD, D= AuCTD, E= DOX.

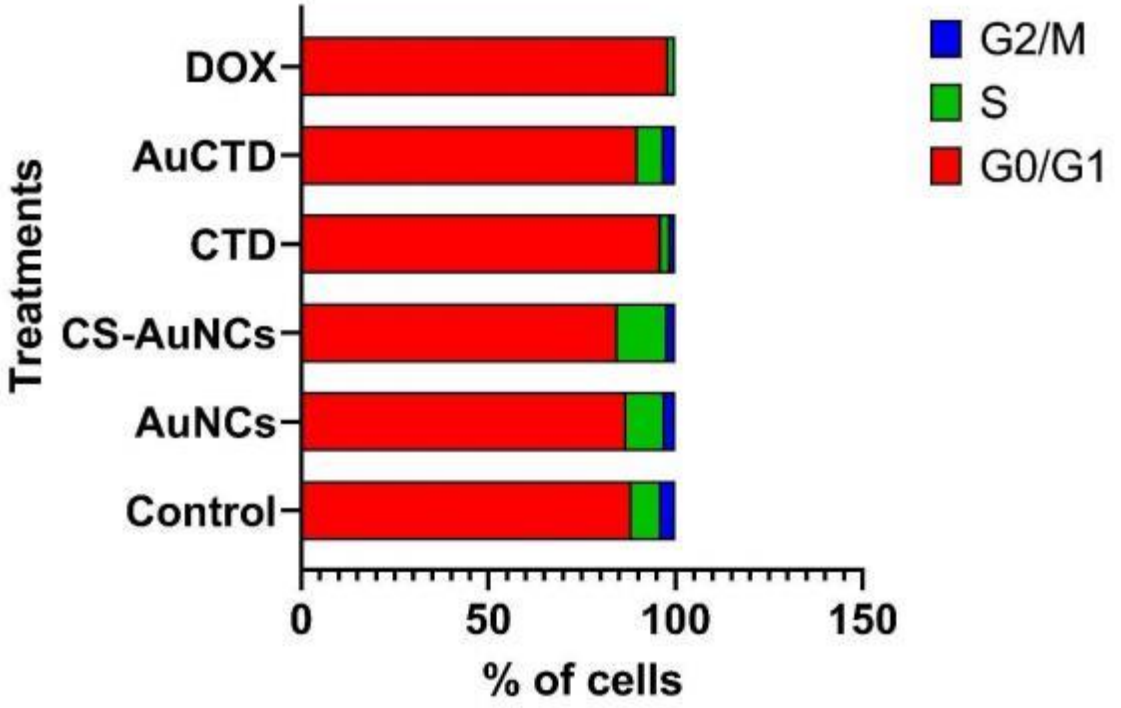

Figure 4.13: Graphical representation of the cell cycle analysis of the MCF-7 cells after treatment at the half-maximal inhibitory concentrations obtained from the cytotoxicity assay.

Chapter 5

Conclusion and Future Studies

CHAPTER FIVE

5. Conclusion and Future Studies

5.1 Conclusion

Over the years, researchers have formulated or refined methods to improve the conventional treatments of cytotoxic drugs using nanotechnology. Nanomedicine has opened up new avenues not only for the treatment of diseases, but also for the diagnosis and imaging of various diseases, including cancer. Gold nanoclusters (AuNCs) embody unique properties that have made them attractive for use in nanomedicine as drug delivery vehicles.

This investigation was focused on breast cancer and the delivery of the anticancer drug DOX to breast cancer cells *in vitro* using chitosan-functionalized gold nanoclusters (AuCTD). The characterisation confirmed the successful synthesis and formulation of all the nanoparticles and nanocomplexes, which possessed a small size and good dispersity. The inclusion of chitosan in the AuNCs served to enhance biocompatibility, stability, drug encapsulation and drug delivery *in vitro*.

The chitosan inclusion in the nanocomplexes increased the drug encapsulation and efficiency, and its cationic nature improved the cellular uptake, which led to increased anticancer activity in the breast cancer cells, while preserving the integrity of healthy cells. Pharmacokinetic studies suggested a sustained drug release over a period of time, which can improve treatment regimens. Cell-based assays displayed high levels of anticancer specificity for the breast cancer cells, with the mechanism of cell death most likely being that of apoptosis. The advantages of AuCTD as a nano-delivery system are due to its small size (won't be prematurely removed from the reticuloendothelial system, low toxcity to healthy cells, biocompatibility, increased drug therapeutic index, site specificity and high levels of stability pertinent to the experimental analysis. The disadvantages associated with AuCTD treatment due to chitosan could be below mechanical resistance, low physiological pH solubility, and difficulty controlling pore size at various pH levels.

The evidence obtained from this study showed that the formulated drug delivery system (AuCTD) can be used as an anticancer drug delivery system and hence requires further studies and optimisations, including *in vivo* studies.

5.2 Future Studies

The *in vitro* aspect of this study can be extended to include more cancer cell lines to identify specificity for a cancer cell type. Other breast cancer cell lines that represent different subtypes of breast cancer could be included to observe the effect on metastatic and hormone-responsive cancers. Future studies may also look at the addition of targeting moieties such as cell-specific ligands, antibodies or peptides. Since chitosan is rich in amino and hydroxyl groups, the addition of the targeting moieties using simple coupling reactions can be achieved. The folate ligand or the epidermal growth factor could be included in the delivery system to target specific breast cancer cells. This would ensure cancer cell specificity and targeted cellular uptake. The use of a co-polymer such as polyethylene glycol with chitosan can be included to improve stability and improve circulation time in an *in vivo* system. This delivery system can be further tested using a combination of anticancer drugs, which are commonly used in chemotherapy. This should be taken further by mechanistic studies that will investigate of the nanomaterial's mode of action and the pathways involved in cell death or apoptosis. Further optimizations with regard to concentrations used in the study during synthesis and for drug delivery can be undertaken before testing this system in an *in vivo* animal model, before pre-clinical trials. However, this preliminary study provides a stepping stone for further studies on these innovatiove systems.

References

References

Abo Mansour, H. E., El-Batsh, M. M., Badawy, N. S., Mehanna, E. T., Mesbah, N. M., and Abo-Elmatty, D. M. (2020). Effect of Co-treatment with Doxorubicin and Verapamil Loaded into Chitosan Nanoparticles on Diethylnitrosamine-induced Hepatocellular Carcinoma in mice. *Human & Experimental Toxicology*. 39 (11), 1528-1544. https://doi.org/10.1177/0960327120930266.

Adepu, S., and Ramakrishna, S. (2021). Controlled Drug Delivery Systems: Current Status and Future Directions. *Molecules*. 26 (19), 5905. https://doi.org/10.3390/molecules26195905.

Akakuru, O. U., and Isiuku, B. O. (2017). Chitosan Hydrogels and their Glutaraldehyde-Crosslinked Counterparts as Potential Drug Release and Tissue Engineering Systems-synthesis, Characterization, Swelling Kinetics and Mechanism. *J. Phys. Chem. Biophys*. 7 (3), 1-7. https://doi.org/10.4172/2161-0398.1000256.

Akinyelu, J., and Singh, M. (2019). Folate-tagged chitosan-functionalized gold nanoparticles for enhanced delivery of 5-fluorouracil to cancer cells. *Applied Nanoscience*. 9, 7-17. https://doi.org/10.1007/s13204-018-0896-4.

Akinyelu, J., Oladimeji, O., Daniels, A., and Singh, M. (2022). Folate-Targeted Doxorubicin Delivery to Breast and Cervical Cancer cells using a Chitosan-Gold Nano-delivery System. *Journal of Drug Delivery Science and Technology*. 67, 102978, https://doi.org/10.1016/j.jddst.2021.102978.

Alghorabi, A. A., Kabel, A. M., and Elmaaboud, M. (2019). Doxorubicin: Insights into Dynamics, Clinical Uses and Adverse Effects. *J. Cancer Res. Treat*. 7 (1), 17-20. https://doi.org/10.12691/jcrt-7-1-3.

Aloss, K., and Hamar, P. (2023). Recent preclinical and clinical progress in liposomal doxorubicin. *Pharmaceutics*. 15 (3), 893. https://doi.org/10.3390/pharmaceutics 15030893.

Augustine, R., Hasan, A., Primavera, R., Wilson, R. J., Thakor, A. S., and Kevadiya, B. D. (2020). Cellular Uptake and Retention of Nanoparticles: Insights on Particle

Properties and Interaction with Cellular Components. *Materials Today Communications*. 25, 101692. https://doi.org/10.1016/j.mtcomm.2020.101692.

Attia, M. F., Anton, N., Wallyn, J., Omran, Z., and Vandamme, T. F. (2019). An overview of active and passive targeting strategies to improve the nanocarriers efficiency to tumour sites. *Journal of Pharmacy and Pharmacology*. 71 (8), 1185-1198. https://doi.org/10.1111/jphp.13098.

Avramović, N., Mandić, B., Savić-Radojević, A., and Simić, T. (2020). Polymeric Nanocarriers of Drug Delivery Systems in Cancer Therapy. *Pharmaceutics*. 12 (4), 298. https://doi.org/10.3390/pharmaceutics12040298.

Aykul, S., and Martinez-Hackert, E. (2016). Determination of Half-maximal Inhibitory Concentration using Biosensor-based Protein Interaction Analysis. *Analytical biochemistry*. 508, 97-103. https://doi.org/10.1016/j.ab.2016.06.025.

Azamjah, N., Soltan-Zadeh, Y., and Zayeri, F. (2019). Global Trend of Breast Cancer Mortality Rate: a 25-year Study. *Asian Pacific journal of cancer prevention: APJCP*. 20 (7), 2015-2020. https://doi.org/10.31557/APJCP.2019.20.7.2015.

Babu, A., and Ramesh, R. (2017). Multifaceted Applications of Chitosan in Cancer Drug Delivery and Therapy. *Marine drugs*. 15 (4), 96. https://doi.org/10.3390/md15040096.

Bae, Y. H., and Park, K. (2011). Targeted Drug Delivery to Tumors: Myths, Reality and Possibility. *Journal of controlled release*. 153 (3), 198-205. https://doi.org/10.1016/j.jconrel.2011.06.001.

Baguley, B. C. (2010). Multiple Drug Resistance Mechanisms in Cancer. *Molecular biotechnology*. 46, 308-316. https://doi.org/10.1007/s12033-010-9321-2.

Bai, Y., Shu, T., Su, L., and Zhang, X. (2020). Fluorescent gold nanoclusters for biosensor and bioimaging application. *Crystals*. 10 (5), 357. https://doi.org/10.3390/cryst10050357.

Baig, S., Seevasant, I., Mohamad, J., Mukheem, A., Huri, H. Z., and Kamarul, T. (2016). Potential of apoptotic pathway-targeted cancer therapeutic research: Where

do we stand?. *Cell death & disease*. 7 (1), e2058. https://doi.org/10.1038/cddis.2015.275.

Bajgelman, M. C. (2019). In *Data processing handbook for complex biological data sources*. Academic Press. pp 119-124. https://doi.org/10.1016/B978-0-12-816548-5.00008-3.

Bansal, R., Singh, R., and Kaur, K. (2021). Quantitative Analysis of Doxorubicin hydrochloride and Arterolane Maleate by Mid IR Spectroscopy using Transmission and Reflectance Modes. *BMC chemistry*. 15 (1), 27. https://doi.org/10.1186/s13065-021-00752-3.

Barclay, T. G., Day, C. M., Petrovsky, N., and Garg, S. (2019). Review of Polysaccharide Particle-based Functional Drug Delivery. *Carbohydrate polymers*. 221, 94-112. https://doi.org/10.1016/j.carbpol.2019.05.067.

Bhattacharjee, S. (2016). DLS and Zeta Potential–What They Are and What They Are Not?. *Journal of controlled release*. 235, 337-351. https://doi.org/10.1016/j.jconrel.2016.06.017.

Behzadi, S., Serpooshan, V., Tao, W., Hamaly, M. A., Alkawareek, M. Y., Dreaden, E. C., Brown, D., Alkilany, M. A., Farokhzad, C. O., and Mahmoudi, M. (2017). Cellular Uptake of Nanoparticles: Journey Inside the Cell. *Chemical society reviews*. 46 (14), 4218-4244. https://doi.org/10.1039/C6CS00636A.

Bhushan, B. (2016). Introduction to nanotechnology: History, Status, and Importance of Nanoscience and Nanotechnology Education. *Global perspectives of nanoscience and engineering education*. 1-31. https://doi.org/10.1007/978-3-319-31833-2_1.

Blanco, E., Shen, H., and Ferrari, M. (2015). Principles of Nanoparticle Design for Overcoming Biological Barriers to Drug Delivery. *Nature biotechnology*. 33 (9), 941-951. https://doi.org/10.1038/nbt.3330.

Bogdanov, A., Bogdanov, A., Chubenko, V., Volkov, N., Moiseenko, F., and Moiseyenko, V. (2022). Tumor acidity: From Hallmark of Cancer to Target of Treatment. *Frontiers in Oncology*. 12, 979154. https://doi.org/10.3389/fonc.2022.979154.

Bugwandeen, A., Singh, K., Daniels, A., Singh, D., David, L. L., and Singh, M. (2023). In vitro Cytotoxicity Profiles of Some Polymers and Inorganic Nanoparticles commonly used in Nanomedicine. *Toxicology*. 19. 1-11.

Bukowski, K., Kciuk, M., and Kontek, R. (2020). Mechanisms of Multidrug Resistance in Cancer Chemotherapy. *International journal of molecular sciences*. 21 (9), 3233. https://doi.org/10.3390/ijms21093233.

Carvalho, C., Santos, R. X., Cardoso, S., Correia, S., Oliveira, P. J., Santos, M. S., and Moreira, P. I. (2009). Doxorubicin: the good, the bad and the ugly effect. *Current Medicinal Chemistry*. 16 (25), 3267-3285.

https://doi.org/10.2174/092986709788803312.

Carvalho, P. M., Felício, M. R., Santos, N. C., Gonçalves, S., and Domingues, M. M. (2018). Application of Light Scattering Techniques to Nanoparticle Characterization and Development. *Frontiers in chemistry*. 6, 237. https://doi.org/10.3389/fchem.2018.00237.

Cecchini, M. J., Amiri, M., and Dick, F. A. (2012). Analysis of cell cycle position in mammalian cells. *Journal of visualized experiments: JoVE*. 59, 3491.

https://doi.org/10.3791/3491.

Chakraborty, I., and Pradeep, T. (2017). Atomically Precise Clusters of Noble Metals: Emerging Link between Atoms and Nanoparticles. *Chemical reviews*. 117 (12), 8208-8271. https://doi.org/10.1021/acs.chemrev.6b00769.

Chakraborty, S., and Rahman, T. (2012). The Difficulties in Cancer Treatment. *Ecancermedicalscience*. 6. https://doi.org/10.3332/ecancer.2012.ed16.

Charoenwongpaiboon, T., Supraditaporn, K., Klaimon, P., Wangpaiboon, K., Pichyangkura, R., Issaragrisil, S., and Lorthongpanich, C. (2019). Effect of Alternan Versus Chitosan on the Biological Properties of Human Mesenchymal Stem Cells. *RSC advances*. 9 (8), 4370-4379. https://doi.org/10.1039/C8RA10263E.

Chatterjee, P., and Kumar, S. (2022). Current Developments in Nanotechnology for Cancer Treatment. *Materials Today: Proceedings*. 48, 1754-1758. https://doi.org/10.1016/j.matpr.2021.10.048.

Chen, T., Xu, S., Zhao, T., Zhu, L., Wei, D., Li, Y., Zhang, H., and Zhao, C. (2012). Gold Nanocluster-conjugated Amphiphilic Block Copolymer for Tumor-targeted Drug Delivery. *ACS applied materials & interfaces*. 4 (11), 5766-5774. https://doi.org/10.1021/am301223n.

Chidambaram, M., Manavalan, R., and Kathiresan, K. (2011). Nanotherapeutics to Overcome Conventional Cancer Chemotherapy Limitations. *Journal of Pharmacy & Pharmaceutical Sciences*. 14 (1), 67–77. https://doi.org/10.18433/J30C7D.

Chu, E., and Sartorelli, A. C. (2018). Cancer Chemotherapy. *Lange's Basic and Clinical Pharmacology.* 948-976. https://doi.org/10.1016/b978-072160558-6.50014-9.

Cong, Y., Wang, X., Zhu, S., Liu, L., and Li, L. (2021). Spiropyran-functionalized Gold Nanoclusters with Photochromic Ability for Light-controlled Fluorescence Bioimaging. *ACS Applied Bio Materials*. 4 (3), 2790-2797. https://doi.org/10.1021/acsabm.1c00011.

Cui, H., Shao, Z. S., Song, Z., Wang, Y. B., and Wang, H. S. (2020). Development of Gold Nanoclusters: From Preparation to Applications in the Field of Biomedicine. *Journal of Materials Chemistry C*. 8 (41), 14312-14333. https://doi.org/10.1039/D0TC03443F.

Damodharan, N. (2020). Mathematical modelling of dissolution kinetics in dosage forms. *Research Journal of Pharmacy and Technology*. 13 (3), 1339-1345. https://doi.org/10.5958/0974-360X.2020.00247.4.

Danhier, F., Feron, O., and Préat, V. (2010). To Exploit the Tumor Microenvironment: Passive and Active Tumor Targeting of Nanocarriers for Anti-cancer Drug

Delivery. *Journal of controlled release*. 148 (2), 135-146. https://doi.org/10.1016/j.jconrel.2010.08.027.

David, L.L., Daniels, A., Habib, S. and Singh, M. (2023) Gold Nanoparticles in Transferrin-targeted dual-drug delivery in vitro. *Journal of Drug Delivery Science and Technology.* 90, 105168. https://doi.org/10.1016/j.jddst.2023.105168.

David, L. L., and Singh, M. (2025). Palladium nanoparticles: Potential for receptor-mediated chemotherapeutic drug delivery to cervical cancer cells. *Nano-Structures & Nano-Objects*. 41, 101428. https://doi.org/10.1016/j.nanoso.2024.101428.

Debela, D. T., Muzazu, S. G., Heraro, K. D., Ndalama, M. T., Mesele, B. W., Haile, D. C., Sophia, K. K., and Manyazewal, T. (2021). New approaches and procedures for cancer treatment: Current perspectives. *SAGE Open Medicine*. 9, 20503121211034366. https: oi.org 1 .1177 2 121211 4//d0/050303366.

Dessale, M., Mengistu, G., and Mengist, H. M. (2022). Nanotechnology: a promising approach for cancer diagnosis, therapeutics and theragnosis. *International Journal of Nanomedicine*. 17, 3735. https://doi.org/10.2147/IJN.S378074.

Dlamini, Z., Molefi, T., Khanyile, R., Mkhabele, M., Damane, B., Kokoua, A., Bida, M., Saini, S. K., Chauke-Malinga, N., Luvengho, E. T., and Hull, R. (2024). From incidence to intervention: a comprehensive look at breast cancer in South Africa. *Oncology and Therapy*. 12 (1), 1-11. https://doi.org/10.1007/s40487-023-00248-1.

Emerich, D. F., and Thanos, C. G. (2003). Nanotechnology and medicine. *Expert Opinion on Biological Therapy*. 3 (4), 655-663. https://doi.org/10.1517/14712598.3.4.655.

Essawy, A. A., and El-Nggar, A. M. (2019). *Biocompatible chitosan in unique applications for tissue engineering*. Elsevier. pp 279-308. https://doi.org/10.1016/B978-0-12-818415-8.00010-3.

Faid, A. H., Shouman, S. A., Badr, Y. A., Sharaky, M., Mostafa, E. M., and Sliem, M. A. (2022). Gold nanoparticles loaded chitosan encapsulate 6-mercaptopurine as a novel nanocomposite for chemo-photothermal therapy on breast cancer. *BMC chemistry*. 16 (1), 94. https://doi.org/10.1186/s13065-022-00892-0.

Fathy, M. M., Mohamed, F. S., Elbialy, N., and Elshemey, W. M. (2018). Multifunctional Chitosan-Capped Gold Nanoparticles for Enhanced Cancer Chemo-radiotherapy: An Invitro Study. *Physica Medica*. 48, 76-83. https://doi.org/10.1016/j.ejmp.2018.04.002.

Finbloom, J. A., Sousa, F., Stevens, M. M., and Desai, T. A. (2020). Engineering the Drug Carrier Biointerface to Overcome Biological Barriers to Drug Delivery. *Advanced drug delivery reviews*. 167, 89-108. https://doi.org/10.1016/j.addr.2020.06.007.

Foroozandeh, P., and Aziz, A. A. (2018). Insight into Cellular Uptake and Intracellular Trafficking of Nanoparticles. *Nanoscale research letters*. 13 (1), 339. https://doi.org/10.1186/s11671-018-2728-6.

Forouhari, S., Beygi, Z., Mansoori, Z., Hajsharifi, S., Heshmatnia, F., and Gheibihayat, S. M. (2022). Liposomes: Ideal Drug Delivery Systems in Breast Cancer. *Biotechnology and Applied Biochemistry*. 69 (5), 1867-1884. https://doi.org/10.1002/bab.2253.

Fukuda, H., Kuramochi, H., Shibuta, Y., and Ichiki, T. (2023). Analysis of Brownian Motion Trajectories of Non-spherical Nanoparticles using Deep Learning. *APL Machine Learning*. 1 (4). https://doi.org/10.1063/5.0160979.

Fulda, S. (2015). *Targeting apoptosis for anticancer therapy*. In Seminars in cancer biology. Academic Press. Vol 31, pp 84-88. https://doi.org/10.1016/j.semcancer.2014.05.002.

Gao, J., Karp, J. M., Langer, R., and Joshi, N. (2023). The future of drug delivery. *Chemistry of Materials*. 35 (2), 359-363. https://doi.org/10.1021/acs.chemmater.2c03003.

Ghasemi, M., Turnbull, T., Sebastian, S., and Kempson, I. (2021). The MTT Assay: Utility, Limitations, Pitfalls, and Interpretation in Bulk and Single-cell Analysis. *International journal of molecular sciences*. 22 (23), 12827. https://doi.org/10.3390/ijms222312827.

Ghazali, R., Mehta, K. J., Bligh, S. A., Tewfik, I., Clemens, D., and Patel, V. B.

(2020). High Omega Arachidonic acid/Docosahexaenoic acid Ratio Induces Mitochondrial Dysfunction and Altered Lipid Metabolism in Human Hepatoma Cells. *World journal of hepatology*. 12 (3), 84. https://doi.org/10.4254/wjh.v12.i3.84.

Gholami, A., Abdouss, H., Pourmadadi, M., Abdouss, M., Rahdar, A., and Pandey, S. (2024). A Comprehensive Perspective of Trastuzumab-based Delivery systems for Breast Cancer Treatment. *Journal of Drug Delivery Science and* Technology. 105592. https://doi.org/10.1016/j.jddst.2024.105592.

Gmeiner, W. H., and Ghosh, S. (2014). Nanotechnology for Cancer Treatment. *Nanotechnology reviews*. 3 (2), 111-122. https://doi.org/10.1515/ntrev-2013-0013.

Goswami, N., Lin, F., Liu, Y., Leong, D. T., and Xie, J. (2016). Highly Luminescent Thiolated Gold Nanoclusters Impregnated in Nanogel. *Chemistry of Materials*. 28 (11), 4009-4016. https://doi.org/10.1021/acs.chemmater.6b01431.

Gounden, V., and Singh, M. (2024). Hydrogels and Wound Healing: Current and Future Prospects. *Gels*. 10 (1), 43. https://doi.org/10.3390/gels10010043.

Gounden, V., and Singh, M. (2025). Gold Nanoparticle-Based Hydrogel: Application in Anticancer Drug Delivery and Wound Healing In Vitro. *Pharmaceutics*. 17 (5), 633. https://doi.org/10.3390/pharmaceutics17050633.

Guo, X., Zhuang, Q., Ji, T., Zhang, Y., Li, C., Wang, Y., Hong, L., Jia, H., Yang, L., and Du, L. (2018). Multi-functionalized Chitosan Nanoparticles for Enhanced Chemotherapy in Lung Cancer. *Carbohydrate polymers*. 195, 311-320. https://doi.org/10.1016/j.carbpol.2018.04.087.

Habashi, F. (2016). Gold–An Historical Introduction. In *Gold Ore Processing*. 1-20. https://doi.org/10.1016/B978-0-444-63658-4.00001-3.

Haleem, A., Javaid, M., Singh, R. P., Rab, S., and Suman, R. (2023). Applications of Nanotechnology in Medical Field: A Brief Review. *Global Health Journal*. 7 (2), 70-77. https://doi.org/10.1016/j.glohj.2023.02.008.

Harrison, B. (2010). Gold science and Applications: Edited by Christopher Corti and Richard Holliday. *Gold Bull*. 43, 131. https://doi.org/10.1007/BF03214978.

He, B., Sui, X., Yu, B., Wang, S., Shen, Y., and Cong, H. (2020). Recent advances in drug delivery systems for enhancing drug penetration into tumors. *Drug delivery*, *27*(1), 1474-1490. https://doi.org/10.1080/10717544.2020.1831106.

Hornyak, G. L., Moore, J. J., Tibbals, H. F., and Dutta, J. (2018). *Fundamentals of nanotechnology*. CRC press. pp 786. https://doi.org/10.1201/9781315222561.

Hu, Q., Li, H., Wang, L., Gu, H., and Fan, C. (2018). DNA Nanotechnology-enabled Drug Delivery Systems. *Chemical reviews*. 119 (10), 6459-6506. https://doi.org/10.1021/acs.chemrev.7b00663.

Iacopetta, D., Ceramella, J., Baldino, N., Sinicropi, M. S., and Catalano, A. (2023). Targeting breast cancer: An overlook on current strategies. *International Journal* of Molecular Sciences. 24 (4), 3643 https://doi.org/10.3390/ijms24043643.

Ignatova, M., Yossifova, L., Gardeva, E., Manolova, N., Toshkova, R., Rashkov, I., and Alexandrov, M. (2011). Antiproliferative activity of nanofibers containing quaternized chitosan and/or doxorubicin against MCF-7 human breast carcinoma cell line by apoptosis. *Journal of bioactive and compatible polymers*. 26 (6), 539-551. https://doi.org/10.1177/0883911511424655.

Islam, M. S., Haque, P., Rashid, T. U., Khan, M. N., Mallik, A. K., Khan, M. N. I., Khan, M., and Rahman, M. M. (2017). Core–shell Drug Carrier from Folate Conjugated Chitosan obtained from Prawn Shell for Targeted Doxorubicin Delivery. *Journal of Materials Science: Materials in Medicine*. 28, 1-10. https://doi.org/10.1007/s10856-017-5859-x.

Jain, K. K. (2008). Drug Delivery Systems: An Overview. Methods Molecular Biology. 4371-4350. doi: 10.1007/978-1-59745-210-6_1.

Jassim, A., Rahrmann, E. P., Simons, B. D., and Gilbertson, R. J. (2023). Cancers make their own luck: theories of cancer origins. *Nature Reviews Cancer*. 23 (10), 710- 724. https://doi.org/10.1038/s41568-023-00602.

Jin, R., Zeng, C., Zhou, M., and Chen, Y. (2016). Atomically Precise Colloidal Metal Nanoclusters and Nanoparticles: Fundamentals and Opportunities. *Chemical Reviews*. 116 (18), 10346-10413. https://doi.org/10.1021/ acs.chemrev.5b00703.

Johnson-Arbor, K., and Dubey, R. (2017). Doxorubicin. In *StatPearls*. StatPearls Publishing. PMID: 29083582.

Jones, I. C., and Dass, C. R. (2022). Doxorubicin-induced cardiotoxicity: causative factors and possible interventions. *Journal of Pharmacy and Pharmacology*. 74 (12), 1677-1688. https://doi.org/10.1093/jpp/rgac063.

Kachalaki, S., Ebrahimi, M., Khosroshahi, L. M., Mohammadinejad, S., and Baradaran, B. (2016). Cancer Chemoresistance; Biochemical and Molecular Aspects: A Brief Overview. *European journal of pharmaceutical sciences*. 89, 20-30. https://doi.org/10.1016/j.ejps.2016.03.025.

Kalaydina, R. V., Bajwa, K., Qorri, B., Decarlo, A., and Szewczuk, M. R. (2018). Recent Advances in "smart" Delivery Systems for Extended Drug Release in Cancer Therapy. *International Journal of Nanomedicine*. 13, 4727-4745. https://doi.org/10.2147/IJN.S168053.

Kaur, N., Aditya, R. N., Singh, A., and Kuo, T. R. (2018). Biomedical Applications for Gold Nanoclusters: Recent Developments and Future Perspectives. *Nanoscale Research Letters. 13 (1), 302. https://doi.org/10.1186/s11671-018-2725-9.*

Kim, S. M., Faix, P. H., and Schnitzer, J. E. (2017). Overcoming Key Biological Barriers to Cancer Drug Delivery and Efficacy. *Journal of Controlled Release*. 267, 15-30. https://doi.org/10.1016/j.jconrel.2017.09.016.

Kong, Y., Santos-Carballal, D., Martin, D., Sergeeva, N. N., Wang, W., Liu, G., Johnson, B., Bhayana, B., Lin, Z., Wang, Y., Le Guével, X., de Leeuw, H. N., Zhou, D., and Wu, M. X. (2021). A NIR-II-emitting Gold Nanocluster-based Drug Delivery System for Smartphone-triggered Photodynamic Theranostics with Rapid Body Clearance. *Materials Today*. *51*, 96-107. https://doi.org/10.1016/ j.mattod.2021.09.022.

Kripke, M., Brody, J. G., Hawk, E., Hernandez, A. B., Hoppin, P. J., Jacobs, M. M., Ruthann, R A., and Rebbeck, T. R. (2020). Rethinking environmental carcinogenesis. *Cancer Epidemiology, Biomarkers & Prevention*. 29 (10), 1870-1875. https://doi.org/10.1158/1055-9965.EPI-20-0541

Kulkarni, S. A., and Feng, S. S. (2013). Effects of Particle Size and Surface Modification on Cellular Uptake and Biodistribution of Polymeric Nanoparticles for Drug Delivery. *Pharmaceutical Research*. 30, 2512-2522. https://doi.org/10.1007/s11095-012-0958-3.

Kumar, G. P., Sanganal, J. S., Phani, A. R., Manohara, C., Tripathi, S. M., Raghavendra, H. L., Janardhana, B. P., Amaresha, S., Swamy, K. B., and Prasad, R. G. S. V. (2015). Anti-cancerous efficacy and pharmacokinetics of 6-mercapto purine loaded chitosan nanoparticles. *Pharmacological Research*. *100*, 47-57. https://doi.org/10.1016/j.phrs.2015.07.025.

Kuo, J. C., Tan, S. H., Hsiao, Y. C., Mutalik, C., Chen, H. M., Yougbaré, S., and Kuo, T. R. (2021). Unveiling the Antibacterial Mechanism of Gold Nanoclusters Via in situ Transmission Electron Microscopy. *ACS Sustainable Chemistry & Engineering*. 10 (1), 464-471. https://doi.org/10.1021/acssuschemeng.1c06714.

Li, G., and Jin, R. (2013). Atomically Precise Gold Nanoclusters as New Model Catalysts. *Accounts of Chemical Research*. 46 (8), 1749-1758. https://doi.org/10.1021/ar300213z.

Li, Q., Pan, Y., Chen, T., Du, Y., Ge, H., Zhang, B., Xie, J., Yu, H., and Zhu, M. (2018). Design and Mechanistic Study of a Novel Gold Nanocluster-based Drug Delivery System. *Nanoscale*. 10 (21), 10166-10172. https://doi.org/10.1039/C8NR02189A.

Li, Z., de Barros, A. L. B., Soares, D. C. F., Moss, S. N., and Alisaraie, L. (2017). Functionalized Single-walled Carbon Nanotubes: Cellular Uptake, Biodistribution and Applications in Drug Delivery. *International journal of pharmaceutics*. 524 (1-2), 41-54. https://doi.org/10.1016/j.ijpharm.2017.03.017.

Liu, D., Yang, F., Xiong, F., and Gu, N. (2016). The Smart Drug Delivery System and its Clinical Potential. *Theranostics*. 6 (9), 1306. https://doi.org/10.7150/thno. 14858.

Liu, J., Cabral, H., and Mi, P. (2024). Nanocarriers address intracellular barriers for efficient drug delivery, overcoming drug resistance, subcellular targeting and controlled release. *Advanced Drug Delivery Reviews*. 115239. https://doi.org/10.1016/j.addr.2024.115239.

Liu, P., Yang, W., Shi, L., Zhang, H., Xu, Y., Wang, P., Zhang, G., Chen, R. W., Zhang, B., and Wang, X. (2019). Concurrent Photothermal Therapy and Photodynamic Therapy for Cutaneous Squamous Cell Carcinoma by Gold Nanoclusters Under a Single NIR Laser Irradiation. *Journal of materials chemistry. B. 7 (44), 6924-6933. https://doi.org/10.1039/C9TB01573F.*

Liu, S., Yang, S., and Ho, P. C. (2018). Intranasal Administration of Carbamazepine-loaded Carboxymethyl Chitosan Nanoparticles for Drug Delivery to the Brain. *Asian Journal of Pharmaceutical Sciences*. 13 (1), 72-81. https://doi.org/10.1016/j.ajps.2017.09.001.

Liu, Z., Jiao, Y., Wang, Y., Zhou, C., and Zhang, Z. (2008). Polysaccharides-based Nanoparticles as Drug Delivery Systems. *Advanced drug delivery reviews*. 60 (15), 1650-1662. https://doi.org/10.1016/j.addr.2008.09.001.

Lohse, S. E., and Murphy, C. J. (2013). The Quest for Shape Control: A History of Gold Nanorod Synthesis. *Chemistry of Materials*. 25 (8), 1250-1261. https://doi.org/10.1021/cm303708p.

Lowry, G. V., Hill, R. J., Harper, S., Rawle, A. F., Hendren, C. O., Klaessig, F., Nobbmann, U., Sayre, P., and Rumble, J. (2016). Guidance to Improve the Scientific Value of Zeta-potential Measurements in NanoEHS. *Environmental Science: Nano*. 3 (5), 953-965. https://doi.org/10.1039/C6EN00136J.

Lu, Z. R., and Qiao, P. (2018). Drug Delivery in Cancer Therapy, Quo Vadis?. *Molecular Pharmaceutics*. 15 (9), 3603-3616. https://doi.org/10.1021/acs.molpharmaceut.8b00037.

Lunardi, C. N., Gomes, A. J., Rocha, F. S., De Tommaso, J., and Patience, G. S. (2021). Experimental Methods in Chemical Engineering: Zeta Potential. *The*

Canadian Journal of Chemical Engineering. 99 (3), 627-639. https://doi.org/10.1002/cjce.23914.

Luo, Z., Yuan, X., Yu, Y., Zhang, Q., Leong, D. T., Lee, J. Y. and Xie, J. (2012). From Aggregation-induced Emission of Au (I)–thiolate Complexes to Ultrabright Au(0) @ Au (I)–thiolate Core–shell Nanoclusters. *Journal of the American Chemical Society*. 134 (40), 16662-16670.

Maiyo, F., Moodley, R., and Singh, M. (2016). Cytotoxicity, antioxidant and apoptosis studies of Quercetin-3-O-glucoside and 4-(β-D-Glucopyranosyl-1→4-α-L-Rhamnopyranosyloxy)-benzyl isothiocyanate from Moringa oleifera. *Anti-cancer Agents in Medicinal Chemistry*. 16 (5), 648 – 656. http://doi: 10.2174/1871520615666151002110424.

Mandru, A., Mane, J., and Mandapati, R. (2023). A Review on UV-visible Spectroscopy. *Journal of Pharma Insights and Research*. 1 (2), 091-096. https://doi.org/ 10.5281/zenodo.10232708.

Maney, V and Singh, M (2017). An *in vitro* assessment of Chitosan/ Bimetallic PtAu nanocomposites as delivery vehicles for Doxorubicin. *Nanomedicine.* 12 (21), 2625-2640. https://doi.org/10.2217/nnm-2017-0228.

Manivasagan, P., Bharathiraja, S., Bui, N. Q., Jang, B., Oh, Y. O., Lim, I. G., and Oh, J. (2016). Doxorubicin-loaded fucoidan capped gold nanoparticles for drug delivery and photoacoustic imaging. *International journal of biological macromolecules*. 91, 578-588. https://doi.org/10.1016/j.ijbiomac.2016.06.007.

Mansoori, G. A. (2017). An Introduction to Nanoscience and Nanotechnology. *Nanoscience and plant–soil systems*. 3-20.

https://doi.org/10.1007/978-3-319-46835-8_1.

Mao, Q., Fang, J., Wang, A., Zhang, Y., Cui, C., Ye, S., Zhao, Y., Feng, Y., Li, J., and Shi, H. (2021). Aggregation of Gold Nanoparticles Triggered by Hydrogen Peroxide-Initiated Chemiluminescence for Activated Tumor Theranostics. *Angewandte Chemie International Edition*. 60 (44), 23805-23811. https://doi.org/10.1002/anie.202109863.

Matthews, H. K., Bertoli, C., and de Bruin, R. A. (2022). Cell cycle control in cancer. *Nature reviews Molecular cell biology*. 23 (1), 74-88. https://doi.org/10.1038/s41580-021-00404-3.

McGuinn, L. A., Ghazarian, A. A., Ellison, G. L., Harvey, C. E., Kaefer, C. M., and Reid, B. C. (2012). Cancer and Environment: Definitions and Misconceptions. *Environmental research*. 112, 230-234. https://doi.org/10.1016/j.envres.2011.10.009.

Meng, F., Gan, F., and Ye, G. (2019). Bimetallic Gold/Silver Nanoclusters as a Fluorescent Probe for Detection of Methotrexate and Doxorubicin in Serum. *Microchimica Acta*. 186, 1-8. https://doi.org/10.1007/s00604-019-3477-7.

Mingos, D. M. P. (2014). Historical Introduction to Gold Colloids, Clusters and Nanoparticles. *Gold Clusters, Colloids and Nanoparticles I*. 161, 1-47. https://doi.org/10.1007/430_2013_138.

Mohamed, M. A., Jaafar, J., Ismail, A. F., Othman, M. H. D., and Rahman, M. A. (2017). Fourier transform infrared (FTIR) spectroscopy. In *Membrane Characterization.* Elsevier. pp 3-29. https://doi.org/10.1016/B978-0-444-63776-5.00001-2.

Mohammed, M. A., Syeda, J. T., Wasan, K. M., and Wasan, E. K. (2017). An Overview of Chitosan Nanoparticles and its Application in Non-parenteral Drug Delivery. *Pharmaceutics*. 9 (4), 53. https://doi.org/10.3390/pharmaceutics9040053.

Mohammed, N., Nawar, S. H., Etawy, M. S., Nassar, G. E., and Hassabo, A. G. (2024). Nanotechnology and its Applications in Industry and Product Design. *Journal of Textiles, Coloration and Polymer Science*. 21 (2), 273-284. https://doi.org/10.21608/jtcps.2024.258215.1251.

Molina, A., and Pituello, F. (2017). Playing with the cell cycle to build the spinal cord. *Developmental biology*. 432 (1), 14-23. https://doi.org/10.1016/j.ydbio.2016.12.022.

Moo, T. A., Sanford, R., Dang, C., and Morrow, M. (2018). Overview of Breast Cancer Therapy. *PET clinics*. 13 (3), 339-354. https://doi.org/10.1016/j.cpet.2018.02.006.

Moodley, T. and Singh, M. (2020). Sterically Stabilised Polymeric Mesoporous Silica Nanoparticles Improve Doxorubicin Efficiency: Tailored Cancer Therapy. *Molecules*.Molecules. 25(3): 742. https://doi:10.3390/molecules25030742**.**

Moreaud, L., Prasad, J., Mazères, S., Marcelot, C., Comby-Zerbino, C., Antoine, R., Heintz, O., and Dujardin, E. (2022). Facile One-pot Synthesis of White Emitting Gold Nanocluster Solutions Composed of Red, Green and Blue emitters. *Journal of Materials Chemistry C*. 10 (6), 2263-2270. https://doi.org/10.1039/D1TC04874K.

Moses, M. A., Brem, H., and Langer, R. (2003). Advancing The Field of Drug Delivery: Taking Aim at Cancer. *Cancer Cell*. 4 (5), 337-341. https://doi.org/S1535-6108(03)00276-9.

Muhesen, R. A., and Rajab, N. A. (2023). Formulation and characterization of olmesartan medoxomil as a nanoparticle. *Research Journal of Pharmacy and Technology*. 16 (7), 3314-3320. https://doi.org/ 10.52711/0974-360X.2023.00547.

Murugadoss, A., and Sakurai, H. (2011). Chitosan-stabilized Gold, Gold–palladium, and Gold–platinum Nanoclusters as Efficient Catalysts for Aerobic Oxidation of Alcohols. *Journal of Molecular Catalysis A: Chemical*. 341 (1-2), 1-6. https://doi.org/10.1016/j.molcata.2011.03.019.

Nag, O. K., and Delehanty, J. B. (2019). Active cellular and subcellular targeting of nanoparticles for drug delivery. *Pharmaceutics*. 11 (10), 543. https://doi.org/10.3390/pharmaceutics11100543.

Nasrollahzadeh, M., Sajadi, S. M., Sajjadi, M., and Issaabadi, Z. (2019). An Introduction to Nanotechnology. *Interface Science and Technology.* 28, 1-27. https://doi.org/10.1016/B978-0-12-813586-0.00001-8.

Navya, P. N., Kaphle, A., Srinivas, S. P., Bhargava, S. K., Rotello, V. M., and Daima, H. K. (2019). Current trends and challenges in cancer management and therapy using designer nanomaterials. *Nano Convergence*. 6 (1), 23. https://doi.org/10.1186/s40580-019-0193-2.

Nelemans, L. C., and Gurevich, L. (2020). Drug Delivery with Polymeric Nanocarriers—Cellular Uptake Mechanisms. *Materials*. 13 (2), 366. https://doi.org/10.3390/ma13020366.

Norouzi, M., Amerian, M., Amerian, M., and Atyabi, F. (2020). Clinical Applications of Nanomedicine in Cancer Therapy. *Drug Discovery Today*. 25 (1), 107-125. https://doi.org/10.1016/j.drudis.2019.09.017.

Obeagu, E. I., and Obeagu, G. U. (2024). Breast cancer: A Review of Risk Factors and Diagnosis. *Medicine*. 103 (3), 36905. https://doi.org/10.1097/MD.0000000000036905.

Oladimeji, O., Akinyelu, J., Daniels, A., and Singh, M. (2021). Modified gold nanoparticles for efficient delivery of betulinic acid to cancer cell mitochondria. *International Journal of Molecular Sciences*. 22 (10), 5072. https://doi.org/10.3390/ijms22105072.

Paduch, R. (2015). Theories of Cancer Origin. *European Journal of Cancer Prevention*. 24 (1), 57-67. https://doi.org/10.1097/CEJ.0000000000000024.

Pal, N. K., and Kryschi, C. (2015). A Facile One-pot Synthesis of Blue and Red Luminescent Thiol Stabilized Gold Nanoclusters: A Thorough Optical and Microscopy Study. *Physical Chemistry Chemical Physics*. 17 (33), 21423-21431. https://doi.org/10.1039/C5CP01773D.

Pan, S. T., Li, Z. L., He, Z. X., Qiu, J. X., and Zhou, S. F. (2016). Molecular Mechanisms for Tumour Resistance to Chemotherapy. *Clinical and Experimental Pharmacology and Physiology*. 43 (8), 723-737. https://doi.org/10.1111/1440-1681.12581.

Panda, M. K., Panda, S. K., Singh, Y. D., Jit, B. P., Behara, R. K., and Dhal, N. K. (2020). Role of nanoparticles and nanomaterials in drug delivery: an overview. *Advances in pharmaceutical biotechnology: recent progress and future applications*. 247-265. https://doi.org/10.1007/978-981-15-2195-9_19.

Pavelka, O., Dyakov, S., Kvakova, K., Vesely, J., Cigler, P., and Valenta, J. (2023). Towards site-specific emission enhancement of gold nanoclusters using plasmonic systems: advantages and limitations. *Nanoscale*. 15 (7),3351-3365. https://doi.org/10.1039/D2NR06680G.

Pedroso-Santana, S., and Fleitas-Salazar, N. (2020). Ionotropic Gelation Method in the Synthesis of Nanoparticles/microparticles for Biomedical Purposes. *Polymer International*. 69 (5), 443-447. https://doi.org/10.1002/pi.5970.

Pissuwan, D., Niidome, T., and Cortie, M. B. (2011). The Forthcoming Applications of Gold Nanoparticles in Drug and Gene Delivery Systems. *Journal of controlled release*. 149 (1), 65-71. https://doi.org/10.1016/j.jconrel.2009.12.006.

Plucinski, A., Lyu, Z., and Schmidt, B. V. (2021). Polysaccharide nanoparticles: From fabrication to applications. *Journal of Materials Chemistry B*. 9 (35), 7030-7062. https://doi.org/10.1039/D1TB00628B.

Qu, X., Li, Y., Li, L., Wang, Y., Liang, J., and Liang, J. (2015). Fluorescent Gold Nanoclusters: Synthesis and Recent Biological Application. *Journal of*

Nanomaterials. 2015 (1). 784097. https://doi.org/10.1155/2015/784097.

Rabanel, J. M., Aoun, V., Elkin, I., Mokhtar, M., and Hildgen, P. (2012). Drug-loaded Nanocarriers: Passive Targeting and Crossing of Biological Barriers. *Current medicinal chemistry*. 19 (19), 3070-3102.

https://doi.org/10.2174/092986712800784702.

Ramsden, J. J. (2023). Applied Nanotechnology. *Language*. 978, 161-163. https://doi.org/10.1016/B978-0-8155-2023-8.00023-6.

Ribble, D., Goldstein, N. B., Norris, D. A., and Shellman, Y. G. (2005). A simple technique for quantifying apoptosis in 96-well plates. *BMC biotechnology*. 5, 1-7. https://doi.org/10.1186/1472-6750-5-12.

Rivankar, S. (2014). An Overview of Doxorubicin Formulations in Cancer Therapy. *Journal of cancer research and therapeutics*. 10 (4), 853-858. https://doi.org/10.4103/0973-1482.139267.

Rodrigues, S., Dionísio, M., Remunan Lopez, C., and Grenha, A. (2012). Biocompatibility of chitosan carriers with application in drug delivery. *Journal of functional biomaterials*. 3 (3), 615-641. https://doi.org/10.3390/jfb3030615.

Saeedi, M., Vahidi, O., Moghbeli, M. R., Ahmadi, S., Asadnia, M., Akhavan, O., Seidi, F., Rabiee, M., Mohammad, R. S., Webster, J. T., Varma, R. S., Sharifi, E., Zarrabi, A., and Rabiee, N. (2022). Customizing Nano-chitosan for Sustainable Drug Delivery. *Journal of Controlled Release*. 350, 175-192. https://doi.org/10.1016/j.jconrel.2022.07.038.

Satalkar, P., Elger, B. S., and Shaw, D. M. (2016). Defining Nano, Nanotechnology and Nanomedicine: Why Should it Matter?. *Science and engineering ethics*. *22*, 1255-1276. https://doi.org/10.1007/s11948-015-9705-6.

Schirrmacher, V. (2019). From Chemotherapy to Biological Therapy: A Review of novel Concepts to Reduce the Side Effects of Systemic Cancer Treatment (Review). International Journal of Oncology. 54, 407-419. https://doi.org/10.3892/ijo.2018.4661.

Schwartz Jr, S. (2017). Unmet Needs in Developing Nanoparticles for Precision Medicine. *Nanomedicine*. 12 (4), 271-274. https://doi.org/10.2217/nnm-2016-0390.

Scimeca, M., Bischetti, S., Lamsira, H. K., Bonfiglio, R., and Bonanno, E. (2018). Energy Dispersive X-ray (EDX) Microanalysis: A Powerful Tool in Biomedical Research and Diagnosis. *European journal of histochemistry: EJH*. 62 (1). https://doi.org/10.4081/ejh.2018.2841.

Sharma, G. N., Dave, R., Sanadya, J., Sharma, P., and Sharma, K. (2010). Various Types and Management of Breast Cancer: An Overview. *Journal of Advanced Pharmaceutical Technology and Research*. 1 (2), 109-126. PMID: 22247839, PMCID: PMC3255438.

Shukla, S. K., Mishra, A. K., Arotiba, O. A., and Mamba, B. B. (2013). Chitosan-based Nanomaterials: A State-of-the-art Review. *International journal of biological macromolecules*. 59, 46-58. https://doi.org/10.1016/j.ijbiomac.2013.04.043.

Siegel, R. L., Miller, K. D., Wagle, N. S., and Jemal, A. (2023). Cancer statistics, 2023. *CA: A Cancer Journal for Clinicians*. 73 (1), 17-48. https://doi.org/10.3322/caac.21763.

Singh, V., Khurana, A., Navik, U., Allawadhi, P., Bharani, K. K., and Weiskirchen, R. (2022). Apoptosis and pharmacological therapies for targeting thereof for cancer therapeutics. *Sci*. 4 (2), 15. https://doi.org/10.3390/sci4020015.

Sobiborowicz-Sadowska, A. M., Kamińska, K., and Cudnoch-Jędrzejewska, A. (2023). Neprilysin Inhibition in the Prevention of Anthracycline-Induced Cardiotoxicity. *Cancers*. 15 (1), 312. https://doi.org/10.3390/cancers15010312.

Sritharan, S., and Sivalingam, N. (2021). A comprehensive review on time-tested anticancer drug doxorubicin. *Life sciences*. 278, 119527. https://doi.org/10.1016/j.lfs.2021.119527.

Surapaneni, S. K., Bashir, S. and Tikoo, K. (2018). Gold Nanoparticles-induced Cytotoxicity in Triple Negative Breast Cancer Involves Different Epigenetic Alterations Depending upon the Surface Charge. *Sci Rep*. 8, 12295. https://doi.org/10.1038/s41598-018-30541-3.

Tan, K., Ma, H., Mu, X., Wang, Z., Wang, Q., Wang, H., and Zhang, X. D. (2024). Application of gold nanoclusters in fluorescence sensing and biological detection. *Analytical and Bioanalytical Chemistry*. 1-21. https://doi.org/10.1007/s00216-024-05220-0.

Tang, W., Fan, W., Lau, J., Deng, L., Shen, Z., and Chen, X. (2019). Emerging Blood–Brain-Barrier-Crossing Nanotechnology for Brain Cancer Theranostics. *Chemical Society Reviews*. 48 (11), 2967-3014. https://doi.org/10.1039/C8CS00805A.

Tannock, I. F. (1998). Conventional cancer therapy: promise broken or promise delayed? *The Lancet*. 351 (suppl. 2) SII9-16. https://doi.org/10.1016/S0140-6736(98)90327-0.

Tian, D., Qian, Z., Xia, Y., and Zhu, C. (2012). Gold Nanocluster-based Fluorescent Probes for Near-infrared and Turn-on Sensing of Glutathione in Living cells. *Langmuir*. 28 (8), 3945-3951. https://doi.org/10.1021/la204380a.

Tewabe, A., Abate, A., Tamrie, M., Seyfu, A., and Abdela Siraj, E. (2021). Targeted drug delivery—from magic bullet to nanomedicine: principles, challenges, and future perspectives. *Journal of Multidisciplinary Healthcare*. 1711-1724. https://doi.org/10.2147/JMDH.S313968.

Thorn, C. F., Oshiro, C., Marsh, S., Hernandez-Boussard, T., McLeod, H., Klein, T. E., and Altman, R. B. (2011). Doxorubicin Pathways: Pharmacodynamics and Adverse Effects. *Pharmacogenetics and genomics*. 21 (7), 440-446. https://doi.org/10.1097/FPC.0b013e32833ffb56.

Torchilin, V. P. (2010). Passive and Active Drug Targeting: Drug Delivery to Tumors as an Example. *Drug delivery*. 3-53. https://doi.org/10.1007/978-3-642-00477-3_1.

Trayes, K. P., and Cokenakes, S. E. (2021). Breast Cancer Treatment. *American family physician*. 104 (2), 171-178. PMID: 34383430.

Turcsányi, Á., Ungor, D., and Csapó, E. (2020). Fluorescent Labeling of Hyaluronic acid-Chitosan Nanocarriers by Protein-stabilized Gold Nanoclusters. *Crystals*. 10 (12), 1113. https://doi.org/10.3390/cryst10121113.

van den Boogaard, W. M., Komninos, D. S., and Vermeij, W. P. (2022). Chemotherapy Side-Effects: Not All DNA Damage is Equal. *Cancers*. 14 (3), 627. https://doi.org/10.3390/cancers14030627.

van de Looij, S. M., Hebels, E. R., Viola, M., Hembury, M., Oliveira, S., and Vermonden, T. (2021). Gold Nanoclusters: Imaging, Therapy, and Theranostic Roles in Biomedical Applications. *Bioconjugate Chemistry*. 33 (1), 4-23. https://doi.org/10.1021/acs.bioconjchem.1c00475.

Venkitaraman, A. R. (2019). How do Mutations Affecting the Breast Cancer Genes BRCA1 and BRCA2 cause Cancer susceptibility?. *DNA repair*. 81, 102668. https://doi.org/10.1016/j.dnarep.2019.102668.

Villela Zumaya, A. L., Mincheva, R., Raquez, J. M., and Hassouna, F. (2022). Nanocluster-based Drug Delivery and Theranostic Systems: Towards Cancer Therapy. *Polymers*. 14 (6), 1188. https://doi.org/10.3390/polym14061188.

Voliani, V. (2020). *Gold Nanoparticles: An Introduction to Synthesis, Properties and Applications*. Walter de Gruyter GmbH & Co KG. pp 33-40. https://doi.org/10.1515/9781501511455-202.

Waheed, S., Li, Z., Zhang, F., Chiarini, A., Armato, U., and Wu, J. (2022). Engineering Nano-drug Biointerface to Overcome Biological Barriers Toward Precision Drug Delivery. *Journal of Nanobiotechnology*. 20 (1), 395. https://doi.org/10.1186/s12951-022-01605-4.

Wakaskar, R. R. (2018). Promising effects of nanomedicine in cancer drug delivery. *Journal of drug targeting*. 26 (4), 319-324. https://doi.org/10.1080/1061186X.2017.1377207.

Waks, A. G., and Winer, E. P. (2019). Breast Cancer Treatment: A Review. *JAMA*. 321 (3), 288-300. https://doi.org/10.1001/jama.2018.19323.

Wang, B., Hu, L., and Siahaan, T. J. (2016). *Drug delivery: principles and applications*. John Wiley & Sons. pp 1-20. https://doi.org/10.1002/0471475734.

Wang, C., Li, J., Amatore, C., Chen, Y., Jiang, H., and Wang, X. M. (2011). Gold Nanoclusters and Graphene Nanocomposites for Drug Delivery and Imaging of Cancer Cells. *Angewandte Chemie*. 123 (49), 11848-11852. https://doi.org/10.1002/ange.201105573.

Wang, H., and Mao, X. (2020). Evaluation of the Efficacy of Neoadjuvant Chemotherapy for Breast Cancer. *Drug Design, Development and Therapy*. 14, 2423–2433. https://doi.org/10.2147/DDDT.S253961.

Wang, Y., and Kohane, D. S. (2017). External Triggering and Triggered Targeting Strategies for Drug Delivery. *Nature Reviews Materials*. 2 (6), 1-14. https://doi.org/10.1038/natrevmats.2017.20.

Watkins, E. J. (2019). Overview of Breast Cancer. *Jaapa*. 32 (10), 13-17. https://doi.org/10.1097/01.JAA.0000580524.95733.3d.

Wrońska, N., Katir, N., Nowak-Lange, M., El Kadib, A., and Lisowska, K. (2023). Biodegradable Chitosan-based Films as an Alternative to Plastic Packaging. *Foods*. 12 (18), 3519. https://doi.org/10.3390/foods12183519.

Wu, B. Y., Wang, C. W., Chen, P. C., and Chang, H. T. (2017). Glutathione Assisted Preparation of Gold Nanoclusters Using Minimum Amount of Protein. *Sensors and Actuators B: Chemical*. 238, 1258-1265. https://doi.org/10.1016/j.snb.2016.09.071.

Wu, Z., Yao, Q., Chai, O. J. H., Ding, N., Xu, W., Zang, S., and Xie, J. (2020). Unraveling the impact of Gold (I)–thiolate Motifs on the Aggregation-induced emission of Gold Nanoclusters. *Angewandte Chemie*. 132 (25), 10020-10025. https://doi.org/10.1002/ange.201916675.

Xie, X., Peng, Z., Hua, X., Wang, Z., Deng, K., Yang, X., and Huang, H. (2020). Selectively Monitoring Glutathione in Human Serum and Growth-associated Living Cells using Gold Nanoclusters. *Biosensors and Bioelectronics*. 148, 111829. https://doi.org/10.1016/j.bios.2019.111829.

Yahia-Ammar, A., Sierra, D., Mérola, F., Hildebrandt, N., and Le Guével, X. (2016). Self-assembled gold nanoclusters for bright fluorescence imaging and enhanced drug delivery. *ACS Nano*. 10 (2), 2591-2599. https://doi.org/10.1021/acsnano.5b07596.

Yan, C., Liu, C., Abroshan, H., Li, Z., Qiu, R., and Li, G. (2016). Surface Modification of Adamantane-terminated Gold Nanoclusters using Cyclodextrins. *Physical Chemistry Chemical Physics*. 18 (33), 23358-23364. https://doi.org/10.1039/C6CP04569C.

Yang, F., Teves, S. S., Kemp, C. J., and Henikoff, S. (2014). Doxorubicin, DNA Torsion, and Chromatin Dynamics. *Biochimica et Biophysica Acta (BBA)-Reviews on Cancer*. 1845 (1), 84-89. https://doi.org/10.1016/j.bbcan.2013.12.002.

Yougbare, S., Chang, T. K., Tan, S. H., Kuo, J. C., Hsu, P. H., Su, C. Y., and Kuo, T. R. (2019). Antimicrobial Gold Nanoclusters: Recent Developments and Future Perspectives. *International journal of molecular sciences*. 20 (12), 2924. https://doi.org/10.3390/ijms20122924.

Yousefpour, P., Atyabi, F., Vasheghani-Farahani, E., Movahedi, A. A. M., and Dinarvand, R. (2022). Targeted Delivery of Doxorubicin Utilizing Chitosan Nanoparticles Surface Functionalized with Anti Her2 Trastuzumab [Corrigendum]. *International Journal of Nanomedicine*. 17, 5047-5048. https://doi.org/10.2147/IJN.S392079.

Zeng, C. (2018). Precision at the Nanoscale: On the Structure and Property Evolution of Gold Nanoclusters. *Pure and Applied Chemistry*. 90 (9), 1409-1427. https://doi.org/10.1515/pac-2018-0511.

Zhang, G., Zeng, X., and Li, P. (2013). Nanomaterials in Cancer-Therapy Drug Delivery System. *Journal of biomedical nanotechnology*. 9 (5), 741-750. https://doi.org/10.1166/jbn.2013.1583.

Zhang, J., Zhan, P., and Tian, H. (2021). Recent updates in the polysaccharides-based Nano-biocarriers for drugs delivery and its application in diseases treatment: A review. *International Journal of Biological Macromolecules*. 182, 115-128. https://doi.org/10.1016/j.ijbiomac.2021.04.009.

Zhang, Y., Yang, M., Portney, N. G., Cui, D., Budak, G., Ozbay, E., Ozakan, M., and Ozkan, C. S. (2008). Zeta potential: a surface electrical characteristic to probe the interaction of nanoparticles with normal and cancer human breast epithelial cells. *Biomedical microdevices*. 10, 321-328. https://doi.org/10.1007/s10544-007-9139-2.

Zhao, H., Zhu, Y., Ye, H., He, Y., Li, H., Sun, Y., Yang, F., and Wang, R. (2023). Atomic-Scale Structure Dynamics of Nanocrystals Revealed by In Situ and Environmental Transmission Electron Microscopy. *Advanced Materials*. 35 (50), 2206911. https://doi.org/10.1002/adma.202206911.

Zheng, Y., Wu, J., Jiang, H., and Wang, X. (2021). Gold Nanoclusters for Theranostic Applications. *Coordination Chemistry Reviews*. 431, 213689. https://doi.org/10.1155/2015/784097.

Appendix

Appendix A

Supplementary NTA data

1. Zeta potential (mV) vs concentration (particles/ ml)

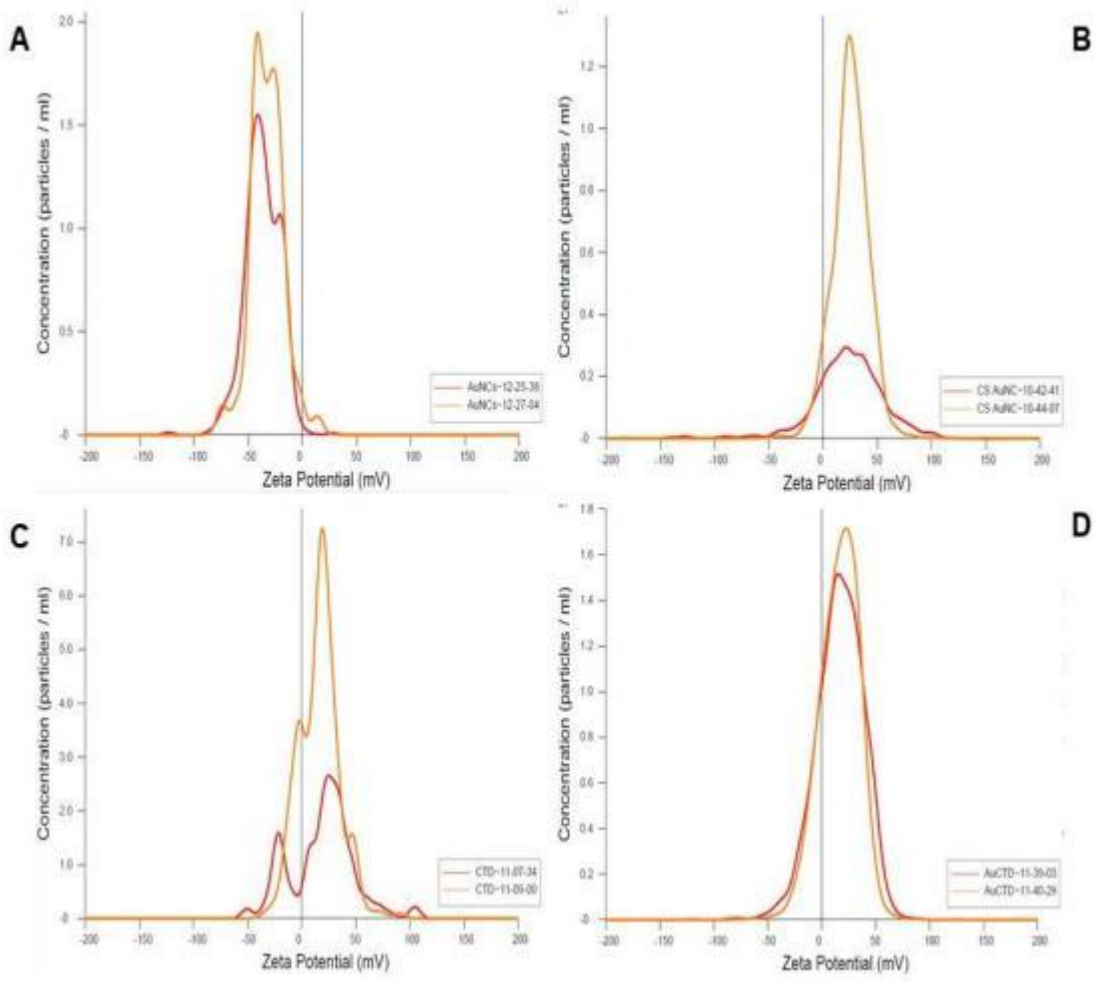

Figure 1: Graphs representation of Zeta Potential vs Concentration (particles/ ml) of synthesized nanocomplexes. A= AuNCs, B= CS-AuNCs, C= CTD, D= AuCTD.

2. Size (nm) vs concentration (particles/ ml)

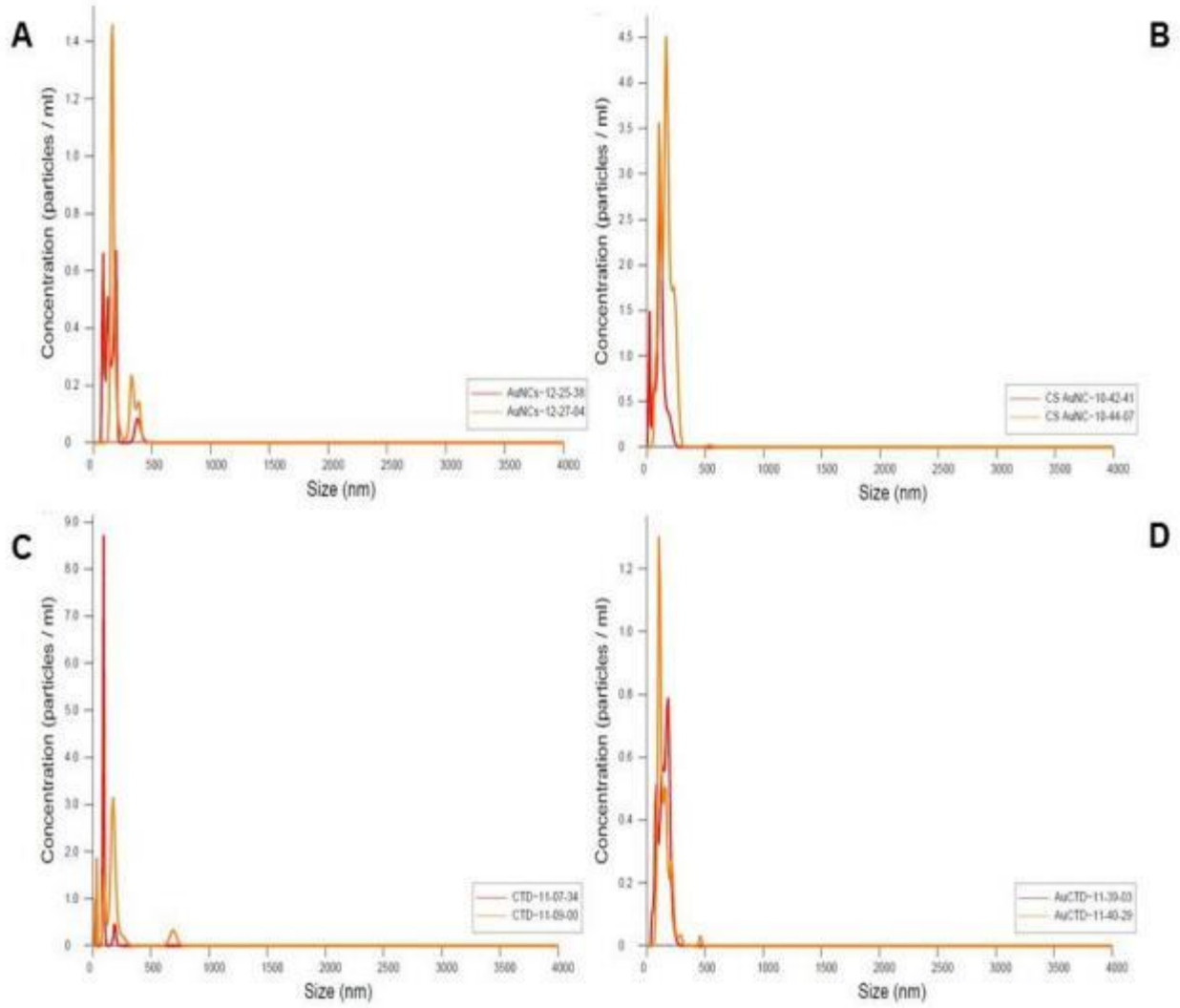

Figure 2: Graphical representation of Size (nm) vs Concentration (particles/ ml) of synthesized nanocomplexes. A= AuNCs, B= CS-AuNCs, C= CTD, D= AuCTD.